Real Time X-Ray Topographic Study of Growth Mechanism of Metallic Single Crystals from the Melt

November 1987

Tatsumasa KOBAYASHI

Real Time X-Ray Topographic Study of Growth Mechanism of Metallic Single Crystals from the Melt

November 1987

Tatsumasa KOBAYASHI

CONTENTS

CHAPTER 1   INTRODUCTION

1.1.   REVIEW OF PREVIOUS WORKS

1.1.1.   Theoretical Studies of Growth Mechanism of Metal Crystals from the Melt

Crystal growth from the melt has been used most widely for the preparation of large single crystals of metals, alloys and semiconductors. Many investigations have been made to understand the mechanism of crystal growth from the melt. However, the mechanism of crystal growth from the melt has not yet been understood as clearly as that from vapor phase or solution, even in the relatively simple case of growth of pure metals.

Since crystal growth occurs at surfaces which contact the parent phase such as vapour, solution or the melt, a clear understanding of interface structure is indispensable. In the case of crystal growth from vapor phase or solution, the surface of a growing crystal can be assumed in general to be flat and smooth on atomic or molecular scale. The theories of crystal growth from vapor phase or solution have been developed by Kossel [1],[2], Stranski-Kalschew [3], Becker-Doring [4], Volmer [5] and Burton-Cabrera-Frank [6]*. In these cases, it is theoretically ascertained that at least a set of low-index crystal surfaces are flat and smooth under ordinary conditions and that fundamental processes are (1) the arrival of atoms at the crystal

---

* A. Ookawa : "Crystal Growth" (Syokabo,Tokyo,1977) in Japanese

surface,   (2) the migration of absorbed molecular (or atoms), (3)
the advance of steps, and (4) nucleation on a growing surface.

On the other hand, the solid-liquid interface of a growing
crystal is not necessarily considered to be flat and smooth on the
atomic scale, and the atomic structure and the nature of the
interface have not yet been clarified as a function of growth
conditions.   In contrast to the density of vapour phase or
solution which is very low compared with that of the crystal, the
density of the melt is as high as that of the crystal.   Since the
melt and the crystal generally have very similar co-ordination
number of atoms, the atomic structure of solid-liquid interface is
believed to be quite different from that of the surface of growing
crystal contacting vapor phase or solution.

K.A.Jackson [7]-[9] introduced the concept of "roughness"
using the two-dimensional Ising model, and investigated
relationship between the roughness of crystal surface and
temperature.   In order to judge whether the crystal surface is
smooth or rough, he introduced a parameter α [8], which is
expressed as follows ;

$$\alpha = (n_1/v)(L_0/kT_E)$$

where, n_1 is the number of nearest neighbors of a single atom on
the plane surface, v the total possible number of nearest
neighbors of an atom in the parent body (so called cordination
number). L_0 the latent heat of the transfomation, k the
Boltzmann's constant and T_E is the equilibrium temperature.   He
proposed the following criterion: (i) when "α" is larger than
two, the crystal surface should be atomistically smooth, (ii) when
"α" is smaller than two, the surface should be atomistically
rough.

D.E.Temkin [10] proposed the concept of diffuseness of the interface on the basis of a multilayer model which was an expansion of Jackson's two dimensional model. Because Temkin's multilayer model neither limits the number of layers nor restricts the temperature of the interface to the melting point, his model holds for all kinds of solid-liquid interface. However, it should be noticed that both of these two models are based on discrete lattice models of solid and liquid near the interface, which are originally invented for the growth from vapor phase or solution.

Cahn et al. [11],[12] studied the solid-liquid interface using a continuous model which was originally applied to second order phase transformation. In this theory, the surface energy of an interface depends on the mean position of the interface with respect to the atomic plane in the crystal, and therefore, the surface energy should vary periodically as the interface moves.

To consider the mechanism of crystal growth from the melt, it is necessary to understand what the unit process of crystal growth is. Theories of crystal growth have been classified into two major processes, namely, (1) atom by atom process and (2) collected atom process [13]. Jackson's theory [7]-[9] and Temkin's theory [10] mentioned above are based on the assumption that the unit process of crystal growth from the melt is atom by atom process. On the other hand, in the theory of Cahn and his co-workers [11],[12], it is conceived that the unit process is the motion of collected atoms. Besides these, there are other versions of growth theory based of the dislocation model of liquid in the melted state [14]-[16]. In these theories, crystal growth from the melt is

-3-

considered to be a recovery process of heavily dislocated materials, namely. the melt. A specific characteristic of these theories is that they take account of the structure of the parent phase, the melt. which is lacking in the aforementioned three theories.

Another viewpoint on the discussion of mechanisms of crystal growth from the melt is provided by kinetics, i.e. the relation between growth rate and undercooling at the interface (supercooling). The kinetics of crystal growth is of importance because it governs the morphologies of a crystal and plays an important role in influencing the stability of growing interface. Theories of kinetics for the crystal growth from the melt have been evolved from that of growth from vapor phase. The relations between growth rate (V) and supercooling (ΔT) are classified roughly into three types in connection with the interface structure, as follows;

(1) $V = A_1 \Delta T$: for growth on rough interface [17]

(2) $V = A_2 \exp(-A_3/\Delta T)$: for two dimensional nucleation and growth on smooth interface [19]

(3) $V = A_4 (\Delta T)^2$: for screw dislocation assisted growth on smooth interface [19]

Detailed classification was made by Brice [20] as shown in table 1. Tiller [21] proposed another classification of the equations for the kinetics.

It should be emphasized that these equations for the kinetics of crystal growth from the melt must be verified experimentally. However, there have been few experiments of that kind on the kinetics of crystal growth of metals, excepting those of low melting temperature such as gallium. because of the difficulty in

Table 1   Growth rates of various types of interface[20].

Case No.	Type of interface	Growth rate
	Perfect singular	
1	(a) Large nuclei spreading slowly	$A_1 \Delta T^{\frac{3}{4}} \exp(-B_1/\Delta T)$
2	(b) Large nuclei spreading rapidly	$A_2 \exp(-B_2/\Delta T)$
3	(c) Small nuclei spreading slowly	$A_3 \Delta T^{1+\frac{1}{2}n^*}$
4	(d) Small nuclei spreading rapdily	$A_4 \Delta T^{1+n^*}$
	Imperfect singular	
5	(a) Constant fraction of sites available	$A_5 \Delta T$
6	(b) Screw dislocation at small super-cooling	$A_6 \Delta T^2$
7	(c) Screw dislocation at large super-cooling	$A_7 \Delta T$
	Rough	
8	(a) Small supercooling	$A_8 \Delta T$
9	(b) Large supercooling	$A_9 \{1 - \exp(-B_3 \Delta T)\}$

A_i and B_i are constants for the various kinds of process. A_i is generally a function of temperature and will decrease slowly as the temperature falls.

n^* is the number of atoms in a critical nucleus.

determining the portion of the interface, temperature and growth rate normal to the interface for a metal with a relatively high melting temperature. Instead, several experiments with computer simulations have been carried out on this problem, as will be mentioned in the next section.

1.1.2.   Experimental Studies of Growth Mechanism of Metallic
           Crystals from the Melt

As mentioned before, a detailed knowledge of the solid-liquid interface during growth is of great importance to infer the mechanism of crystal growth from the melt. It is impossible, however, to observe the structure of solid-liquid interface during growth on an atomic scale (recently, the improvement on resolution of electron microscopes allows us to carry out real time observations of solid-liquid interface in equilibrium state of atomic scale[54], but similar observations during growth have not yet been carried out). Direct observations of macroscopical interface morphology, therefore, have been made for many years.

Most of the early studies on the interface morphology were made by examining the quenched or the so-called "decanted" interface at room temperature. Weinberg and Chalmers [22]-[24] showed that the solid-liquid interface could be revealed by pouring or accelerating away the unsolidified liquid (decanting procedures). The decanting method brought us considerable information about the complex processes occurring at a solid-liquid interface. For example, the first evidence of the transition from planar to cellular growth was obtained from the

optical micrography of decanted surfaces [25]-[27]. However, the limitations of the decanting method were indicated by Chadwick [31]. He showed that a film of retained liquid would invariably remain on portions of a decanted interface and that subsequent freezing of the retained liquid would mask the true microstructural details.

To avoid these shortcomings of quenching or decanting method, experimental techniques of direct and real time observation of the interfacial morphology have been devised, based on optical microscopy [32]-[40], electron microscopy [28]-[30], and X-ray topography, etc. However, most of the direct observations of crystal growth from the melt by optical microscopy or electron microscopy have been limited to systems freezing at relatively low rates (less than about 10^{-1} μm/s) due to the high magnification.

Numerous studies concerning with the interface morphology have been made by optical microscopy. Because it is relatively easy to make direct observations of solidification phenomena in transparent systems, a great deal has been learned from them about the growth mechanism of pure materials [32]-[34], dendritic solidification [35]-[38], and eutectic solidification [39],[40], etc.

The study of metallic crystals by the direct method has been made through the use of reflection microscopy because of the opaqueness of metals. Pennington et al. [41] N.V.Stoichev et al. [42] and I.Gutzow et al. [43] made direct measurements of the relation between growth rate and supercooling on gallium and its alloys. Cline [44] studied eutectic growth of Pb-Sn systems.

observing that the faint contrast between the lead-rich solid and the liquid phase arises from slight differences in their optical reflectivities. Such morphological information on the solid-liquid interface of metallic crystals can be obtained through optical microscopy. However, lattice defects such as dislocations of metallic crystals cannot be detected by this method and observations of the interaction between dislocations and growing interface cannot be made, which would provide us with significant information on mechanism of crystal growth from the melt. In addition, real-time observation of growing interface by optical microscopy is limited to the free surface observation in the case of opaque materials and to metals with a relatively low melting temperature.

The application of transmission electron microscopy to the study of crystal growth of a metallic crystal has made it possible to observe micromorphological structure of the solid-liquid interface during growth of a foil specimen of less than one micron thick. Glicksman and Vold [45] observed growth of interface of pure bismuth intermittently ; during the image formation, melting and growth had to be disrupted. Such an observation of solid-liquid interface may be considered "direct" when the effect of this disruption is negligible for the growth of the interface. Recently, the developments of high voltage electron microscope (1 MeV) and TV imaging systems enable us to make in situ observations of the morphology of solid-liquid interface of growing metallic crystals. With this technique, dynamic observations of solidification process have been attempted on pure metals [46] or metallic alloys [46]-[48].

Although electron microscopy makes it possible to observe the

dynamic behavior of melting and growth processes of metallic crystals with very high resolution, several disadvantages of this metod have been pointed out as follows [49]:

(1) The extreme thinness of the specimen used may give rise to unusual situations which will never be encountered in any usual macroscopic solidification process, for example, the absence of thermal convection and very large thermal gradient. Under typical experimental conditions, the thermal gradient at the solid-liquid interface is estimated to be about $10^2 - 10^3$ K/mm, which is very unusual.

(2) Its application is limited to a low growth rate, and to the specimens with sufficiently low vapor pressure at the melting point.

Therefore, considerable precaution must be taken in comparing the phenomena observed by the electron microscope with those in the growth process of bulk crystals.

X-ray topography has many advantages, but in a sense it is complementary to electron microscopy. Dynamic observations of melting and growth processes by means of this method has been desired because it can eliminate the disadvantages of electron microscopy. Recent development of TV imaging systems combined with high intensity X-ray generators permits direct and real time observations of melting and solidification phenomena of opaque crystals such as metals and semiconductors.

Chikawa [50] has presented the first report on real-time X-ray topographic observation of growth of silicon crystals. In the following works [51]-[53], he and his co-workers studied interface morphology during melting and growth from the melt and found that a strong contrast was observed in the liquid near the interface

during growth,which did not appear during the melting process. They concluded that this contrast is due to crystallites which are formed in the supercooled melt along the interface. Also in these works, they studied behavior of dislocations near the interface and the effect of dislocations on faceted growth. The method they used for observation involved direct heating of the surface of the plate- shaped speciman by two carbon heaters (FZ method) [51] so that the middle part of the specimen was melted into an elliptical shape.

However, there have been actually no real time observations so far on interface morphology of growing metallic crystals in an ordinary condition. (After we have published papers on real-time observations of growing crystals, Nittono et al. [54] observed melting and growth processes of a tin single crystal by X-ray topography using synchrotron radiation with a method similar to that of Chikawa et al.)

On the one hand, experiments on the kinetics of crystal growth from the melt are very rare and limited to metals with low melting temperature such as gallium and its alloys [55]-[58] because of the difficulty involved in determining the interface temperature. In this kind of study, the capillary technique has been employed in which a crystal is grown in a fine bore tube [55]-[58]. The superiority of this technique lies in the fact that this technique makes it possible to grow dislocation-free single crystals and also makes it possible to determine the temperature of the interface when the growth rate is sufficiently small. In these works, three kinds of growth such as (a) lateral growth by two dimensional nucleation, (b) lateral growth by the screw

dislocation. (c) continuous growth. were observed from the measurment of the growth rate as a function of supercooling. In this way, if it is possible to carry out precise measurements of growth rate as a function of supercooling, the mechanism of crystal growth from the melt can be determined by comparing the observed relation between growth rate and supercooling with that theoretically derived, for example, as shown in Table 1. However, it is very difficult to apply the capillary method to a metal with relatively high melting temperature, and there have been no experimental studies on growth kinetics of such metals by direct and real-time observation.

Instead of this. several computer simulations have been attempted on the structure of solid-liquid interface in equilibrium state [59]-[62],[65] or during growth [63]-[65]. and on the kinetics of crystal growth on the basis of statistical or dynamical model [63]-[65]. Computer simulation enables one to investigate the growing process in an atomic level or examine whether the postulated model is proper or not.

However, it has been pointed out that even if the result of computer simulation gives a satisfactory agreement with the presumed interface kinetics, there still remains a problem as to whether or not the presumed mechanism describes properly the process of crystal growth from the melt because of the assumption about liquid state [65]. It was also pointed out that there is a discrepancy between the experimental result of growth kinetics [57] and the kinetics expected from Jackson's theory [8].

1.2. THE AIM OF THE PRESENT STUDY

The primary objective of crystal growth is the production of materials with predicted and controlled properties. The control of the crystal growth. in particular, the growth of dislocation-free crystals has become. in part, feasible industrially. However,the understanding of the mechanism of crystal growth from the melt. which is necessary to control the crystal growth from the melt. is insufficient.

One of the most effective experimental methods for investigating the growth mechanism is direct and dynamic observation of the morphology of the solid-liquid interface during growth. The morphology of the solid-liquid interface is closely related to growth mechanisms. When the interface is far from isothermal. i.e.. when macroscopic faceting of the interface is observed. the growth rate is highly anisotropic. When, on the other hand, the interface is always observed along the isothermal plane, the growth is isotropic. According to theoretical predictions [9], a continuous growth mechanism would imply isotropic growth, while a lateral growth mechanism would imply anisotropic growth. However, the reverse arguments cannot be made with any generality, because the observed degree of anisotropy must always be considered in relation to the existing temperature differences in the system.

The method of unidirectional solidification makes it possible to correlate the observed interface morphologies with the growth mechanisms. In this unidirectional solidification. in which growth occurs onto a part of the crystal while a heat sink is attached to

the remainder, the latent heat generated during the growth process can be removed by conduction into the solid rather than into the liquid. As a result, the existence of extensive zones of supercooling in the liquid can be avoided there by preventing instability in the growing surface which leads to chemical inhomogeneity in crystals with impurities.

The aim of the present study is to provide more direct information on the mechanism of crystal growth from the melt by observing solid-liquid interface with the aid of real time X-ray topography and to make our understanding on the mechanism of crystal growth clear by confronting the experimental observations with the existing theories.

In the present studies, at first, in order to observe dynamically unidirectional melting and growth processes of metallic single crystals, Bridgman furnaces were newly constructed for real time X-ray topography (Chapter 2).

With the aid of these furnaces which were combined with a high intensity X-ray generator and a TV imaging system, morphologies of solid-liquid interface during melting and growth processes of metallic crystals, which are opaque to visible light, were observed, and growth mechanism was investigated from the observation of interface morphology and effect of dislocations on it (Chapter 3). Measurements of growth rate as a function of super-cooling were also made with these furnaces and growth mechanism was inferred by comparing the experimental results with the theories on growth kinetics (Chapter 3).

In order to grow crystals with high perfection, it is necessary to make clear the formation mechanism of dislocations during crystal growth. To do this, real time observations of the

processes of generation and propagation of dislocations is a most suitable experiment. Real-time X-ray topography was applied to the study of the generation mechanism of dislocations and the mechanism of crystal growth from the melt was discussed (Chapter 4).

In these studies, aluminium and gallium single crystals were used. Aluminium has f.c.c. structure and a relatively low melting temperature, and the thickness of aluminium specimen t for satisfying $\mu t=1$, where μ is linear absorption coefficient, is about 0.7 mm for Ag $K_{\alpha 1}$ radiation. This is very favorable for the observation of melting and growth process with real time X-ray topography under conditions similar to common macroscopic growth. Gallium has face-centered orthorohmbic structure, and Jackson's parameter α [8] is nearly equal to 2. Accordingly, Jackson's theory suggests a possibility of growth either by lateral mechanism or by adhesive mechanism, or by both for this material, depending on a growth condition.

Dendritic growth is the most common mechanism of crystallization from the melt in alloys, and the fineness of the dendrite influences the mechanical properties and homogenization kinetics of materials. Because of the industrial necessity of controlling its structure, many studies have been made. However, most of the studies on this problem of alloys have been made "ex post facto" to the actual process by a photographic method. Real time observation by X-ray topography has been first applied to the investigation of dendritic growth of alloys (Chapter 5). Observations have been made using Al-Mg alloys on the following subjects :

(1) Sequential growth and morphology of the dendrite arms during

solidification as a function of growth rate.

(2) Morphological changes of dendrite arms as a function of Mg content.

(3) Morphological changes and solute redistribution during cooling and isothermal annealing after silidification.

(4) Melting process of previously grown dendrite.

REFERENCES

(1) W. Kossel : Nach. Ges Wiss Goettingen (1927) 135

(2) W. Kossel : Naturwissenschafteem **18** (1930) 901

(3) I. N. Stranski and R. Kaischew : Z. Phys. Chem (B)26 (1934) 31

(4) R. Becker and W. Doring : Ann. Phys. **24** (1935) 719

(5) M. Volmer : Kinetik der Phasenbildung (1939)

(6) W. K. Burton, N. Cabrera and F. C. Frank : Phil. trans. Roy. Soc. **A243** (1950-1951) 299

(7) K. A. Jackson, and D. Chalmer : Can. J. Phys. **34** (1956) 473

(8) K. A. Jackson : "Liquid Metals and Solidification" (American Society for Metals, Cleveland,1958) 174

(9) K. A. Jackson, D. R. Vhlmann and J. D. Hunt : J. Cryst. Growth **1** (1967) 1

(10) D. E. Temkn : "Crystallization Process" (Consultant Bureau, New York. 1966) 15

(11) J. W. Cahn : Acta Met. **8** (1960) 554

(12) J.W. Cahn, W. B. Hillig and G. W. Sears : 12 (1964) 1421

(13) A. Ookawa : "Crystal Growth" (Syokabo, Tokyo, 1977) in Japanese

(14) A. Ookawa : J. Phys. Soc. Japan **12** (1960) 2191

(15) R. M. Cotterill, E. J. Jensen, W. D. Kristensen and R. Paetsch : J. de Physique **36** (1975) C2

(16) H. Suzuki : Bull. Japan Institute of Metals, **13** (1974) 733

(17) H. A. Wilson : Phil. Mag. **50** (1900) 238

(18) M. I. Volmer and M. Marder : Z. Phys. Chem. **A154** (1931) 97

(19) W. B. Hillig and D. Turnbull : J. Chem. Phys. **24** (1956) 914

(20) J. C. Brice : "The Growth of Crystals from Liquids" (North-Holland 1973) 19

(21) W. A. Tiller : "Solidification" (Amer. Soc. Metals 1971) 59

(22) F. Weinberg and B. Chalmers : Can. J. Phys. **31** (1951) 382

(23) Winegard, S. Majaka, B. Mthall : Can. J. Phys. **29** (1951) 320

(24) F. Weinberg and B. Chalmers : Can. J. Phys. **30** (1952) 488

(25) J. W. Rutter and B. Chalmers : Can. J. Phys. **31** (1953) 15

(26) C. Elbaum and B.Chalmers : Can. J. Phys. **33** (1955) 196

(27) C. Elbaum and B. Chalmers : Can. J. Phys. **34** (1966) 473

(28) D. G. McCartney and J. D. Hunt : Acta Met. **29** (1981) 1851

(29) G. A. Chadwick : Acta Met. **10** (1962) 1

(30) T. Okamoto and K. Kishitake : J. Cryst. Growth **29** (1975) 137

(31) G. A. Chadwick : Acta Met. **10** (1962) 1

(32) K. A. Jackson, D. R. Vhlmann and J. D. Hunt : J. Cryst. Growth **1** 1

(33) D. E. Glicksman and P. W. Voophees : Metallur. Ttans. **15A** (1984) 995

(34) I. Gutzow and E. Parcheva : Krystall und Technik 11 (1976) 793

(35) M. E. Glicksman and R. J. Schaefer : J. Cryst. Growth 1 (1967) 297

(36) K. A. Jackson and J. D. Hunt : Acta Met. 13 (1965) 1212

(37) K. A. Jackson, J. D. Hunt, D. R. Vhlman and T. P. Seward III : Trans AIME **236** (1966) 149

(38) M. E. Glicksman and P. W. Voophees : Metallur Trans. **15A** (1984) 995

(39) J. D. Hunt and K. A. Jackson : Trans AIME **236** (1966) 843

(40) J. D. Hunt and K. A. Jackson : Trans AIME **239** (1967) 864

(41) P. R. Pennington, S. E. Ravite and G. Abbashain : Acta Met. **68** (1970) 943

(42) N. V. Stoichev, G. A. Alfintsev and D. E. Ovsienko : Sov. Phys. Crystallogr. **20** (1976) 504

(43) I. Gutzow, A. Razpopov and R. Kaischew : Phys. Stat. Sol. (a) **1** (1970) 159

(44) H. E. Cline : Trans AIME **239** (1967) 1489

(45) M. E. Glicksman and C. L. Vold : Acta Met. 15 (1967) 1409

(46) C. Lemaigman, D. Camel and J. Pelissier : J. Cryst. Growth **52** (1981) 67

(47) R. Hamar and C. Lemaigman : J. Cryst. Growth 53 (1981) 586

(48) H. Saka, A. Sakai, T. Kamino and T. Imura : Phil. Mag. (a) 52 (1985) L29

(49) M. E. Glicksman : "Solidification" T. J. Hughel and G. F. Bolling eds. (American Society for Metals, Metal Park 1970) pp. 155

(50) J. Chikawa : J. Cryst. Growth **24/25** (1974) 61

(51) J. Chikawa and S. Shirai : J. Cryst Growth **39** (1977) 328

(52) J. Chikawa and F. Sato : "Defects and Radiation Effects in Semiconductors, 1980) ed. R. R. Hasiguti (The Institute of Phisics. 1981) p.95

(53) J. Chikawa and F. Sato : "Defects in Semiconductors" eds. Narayan and Jan (North-Holland, 1981) p.317

(54) O. Nittono, T Ogawa, S. K. Gong and S. Nagakura : Jpn. J. Appl. Phys. **23** (1984) L581

(55) N. V. Stoichev, G. A. Alfintsev and D. E. Ovsienko : Sov. Phys. Crystallogr. **20** (1976) 504

(56) V. T. Borisov, I. N. Golikov and Yu. E. Matveev : Sov. Phys. Crystallogr. **13** (1959) 756

(57) P. R. Pennington, S. F. Ravitz and G. Abbaschian : Acta Met. **18** (1970) 943

(58) G. J. Abbaschian and S. F. Ravitz : J. Cryst. Growth **44** (1978) 453

(59) C. van. Leeuwen : J. Cryst. Growth **19** (1973) 133

(60) D. J. van. Dijk, C. van. Leeuwen and P. Bennema : J. Cryst. Growth **23** (1974) 81

(61) H. J. Leamy and G. H. Gilmer : J. Cryst. Growth **24/25** (1974)

(62) V. D. Esin, V. I. Danilyuk, Yu. M. Plishkin and G. L. Podchinenova : Sov.Phys. Cryscallogr. **18** (1974) 578

(63) G. H. Gilmer, H. J. Leamy and K. A. Jackson : J. Cryst. Growth **24/25** (1974) 495

(64) J. P. Vander Earden, C. van. Leeuwen, P. Bennema, W. L. Vander Kruk and B. P. Th. Veltman : J. Appl. Phys. **48** (1977) 495

(65) J. P. van. der Earden, P. Bennema and T. A. Cherpanova :

.

CHAPTER 2 APPARATUS FOR REAL TIME OBSERVATIONS OF CRYSTAL GROWTH BY X-RAY TOPOGRAPHY

2.1 INTRODUCTION

X-ray topography, optical as well as electron microscopy and the dislocation etching method have been used for the studies of crystal perfection and mechanism of crystal growth. Among these methods, transmission X-ray topography, especially the Lang method, [1] is the most effective and universal method for the study of crystal growth, because it enables one to observe non-destructively crystal defects in a large area of relatively thick crystal which is opaque to visual light. However, when a conventional X-ray source is used, a long exposure is usually needed to record diffracted images of crystal defects because of the weakness of X-ray intensities. Consequently most of the studies on crystal growth with X-ray topography have been made so far statically by observing the structure of as-grown crystal at room temperature. Therefore, the studies on the mechanism of crystal growth have usually been based on such static observations on the morphology of as grown crystals and on the grown-in crystal defects, such as dislocations, growth striations, etc.

By using a recently developed ultra high power X-ray generator (RU-1500, RIGAKU DENKI) [2] or Synchrotron Orbital Radiation unit (SOR) [3] as a X-ray source and by using TV-VTR system as a continuous recording system [4], it has become

possible to observe dynamical behaviors of defects in growing crystals [5]-[9] or phase transformation of crystals [10]-[12]. However, very limited studies have been reported on real time observation of melting and growth processes. The solid-liquid interface of Si [13]-[15] and Sn [16] single crystal has been studied by a local melting technique. However, no reports have been found on real time X-ray topographic observation of melting and growth processes of metallic crystals using the uni-directional solidification method, which is the usual method to grow metallic single crystals. With this uni-directional method, one can avoid the formation of a new nuclei and avoid instability in the growing surface, which leads to chemical inhomogeneity in the crystals with impurities.

For the purpose of studying the crystal growth from the melt of metallic materials with relatively high melting temperatures, high-temperature furnaces of uni-directional solidification for use with X-ray topographic goniometer have been newly developed in the present experiment. For the furnace for real-time X-ray topographic observations, the following functional features are the minimun requirment : (1) the furnace can be set on a topographic goniometer stage and a large area of the specimen (45 mm, in the present apparatus) can be observed with a high resolution, (2) measurement of the temperature of the specimen near the solid-liquid interface can be made in parallel with a given constant growth rate, (3) the temperature gradient of the specimen should be uni-directional, (4) a given temperature gradient of the solid-liquid interface can be kept constant during growth and on the other hand, a variety of temperature gradient of 1 K/mm to 10 K/mm can be obtained on request, (5)

melting and growth can be made in any environmental gas atmosphere or in a vacuum at any desired temperature below 1200 K, (6) the Bragg condition should be kept strictly and, if necessary, its adjustment can be made during the observation.

The purpose of this chapter is to outline the instruments used for real time x-ray topography and describe the furnaces newly developed for real time observations of crystal growth by X-ray topography.

2.2. REAL TIME X-RAY TOPOGRAPHY APPARATUS

2.2.1. X-ray generator

For real time observation of melting and growth processes of metallic crystals, an X-ray diffraction topographic system which consisted of a 90 kW-class high power X-ray generator (RU-1500, Rigaku Denki) [2], a large topographic goniometer and a TV imaging system were employed. In the case of transmission topography (Lang method in the present experiment), the generator with a rotating Ag target was operated at 50 kV,1200 mA and a bias voltage of 1000 V, and Ag $K\alpha$ radiations were used for topography. For reflection topography, Cu $K\alpha$ radiations from a rotating Cu target operated at 55 kV and 1300 mA were used. The effective size of the focus was 1.0 x 1.0 mm^2 and the distance between the focus and the specimen was 1200 mm, so that the geometrical resolution was about 3 µm in the horizontal direction and 25 µm in the vertical direction. A block diagram of the topographic system is

X-Ray Focus

Beam

Slit

Graphite Heater

Graphite Crucible

Specimen

Be Window

TV Camera
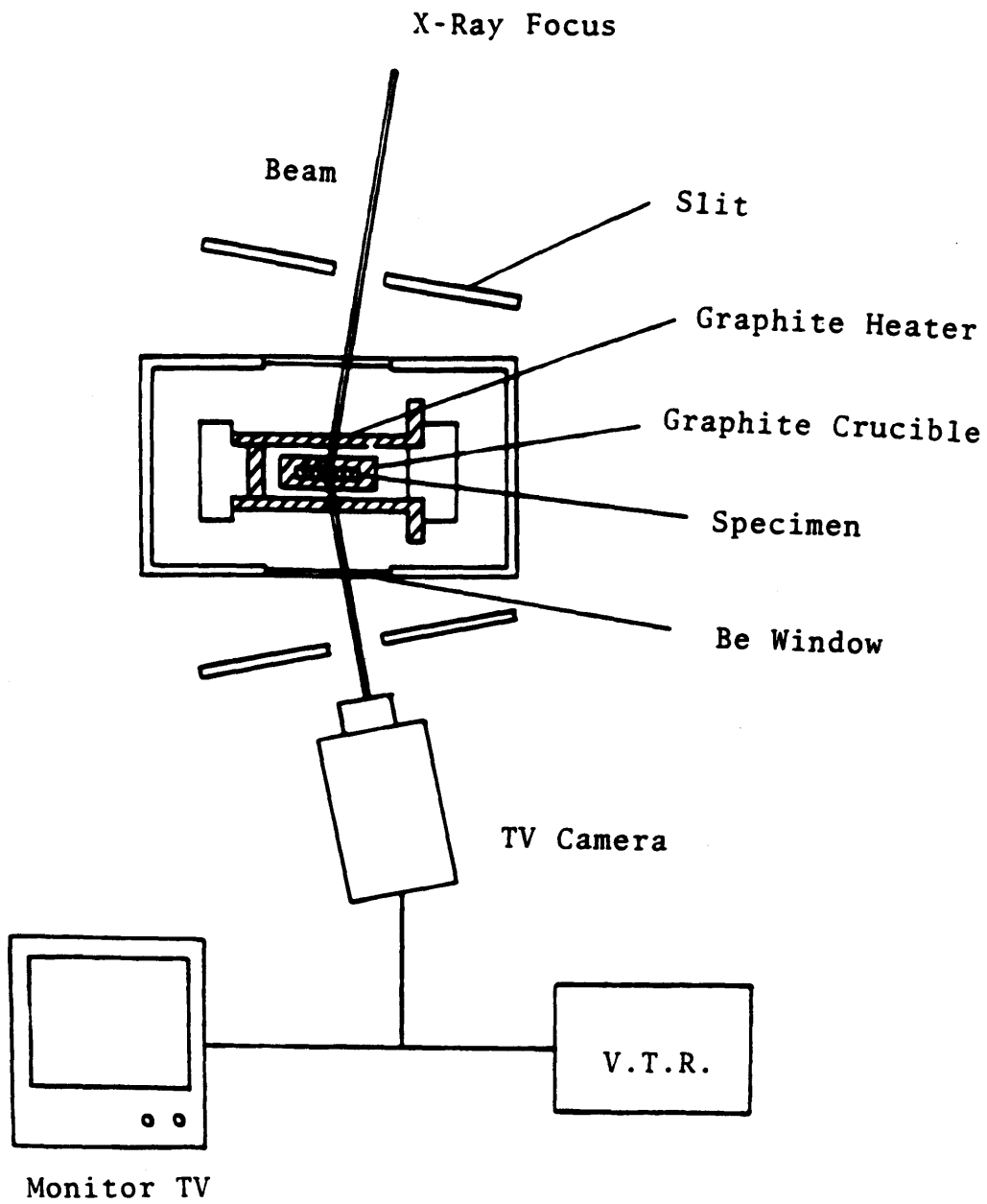
V.T.R.

Monitor TV

Figure 2.1   Schematic diagram of X-ray topography
with the T.V. unit and the Bridgman-furnace.

shown in Fig. 2.1.

2.2.2.   Lang Camera

The goniometer used was of a type of Lang camera [1], which

can be used for both Lang method and Berg-Barrett method [17]. The

distance between the X-ray source and the specimen was 1200 mm and

that between the specimen and the film or the specimen and TV

camera was 6 - 80 mm. The remote control of θ adjustment,

sample rotation and selection of imaging area can be made. The

geometry of observation is shown in Fig. 2.2.

2.2.3.   TV Imaging and Recording System

The TV imaging system consists of a TV camera unit with a PbO

vidicon tube (Hamamatsu T.V., N-603, imaging area: 12x9 mm^2,

spatial resolution: 20 - 25 μm) video amplifier, a camera control

unit, a digital image processor (Avionics,Image Σ) and a TV

monitor operating as a normal closed-circuit TV system (Fig. 2.2).

TV frame speed is 30 frames/s and a number of scanning line   is

525. By orienting the crystal so as to satisfy the Bragg condition

for slightly divergent incident X-ray beam , two images due to the

diffracted $K_{\alpha 1}$ and $K_{\alpha 2}$, each with a width of 1 mm are received by

the vidicon tube. These two band-shaped images are directly

converted into video signals and displayed simultaneously with a

magnification of about 20 times on the TV monitor. Such images are

called "direct-view images" [18]. To observe a larger area of the

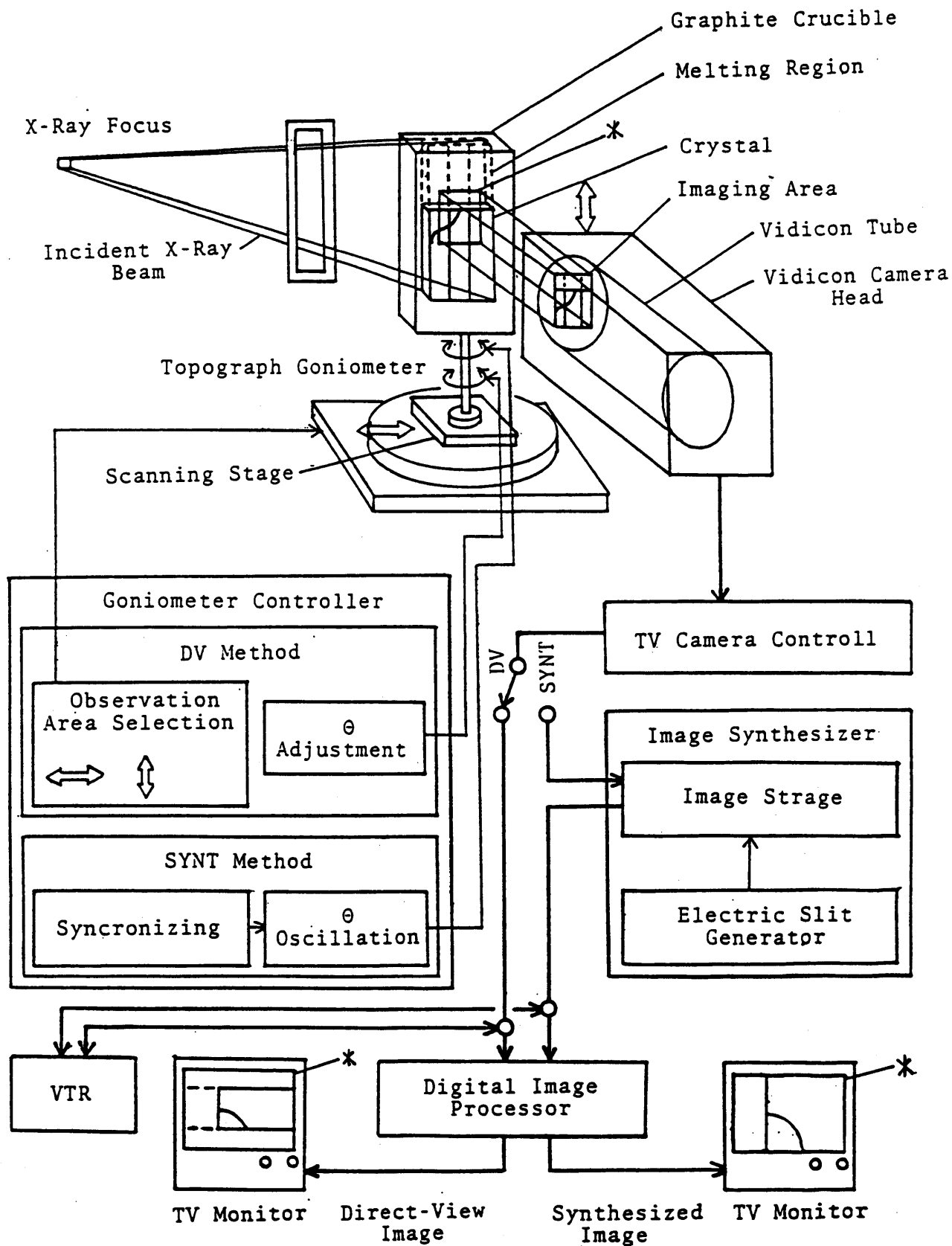specimen, the video signals due to $K_{\alpha 1}$ (or $K_{\alpha 2}$) are selected

Figure 2.2 Block diagram of the imaging system for X-ray topography.

electrically and stored in the image storage, while the goniometer is oscillated between $\pm$ 40' (oscillation topography). The electric slit is also oscillated in syncronization with the selected $K_{\alpha 1}$ (or $K_{\alpha 2}$) image, and at the end of the oscillation, a Lang topograph with the imaging area of the vidicon tube (9 x 12 mm^2) is displayed on the TV monitor. Such images are referred to as "synthesized images" [18]. The dynamic behaviors of the solid-liquid interface and dislocations near the interface during melting and growth processes of them were continuously observed on the monitor TV, and video images were recorded by a video tape recorder (VTR) in parallel with the observation. However, when the signal-to-noise ratio (S/N ratio) of an image was not high enough to observe images of individual dislocations, the S/N ratio was improved, if necessary, by averaging of n TV frames with the digital image processor (Image Σ, Avionics). The averaging of n TV frames improves the S/N ratio by a factor of $(2n-1)^{1/2}$. This image processing was made for both "direct-view image" and "synthesized image". As the spacial resolution of the TV imaging system was lower than the geometrical one, the images were also recorded intermittently on Ilford-L4 nuclear research plates to reveal the details of dislocation configuration or to determine the Burgers vectors of dislocations by the invisibility criterion.

2.3. FURNACES DESIGNED FOR OBSERVATIONS OF UNI-DIRECTIONAL GROWTH
      OF METALLIC CRYSTALS

For the observation of uni-directional melting and growth processes of metallic crystals by real time X-ray topography, two types of in situ heating furnaces were developed, both of which can be set on the topographic goniometer stage.

Figure 2.3 (a) and (b) show the whole view and schematic illustration of the furnace with a graphite heater. The furnace is composed of a vacuum chamber with Be windows, a graphite heater which can be moved up and down, and a graphite crucible with hot junctions of thermocouples. Any temperature up to about 1200 K can be obtained with a U-shaped graphite heater. The water-cooled furnace is either evacuated to 1×10^{-4} Torr or filled with a desired environmental gas. The depth of the vacuum chamber, i.e., the distance between the specimen and Be window located on the side of TV camera was made narrow enough to get better resolution. The graphite heater can be moved up and down by rotating a micrometer screw, which is driven by a synchronous motor through a worm gear. This enables us to grow crystals with a constant temperature gradient near the solid-liquid interface. A plate - shaped specimen of a single crystal is put in the graphite crucible and heated by the graphite heater from both sides of the crucible. Graphite is very suitable for the crucible of this furnace because it is sufficiently chemically unreactive to aluminium and its alloys below 1070 K [21] and X-ray beams are scarcely absorbed by it. The crucible consists of three graphite plates,and the two plates which contact front and back surfaces of the specimen are about 0.5 mm in thickness. The out side size of the crucible is about 50 (long) x 10 (wide) x 2 (thick) mm^3. The temperature of the specimen is measured by ceramic coated chromel-
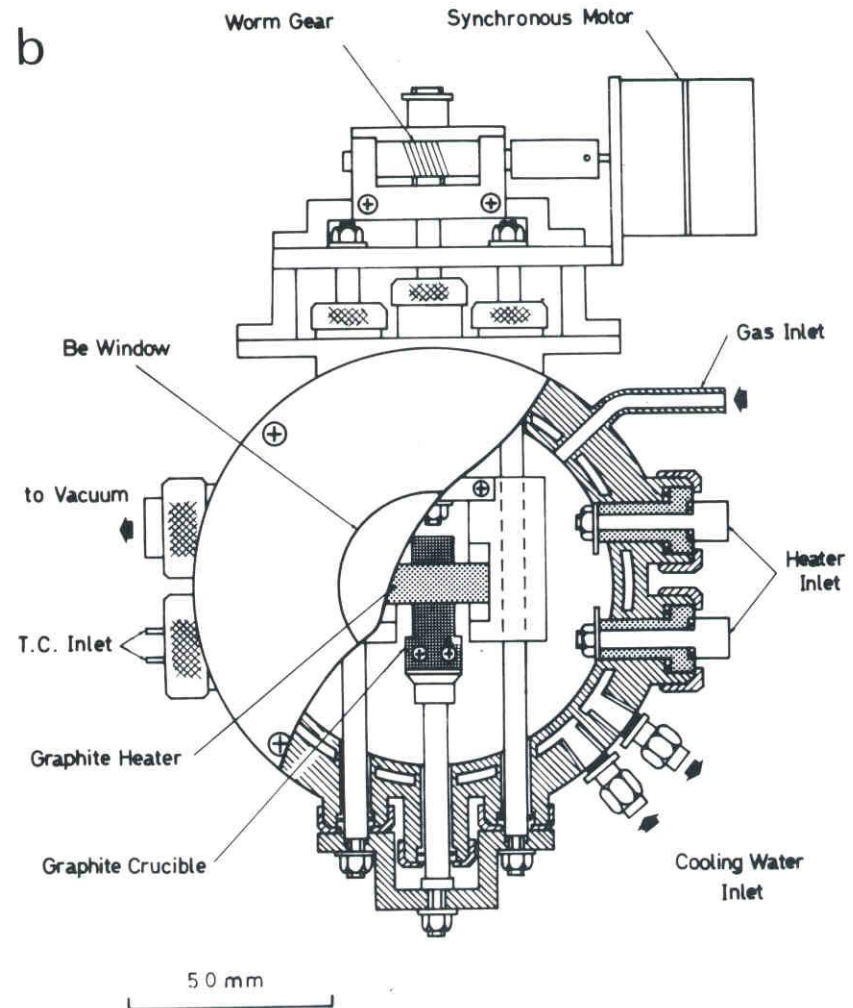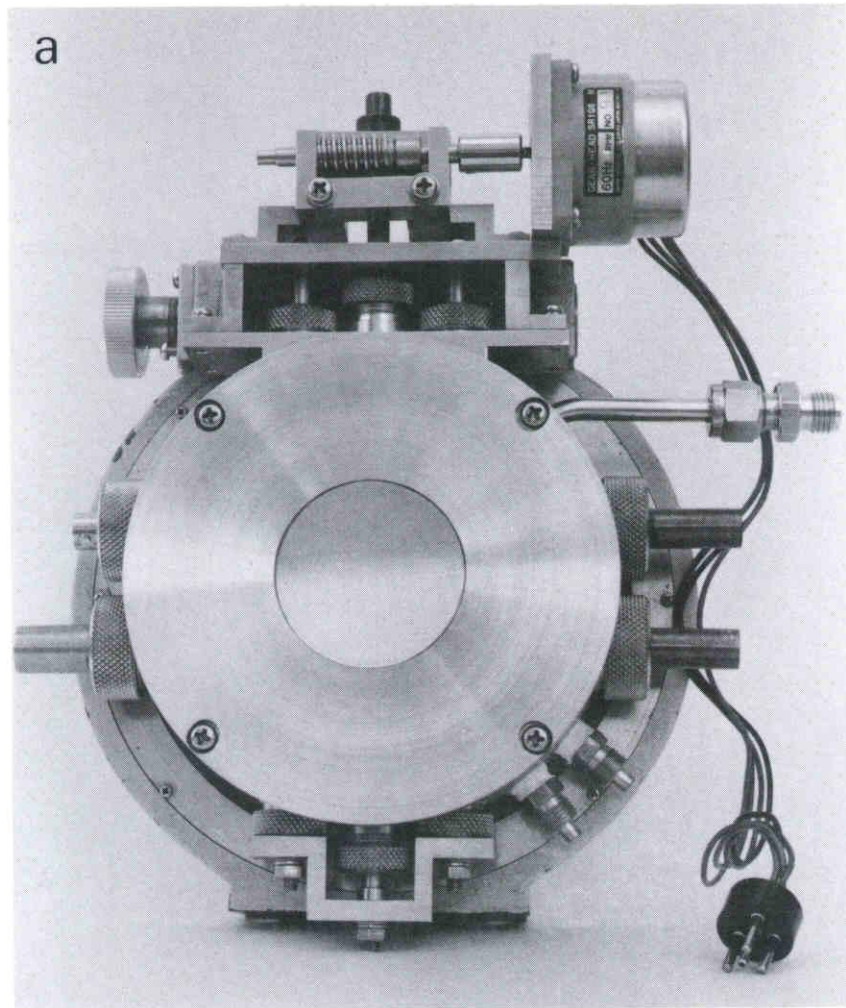
Figure 2.3 (a) A overview of the Bridgman furnace for the in situ observation of the melting and growth processes with X-ray topography. (b) A schematic illustration of the furnace.

alumel thermocouple of 0.1 mm in diameter, which contacts the specimen. The temperature gradient of the specimen is uni-directional as shown in Figure 2.4. The maximum temperature gradient of the specimen obtained is about 10 K/mm.

The furnace has two Be windows (46 mm in diameter) on either side of it. Incident and diffracted X-ray beams pass through the Be windows, the graphite heater and the graphite crucible. To examine the influence of these graphite plates on the spatial resolution, topographs of silicon crystal interposed between graphite plates (1 mm in thickness) and the crystal without graphite plates were taken by the Lang method, which are shown in Figure 2.5. As seen in Fig. 2.5, it can be concluded that graphite plates have little influence on the resolution of topographic images.

Figure 2.6 shows a schematic illustration of another type of the furnace for uni-directional solidification. In this case, the crucible which contains a specimen is heated by four metallic resistors. These heaters consist of alumina cores and Ni-Cr wires of 0.6 mm in diameter which are wound along the cores. By adjusting the current of the upper and the lower heaters, the temperature gradient of the specimen can be changed in the range of 0.7 K/mm to 1.2 K/mm. The typical temperature gradient of the specimen near the melting point (600 K - 660 K) was 1.0 K/mm, as shown in Figure 2.7. Solidification was brought about by decreasing the temperature of the heaters slightly. In this case, there should be a possibility of variation of the temperature gradient of the specimen near the solid-liquid interface, but it had little influence on the morphology of the interface or

a

Graphite
Heater

Crystal

Graphite
Crucible

b

mm

30

Specimen

Heater

20

10

10 K/mm

0

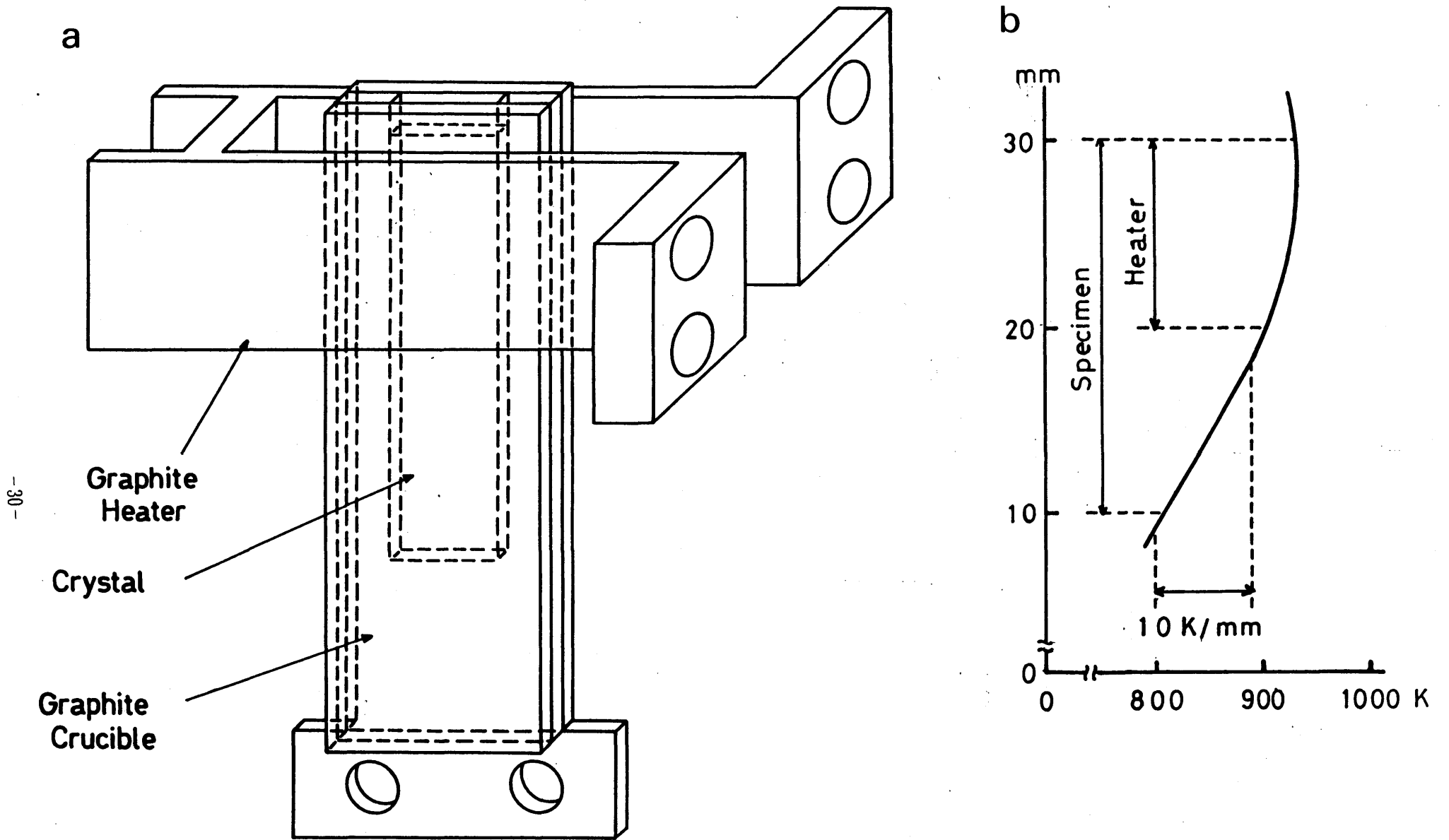0   800   900   1000 K

Figure 2.4   Schematic illustration of (a) graphite heater and graphite crucible

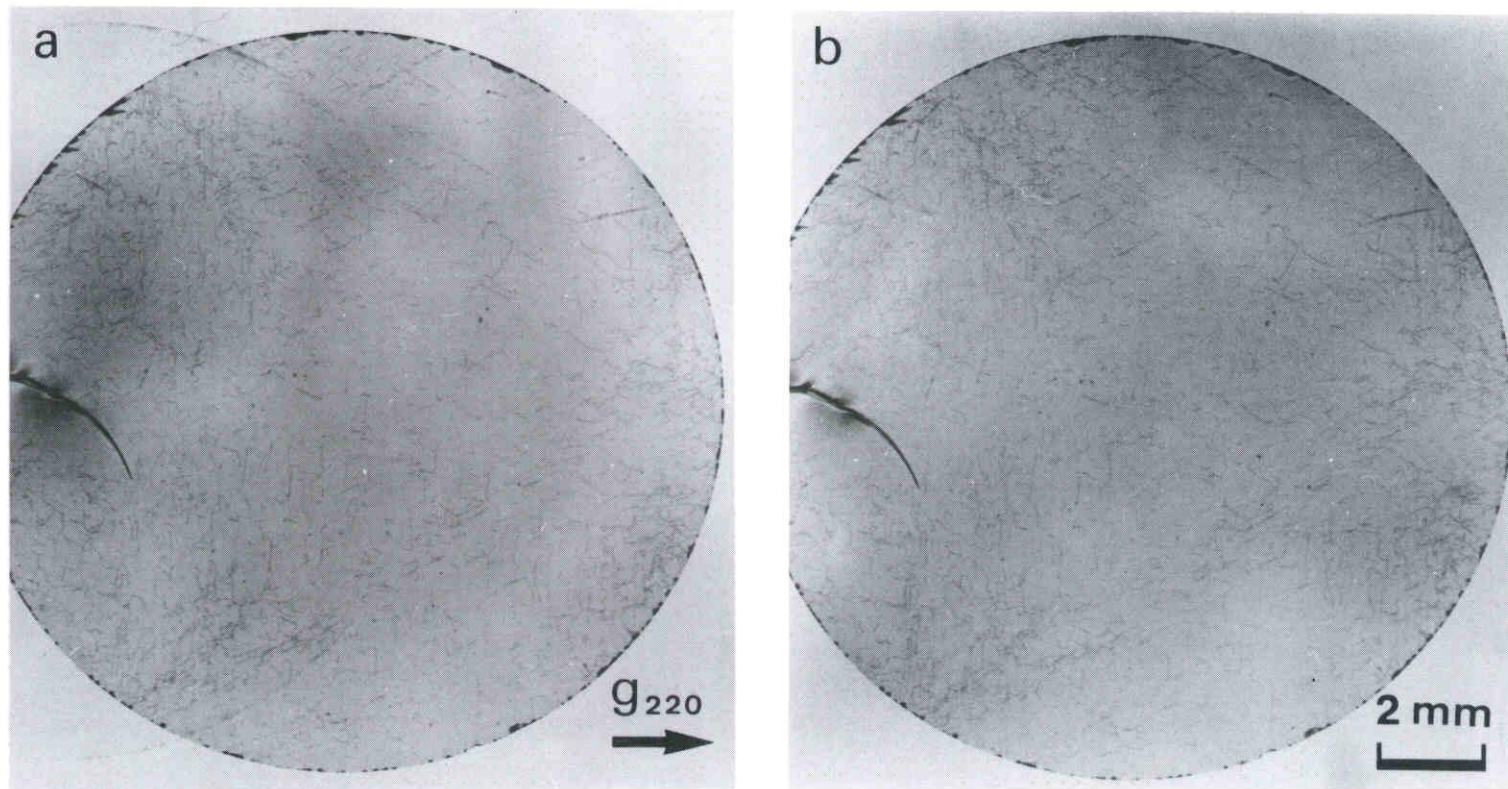and (b) the temperature gradient in the crucible.

Figure 2.5   X-ray topographs of Si crystal (a) crystal without graphite plates,
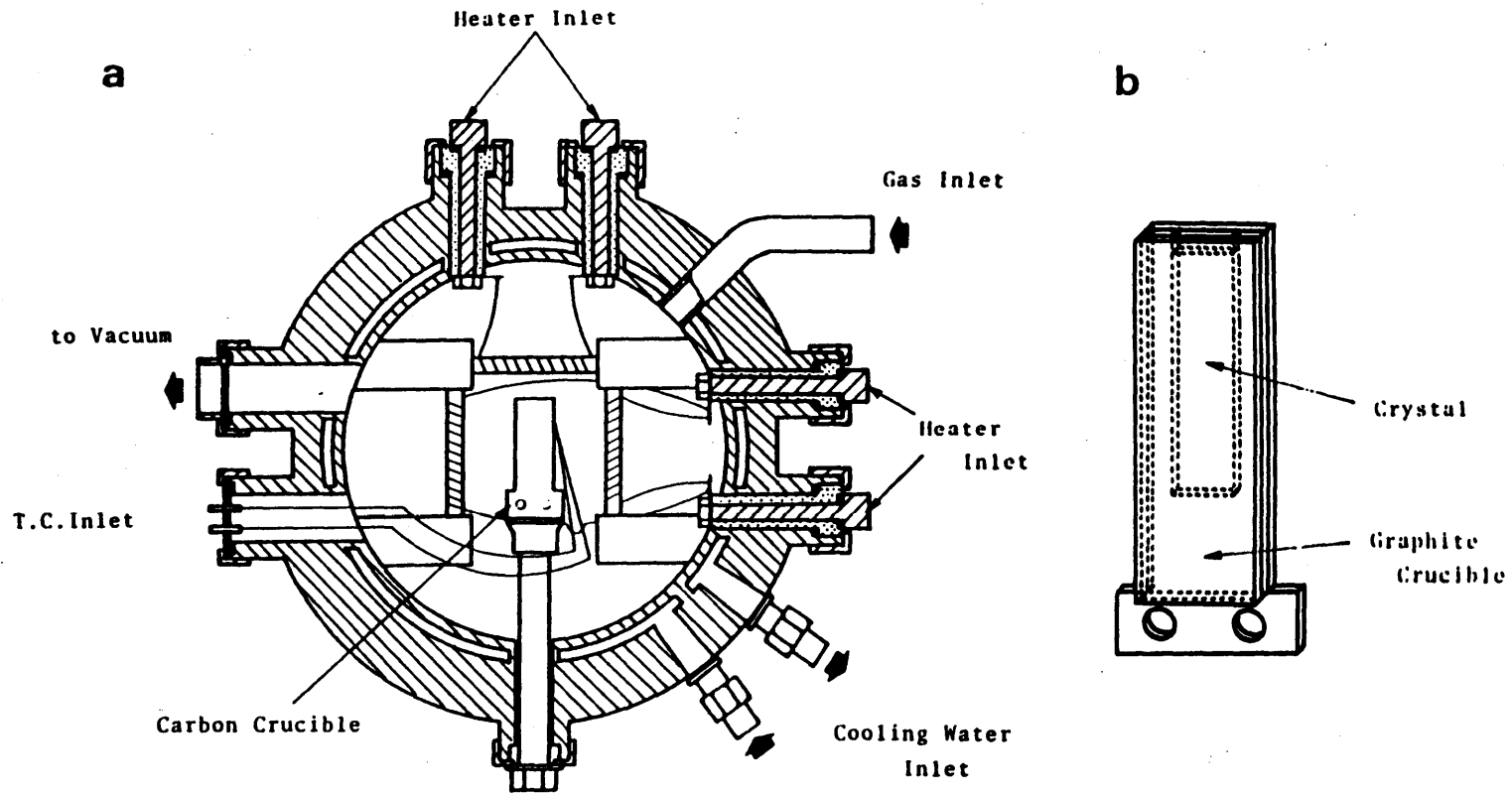(b) crystal interposed between graphite plates.

Figure 2.6 Schematic illustrations of (a) the Bridgman furnace for in situ observation with X-ray topography and (b) the grapite crucible.
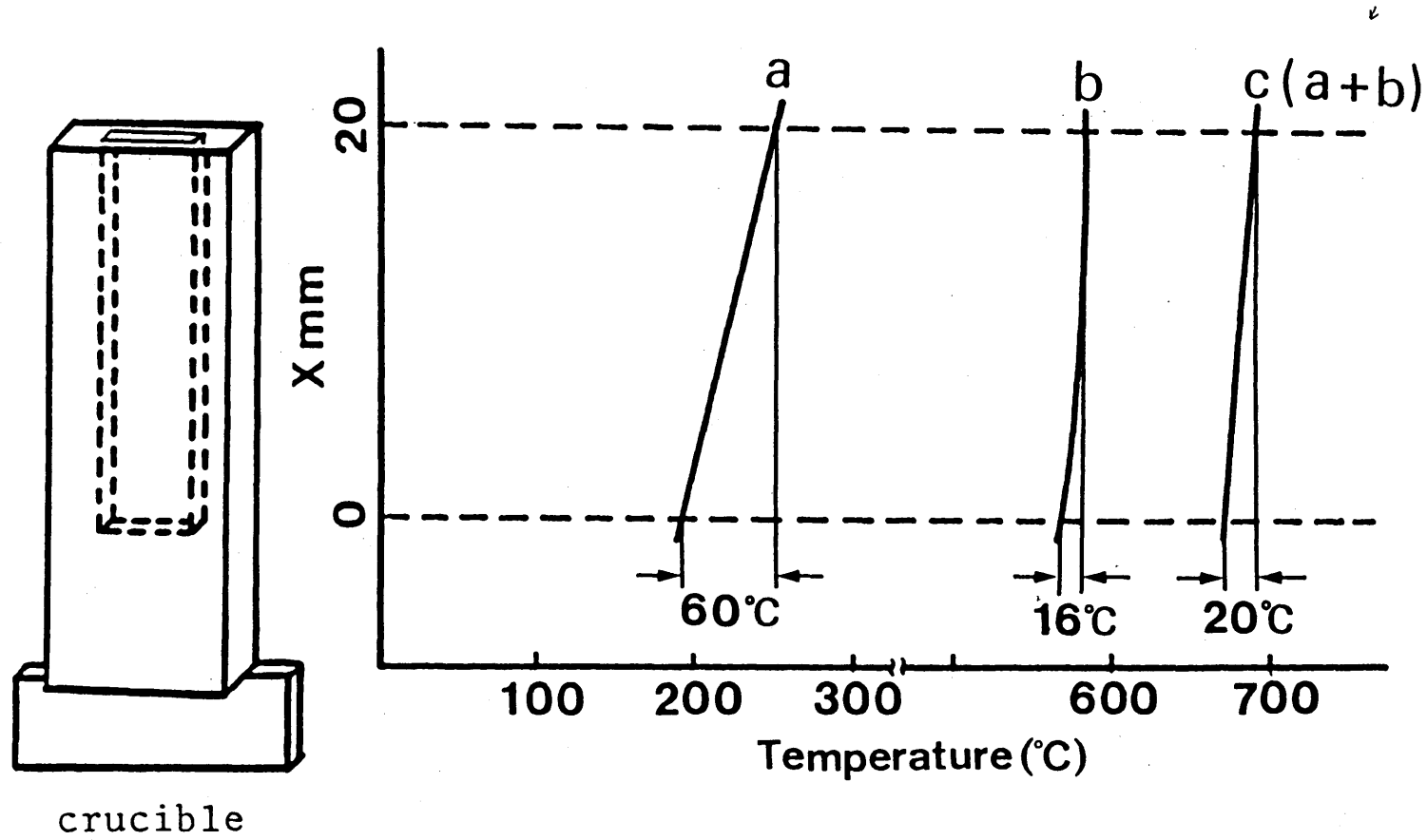
Figure 2.7 Temperature gradients of the specimen in the crucible heated by upper heater only (a), by side heaters only (b), and by the upper and the side heaters (c).

behavior of crystal defects (the variation of the temperature gradient near the interface can be estimated roughly less than 10^{-1} K/mm), as shown in the latter chapter. The crucible used for this furnace was almost the same as that for the furnace with a graphite heater (Fig. 2.4). Other conditions of the observation were the same as in the case of the aforementioned furnace.

In the observation of melting and growth processes of gallium single crystals, a graphite crucible of modified type was used, which is shown in Figure 2.8 with the geometry of the observations. A plate-shaped specimen of gallium single crystal was put in a graphite crucible, the inside of which was covered by Teflon sheets. The crucible and also the specimen were heated by upper resistance heater of the furnace shown in Fig. 2.6; this resulted in uni-directional melting and growth. The temperature gradient of the specimen was about 0.4 K/mm.

With these apparatuses, real time observations of melting and growth processes of single crystals of aluminium, gallium and Al-Mg binary alloys have been made. The specimen was melted from the upper part to the lower part unidirectionally in a pure argon gas atmosphere, and melting was stopped leaving a part of crystal unmolten (see Fig 2.9). After keeping the system in equilibrium for a while, crystal was grown upwards from the seed (un-molten part) unidirectionally. During the melting process and in the equilibrium state, the macroscopic solid-liquid interface always appeared along the iso-thermal plane corresponding to the melting point of the specimen, which was the same in spite of azimuth rotation of the crystal.
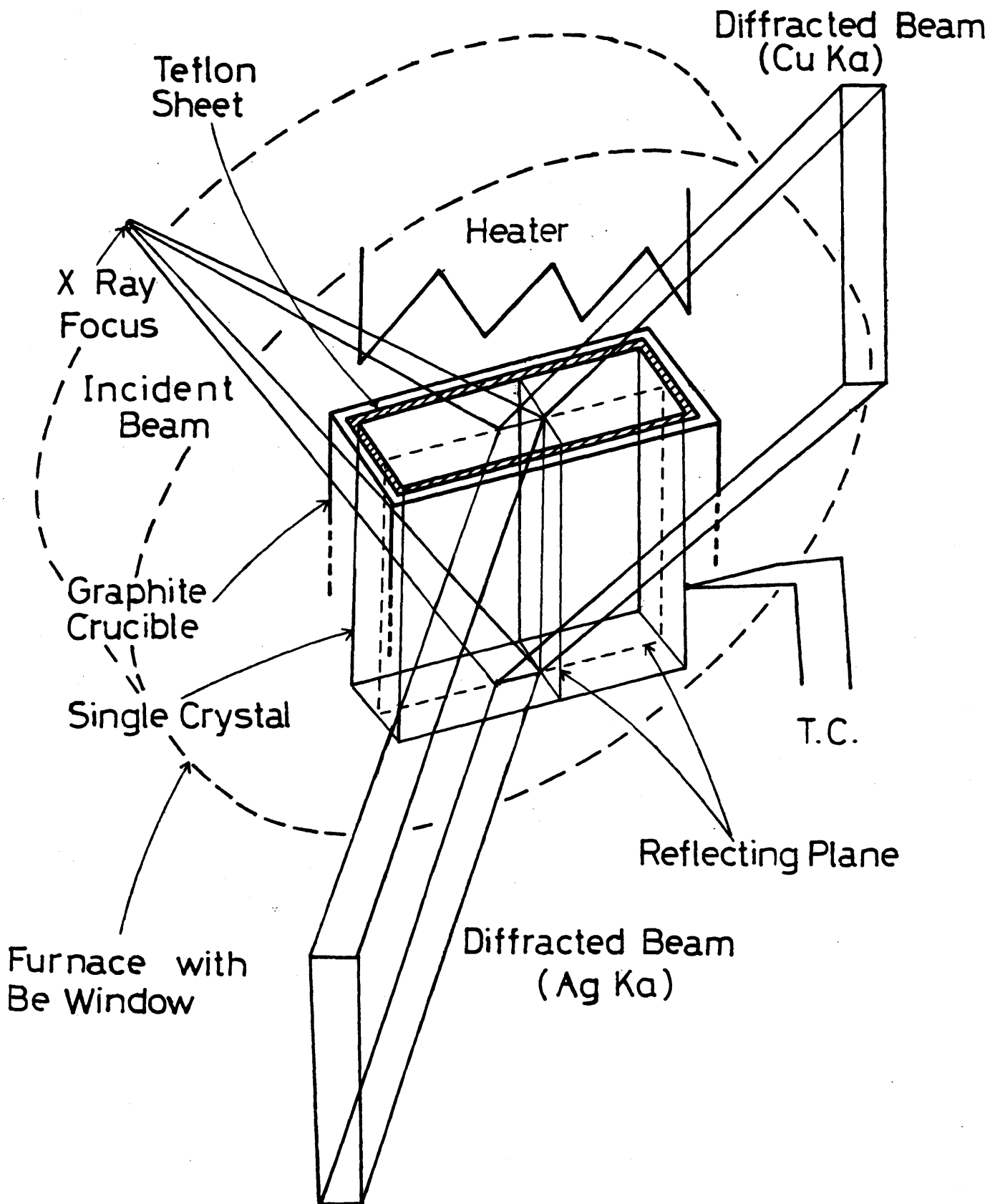
Figure 2.8 Schematic illustration of the disposition of X-ray source, Bridgman furnace and diffracted beam for in situ X-ray topographic observation of melting and growth processes of gallium.
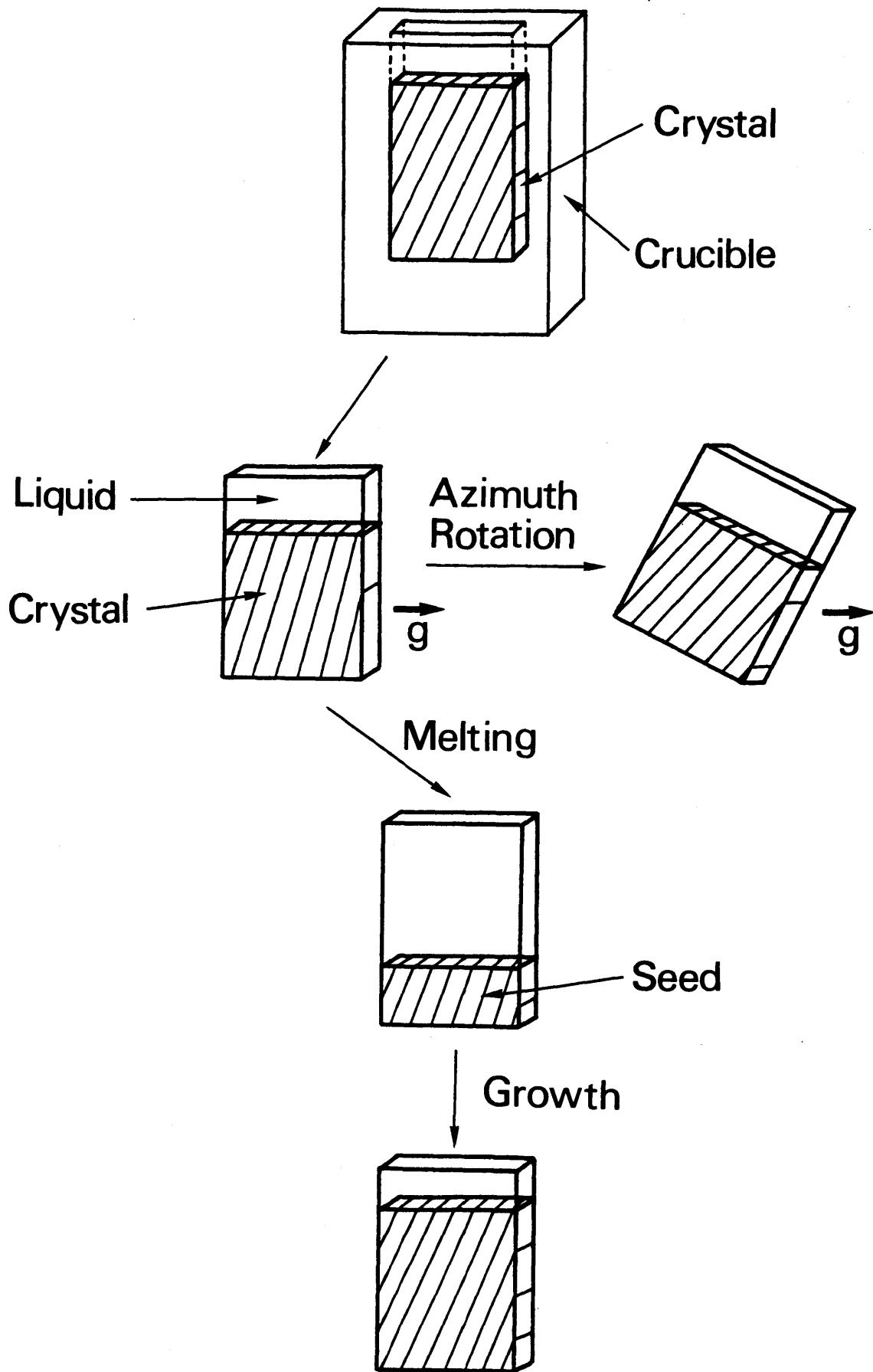
Figure 2.9   Schematic illustration of situation of the specimen in the process of the observation of melting and growth.

REFERENCES

(1)   A. R. LANG : "Modern Diffraction abd Imaging Techniques in Materials Science" S. Amelinckx, R. Gevers, G. Remaut and J. Landuyt eds. (North-Holland, Amsterdam 1970) pp.407

(2)   N. Kato and H. Yamamoto : "Reseach Roport of Ultra High X-ray Diffraction Labratory, NAGOYA UNIVERSITY" No.1 (1979) p.5

(3)   M. Ando, J. Chikawa, H. Hshizumi, K. Hayakawa, T. Imura, T. Ishikawa, S. Kishino, S. Nagakura, O. Nittono and S. Suzuki : "PHOTON FACTORY ACTIVITY REPORT" (1982/83) VI-100

(4)   J. Chikawa : J. Cryst. Growth **24/25** (1974) 61

(5)   Y. Nishino, M. Suzuki, T. Tono, H, Saka and T. Imura : Jpn. J. Appl. Phys. **20** (1981) 1553

(6)   Y. Nishino, H. Saka and T. Imura : Phys. Status Solidi (a) **70** 729

(7)   Y. Nishino and T. Imura : Jpn. J. Appl. Phys. **21** (1982) 1283

(8)   Y. Nishino and T. Imura : Phys. Status Solidi (a) **73** (1982) 173

(9)   T. Imura and Y. Nishino : J. Crystallogr. Soc. Jpn. **24** (1982) (in Japanese) in press. "Development of Deformation Appratus for In-Situ Observation by X-Ray Topography"

(10)   K. Gouhara, Y. H. Li and N. Kato : J. Phys. Soc. Jpn., **52** (1983) 3821

(11)   K. Gouhara, Y. H. Li and N. Kato : J. Phys. Soc. Jpn., **52** (1983) 3697

(12)   Gouhara and N. Kato : Photon Factory Activity Report, (1983/84), VI-63, NLHEP, KEK, (1984)

(13)   J. Chikawa and S. Shirai : J. Cryst. Growth **39** (1977) 328

(14) J. Chikawa and F. Sato : "Defects in Semiconductors" Narayan and Tan, eds. (North-Holland, Inc. 1981) pp.317

(15) J. Chikawa and F. Sato : "Defects and Radiation Effects in Semiconductors, 1980" R. R. Hasiguti ed. (The Institute of Physics, London, 1981) p.95

(16) O. Nittono, T. Ogawa, S. K. Gong and S. Nagakura : Jpn. J. Appl. Physics 8 (1984) L.581

(17) S. B. Austerman and J. B. Newkirk : Advances in X-ray Analysis 10 (1968) 134

(18) J. Chikawa : J. Cryst. Growth 24/25 (1974) 61

CHAPTER 3 MORPHOLOGY OF SOLID-LIQUID INTERFACE AND GROWTH MECHANISM OF ALUMINIUM AND GALLIUM SINGLE CRYSTLS

3.1. INTRODUCTION

Morphology of growing crystals reflects growth rate anisotropy, and growth rate anisotropy is related to growth mechanism. Therefore, growth mechanism can be inferred from the observation of the morphology of the solid-liquid interface during growth. According to Jackson [1], when the growth rate is highly anisotropic, the interface is far from isothermal; when the growth rate is not so anisotropic the interface is, to a good approximation isothermal and advances in the direction normal to the isotherms of the system. If a crystal grows by a lateral growth mechanism. the growth rate will be anisotropic, while if a continuous growth mechanism governs the growth of a crystal, the growth rate will be isotropic. Under the condition of controlled temperature gradient, the reverse suppositions can be made. The mechanism of crystal growth, therefore, can be presumed from the morphology of the interface.

Observation of dislocation effect on the morphology of the interface will also help to understand the mechanism of crystal growth. According to Jackson's two-level model [2], for example, dislocations have an effect only on the lateral growth, although nucleation of steps is not needed in this case. Furthermore, observation of the effect of dislocation to the interfacial

morphology gives us information about roughness [2] of the interface. For instance, screw dislocation effect on the faceted growth, which was observed in silicon [3],[4], is an evidence of the fact that the surface of the crystal which contacts with its melt is not rough, but smooth in the atomic scale, and is also an evidence of the fact that the nucleation for growth takes place at the intersection of the dislocation with the surface.

Jackson's parameter, α [2], clarifies our knowledge of the roughness of the solid-liquid interface, and according to the Jackson's criterion the morphological features of the interface can be predicted from the parameter, α. When α of a given face of a material is greater than 2, the interface will be atomically smooth , and sizable growth rate anisotropy is anticipated. For the case of materials with α smaller than 2, the interface should be rough, and the growth rate anisotropy should be small. These expectation can be confirmed by observation of the solid-liquid interface during growth, and conversely, the Jackson's parameter can be estimated from real time observation of solid-liquid interface during growth.

It should be emphasized that in order to infer the growth mechanism the roughness of the interface must be estimated during the growth process and not during melting or in the equilibrium state. The morphologies of the interface during the melting process or in the equilibrium state have nothing to do with the growth mechanism, and are controlled by the temperature gradient or by anisotropy of surface free energy.

The kinetics of crystal growth are concerned with the relation between growth rate and driving force necessary for

growth. In the case of growth from the melt, the parameter which determines this driving force is the undercooling of the melt in the region of the interface. Measurement of interface kinetics is a most appropriate method to clarify the growth mechanism. However, a direct measurement of the interface temperature is extremely difficult for two reasons: (1) a measuring probe placed at the interface may disturb the system and (2) it is necessary to measure the temperature with high accuracy. In addition, the measurement of the growth rate must be made on each face when several faces of different crystallographic directions appear simultaneously at the interface. It is difficult to do this by the optical method on crystals such as metals which are opaque to visual light.

The purpose of this chapter is to investigate the mechanism of crystal growth from the melt on aluminium and gallium. From the observations of interfacial morphology during melting and growth process, roughness of the interface and growth mechanisms were inferred.

Growth mechanism was investigated also through the ovservation of dislocation effect on the faceted growth. To investigate the dislocation effect on the faceted growth, the growth conditions which are controlled by the presence or absence of dislocations must be set up. Gallium is favorable for such control and for the study of growth kinetics. It is readily available at a very high purity, and when very pure, dislocation-free crystals can be grown with relative ease. Jackson's parameter for gallium is greater than 2 on (010) face and less than 2 on other faces [5]. According to Jackson's theory [1], some habit planes (facets) are expected to appear on (010) and not expected

to appear on other habit planes in gallium crystals during the growth from the melt. Jackson's parameter α of aluminium and gallium is shown in Table 3.1.

Table 3.1 Jackson's parameter α of aluminium and gallium crystals [5].

	habit plane	Jackson's parameter
aluminium	all	α = 1.3
gallium	(010)	α = 2.24
	the others	α = 1.12

The measurement of the relation between growth rate and supercooling has been attempted on aluminium with real time X-ray topography.

3.2. EXPERIMENTAL PROCEDURES

Single crystals of aluminium and gallium with low dislocation

density were prepared by the strain-anneal [6] method and the Bridgman method, respectively.

Aluminium single crystal plates were prepared with the procedure illustrated in Fig.3.1. Hot rolled sheets of aluminium of 99.998 % and 99.999 % (zone refined) in purity and of a size about 200 x 20 x 3 mm^3 were annealed at about 610 K, followed by cold-rolling for producing sheets of 1 mm in thickness (the composition of the crystals are shown in Table 3.2). These sheets were again annealed, etched chemically with a solution (aqua-regia + HF acid) and then strained by tension.

Table 3.2   Composition of aluminium single crystals

	Cu %	Fe %	Si %	Zn
99.998 % Al	0.0004	0.0009	0.0003	tr.
99.999 % Al	0.00008	0.0010	0.0000..	tr.

Strains ranging from 1 to 4 % were introduced : the most appropriate strains were found to be 2 % and 3 % for aluminium of 99.998 % and 99.999 % , respectively. The second anneal was then made to these two groups of lightly strained specimens at 928 K (maximum temperature) in a travelling furnace, at the travelling rate of 10 mm/hr and 20 mm/hr respectively. The crystallographic

cold roll

anneal

tension

anneal

Al Single Crystal
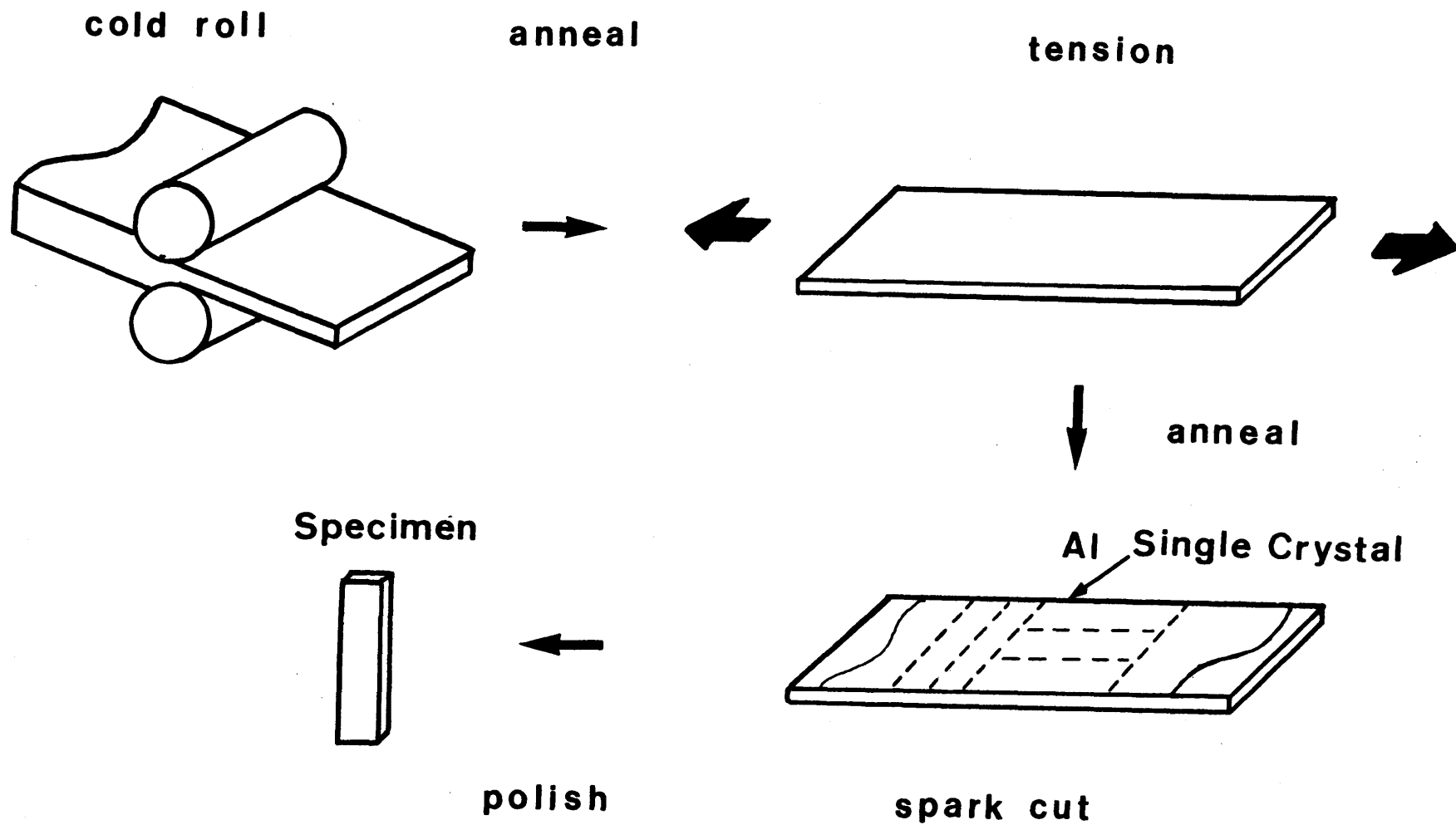
Specimen

polish

spark cut

Figure 3.1 Procedure of preparation of aluminium single crystals by strain-anneal method.

orientations of the crystals were determined by the X-ray method. These single crystals were spark-cut into smaller specimens of about 30 x 5 mm^2, and annealed at about 900 K. A final electropolish was given to all specimens in a solution of 1 part HClO$_4$ and 4 parts CH$_3$COOH (by volume). The specimen thus obtained had a length of about 30 mm, a width of about 4 mm and a thickness of 0.7-0.8 mm.

Table 3.3   Composition of gallium crystal specimens measured by mass spectrographic analysis

Mg ppm	Al ppm	Si ppm	Ca ppm
0.03	0.3	0.03	0.04

Specimens of gallium single crystal used were prepared from nearly dislocation-free single crystals grown by the Bridgman method. Procedure for preparation of specimens for the X-ray topographic observation is schematically illustrated in Figure 3.2. The material used was gallium of 99.9999 % in purity and its composition is shown in table 3.3. Crucible of vinyl resin. which contained such high-purity gallium of 15 mm in diameter, was put into a glass container filled with water which was kept at about 305 K. After the gallium bar had been completely melted, the glass

Ga

Ga Single Crystal

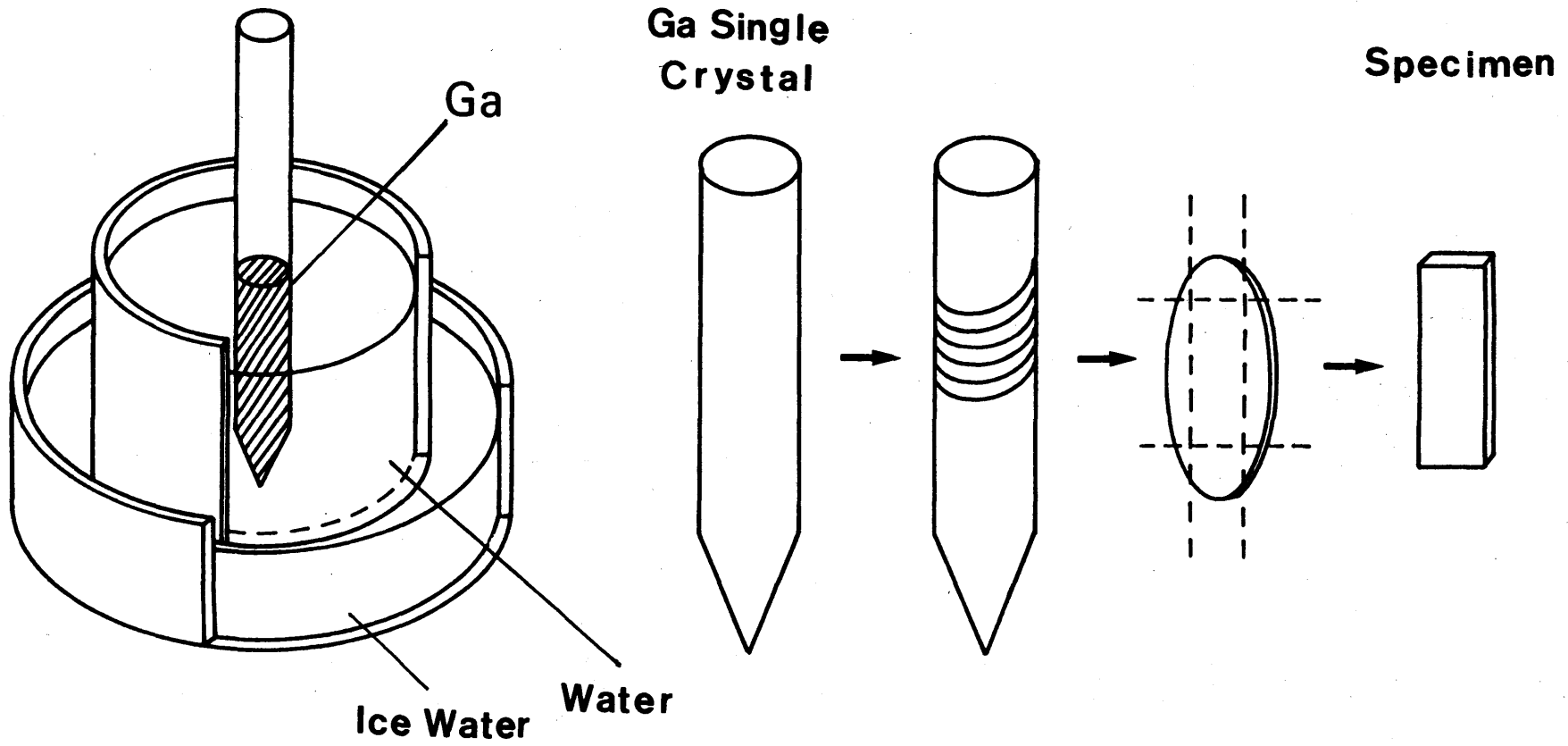Specimen

Ice Water   Water

Figure 3.2   Procedure of preparation of gallium single crystals by Bridgman method.

container was gradually cooled down below the melting point of gallium (302.8 K). Because the temperature of the water in the container was lower in the lower part than that in the upper part, gallium single crystal of 15 mm in diameter and about 40 mm in length was grown upward in such a container. In spite of this simple method, nearly dislocation-free (dislocation free except for region near the surfaces) single crystals of high-purity gallium were grown with relative ease. These crystals were cut into slices of about 0.25 mm thick for transmission X-ray topography and 0.85 mm thick for reflection X-ray topography with the aid of a multi-wire saw. Finally, each slice was cut into a size of about 20 x 4 mm^2. Each specimen was mechanically polished with emery papers followed by electropolishing using a solution of 1 part $HClO_4$ and 4 parts CH_3OH (by volume). The final thickness of the specimens was 0.1 mm for transmission topography and 0.6 mm for reflection topography.

To measure the relation between growth rate and supercooling, aluminium single crystals of 99.999 % in purity and the size of 25 mm in diameter and 60 mm in length were grown by the Bridgman method. The single crystal was cut parallel to (112) surface into slices of about 0.85 mm thick with the aid of a multi-wire saw. Each slice was cut into a size of about 35 x 5 mm^2. Each specimen was chemically and electrolytically polished and the final thickness of about 0.7 μm was obtained.

The measurement of supercooling was made using chromel-alumel thermocouples of 0.1 mm in diameter, the surface of which was ceramic coated and which was placed in contact with the specimen. Two-types of crucibles, indicated schematically in Figure 3.3, were used. The crucible shown in Fig. 3.3 (a) was used for the
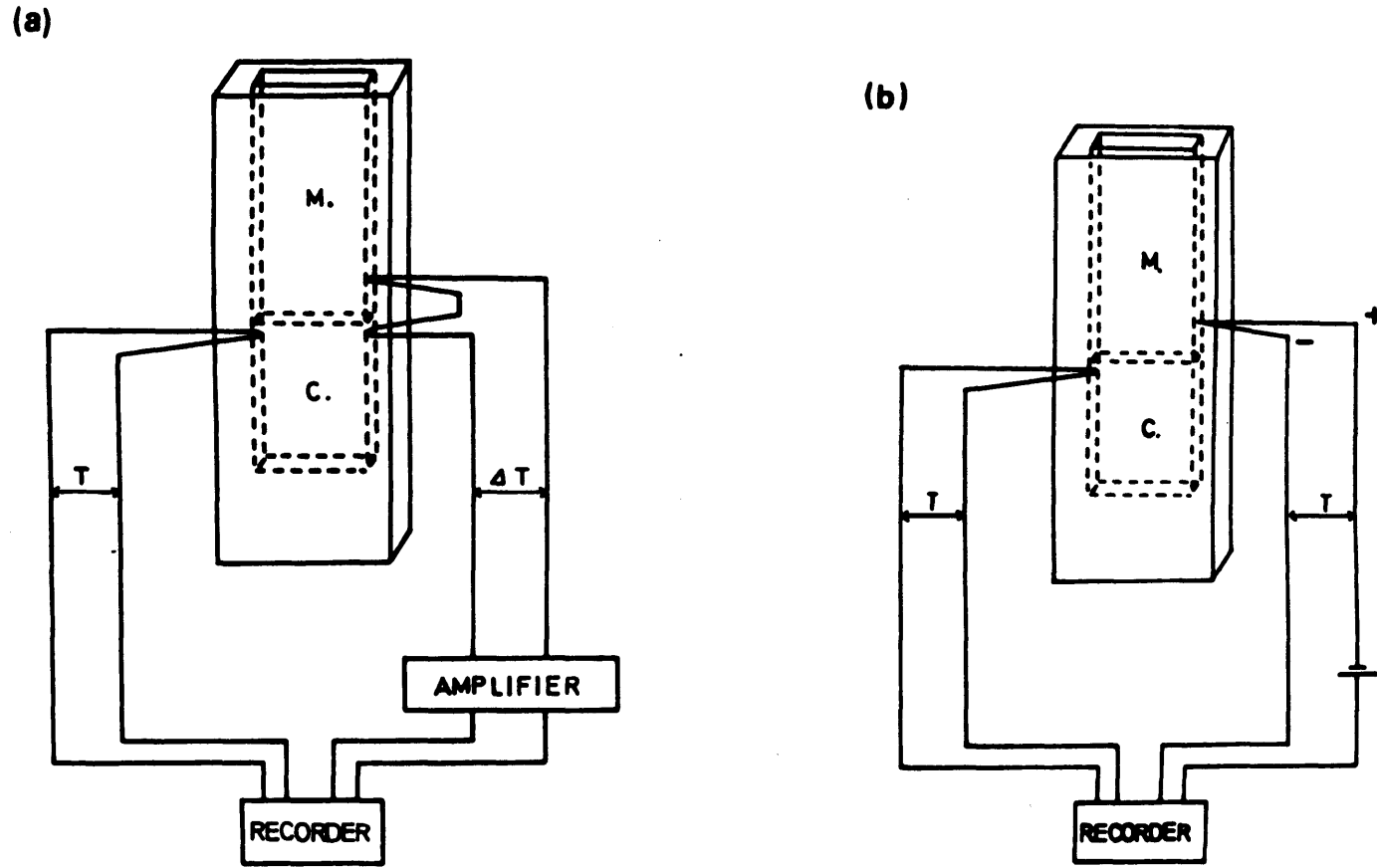
(a)

(b)

Figure 3.3 Schematic diagrams of the crucible and T. C. used for the measurement of supercooling (a) and for the measurement of cooling rate.

measurment of supercooling. In this crucible, two sets of thermocouples were connected in such a way as was indicated in Fig. 3.3(a) in order to measure the difference between the temperature of the crystal and that of the melt near the interface. The distance between the two hot junctions of those thermocouples was about 1 mm. The thermo-electromotive force was amplified and then recorded on a recorder. Fig. 3.3 (b) shows the crucible used for the measurement of cooling rate. A slight change of the temperature in the specimen can be detected.

The growth rate was measured from the photographs of images on the TV monitor.

Measurements for the kinetic study were made on crystal growth in [100], [110] and [111] directions.

3.3 EXPERIMENTAL RESULTS

3.3.1   Observations of Solid-Liquid Interface during Melting

Melting process of aluminium single crystals

Fig.3.4 is a series of transmission X-ray topographs showing the uni-directional melting process of aluminium (99.99 % in purity) with the use of the furnace shown in Fig. 2.3. All the photographs are TV images shown with negative contrast through an imaging processor and therefore, crystal defects such as dislocations show up as black images. The temperature gradient of the specimen at the temperature near the melting point was about 10 K/mm. Fig. 3.4 (a) was obtained at room temperature. The broad images observed at the lower part are subgrain boundaries. Fig. 3.4 (b) shows the state just before the melting began. A number of dislocations were generated by thermal stresses in a range 670 to 930 K during temperature increase up to the melting point.

Fig. 3.4 (c)-(e) are the images taken during the melting process. When the melting began from the upper part of the specimen to the lower part uni-directionally, a macroscopically straight interface was observed along the isothermal plane of the specimen, and no fringe was observed due to thickness variation. This indicates that the temperature gradient in the specimen was almost completely uni-directional. The surface of the crystal in contact with its melt was indicated by bold arrows. In Fig. 3.4 (c)-(e), the upper region, which was the molten part, shows no contrast because the Bragg condition is never satisfied for the melt. It can be seen that the region of the crystal near the interface shows no anomalous image before the melting, and perfection of the region was almost the same as that before the melting. These observations also showed that most of the dislocations were not mobile until they come into contact with the interface during melting. The mean melting rate was estimeted to be about 12 μm/s from the topographs.
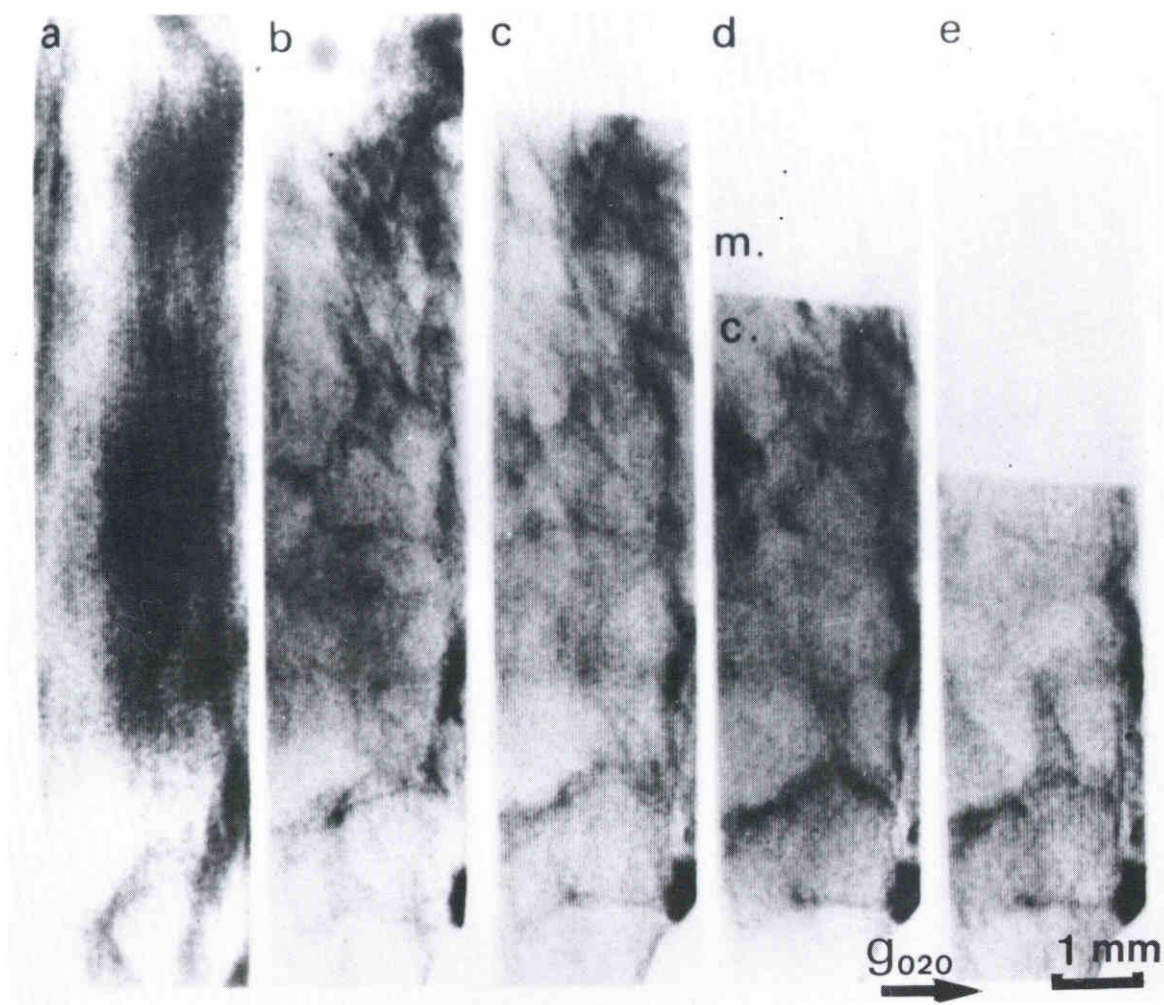
Figure 3.4 A series of X-ray topographs (TV images) of aluminium single crystal (99.99 %) prepared by strain anneal method: (a) at room temperature, (b) just before the melting and (c) - (e) during melting process. Temperature gradient of the crystal was 10 K/mm near the melting point, and the mean melting rate was about 12 um/s.

Figure 3.5 shows another series of topographs of TV images taken during the melting process of aluminium single crystal (99.99 % in purity) under condition of small temperature gradient (1.0 K/mm) with the use of the furnace shown in Fig. 2.5. The solid-liquid interface, which is indicated by bold arrows, appeared along isotherms of the crystal. Black lines caused by bundles of many dislocations are seen in the crystal and they intersect almost perpendicularly with the interface. Similar to the result shown in Fig. 3.4. no contrast change was observed along the interface and the dislocation bundles did not move until they came into contact with the interface.

Another observation of the melting process of aluminium (99.99 % in purity) was made during melting along the horizontal direction in which the temperature gradient was 1.0 K/mm. Fig. 3.6 (a) and (b) are transmission topographs taken during the melting process and (c) is that taken in equilibrium state. The broad black lines which contact with the interface obliquely are subgrain boundaries. As mentioned above, macroscopical solid-liquid interface was observed along the iso-thermal plane throughout the observation.

Melting process of gallium single crystal

Figure 3.7 is a series of reflection topographs of TV images taken during the melting process of gallium single crystal. The direction of the temperature gradient was normal to the solid-liquid interface indicated by bold white arrows. Fig. 3.7 (a) and (b) are images during melting and Fig. 3.7 (c) is that in
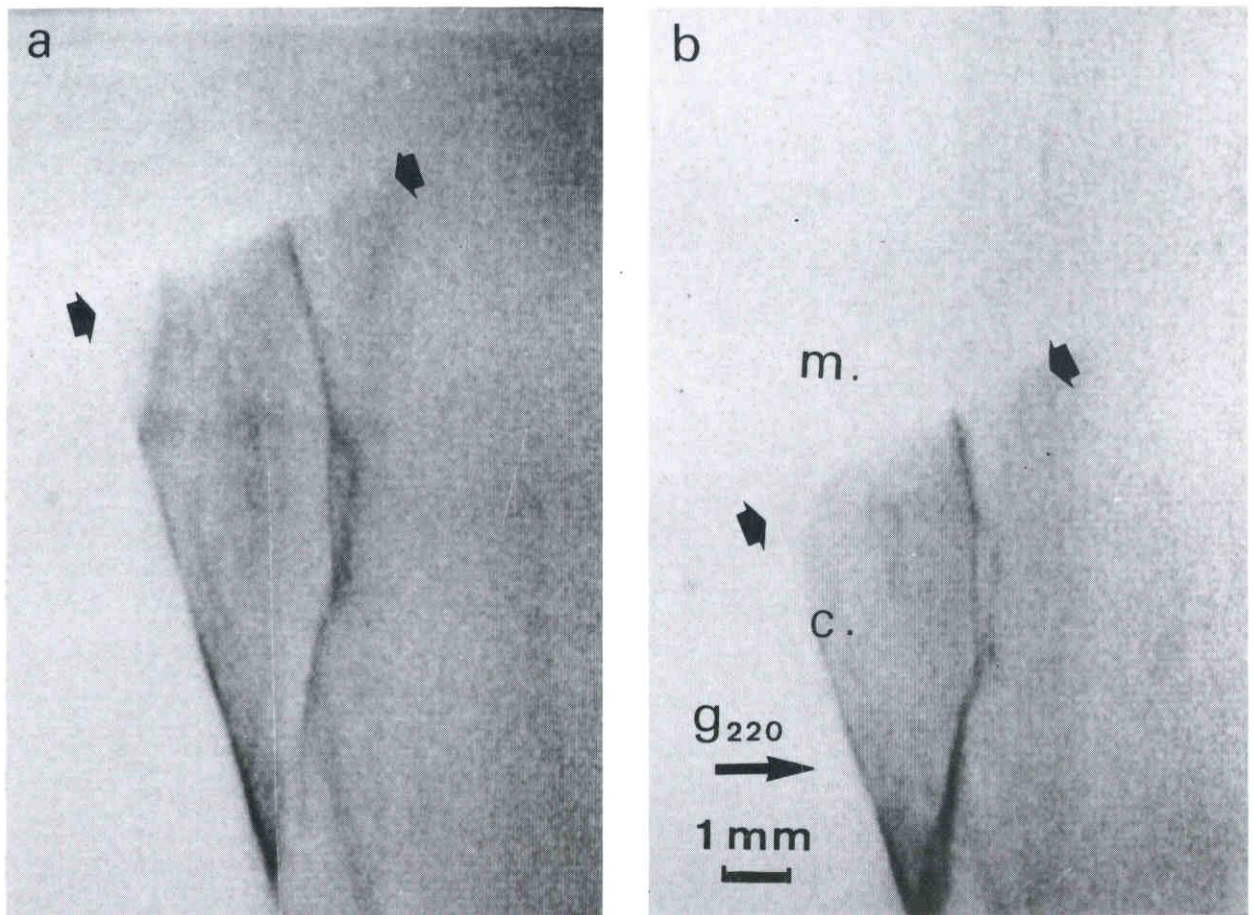
Figure 3.5 X-ray topographs of aluminium single crystal (99.99%) during melting process. The temperature gradient of the crystal was 1.0 K/mm.
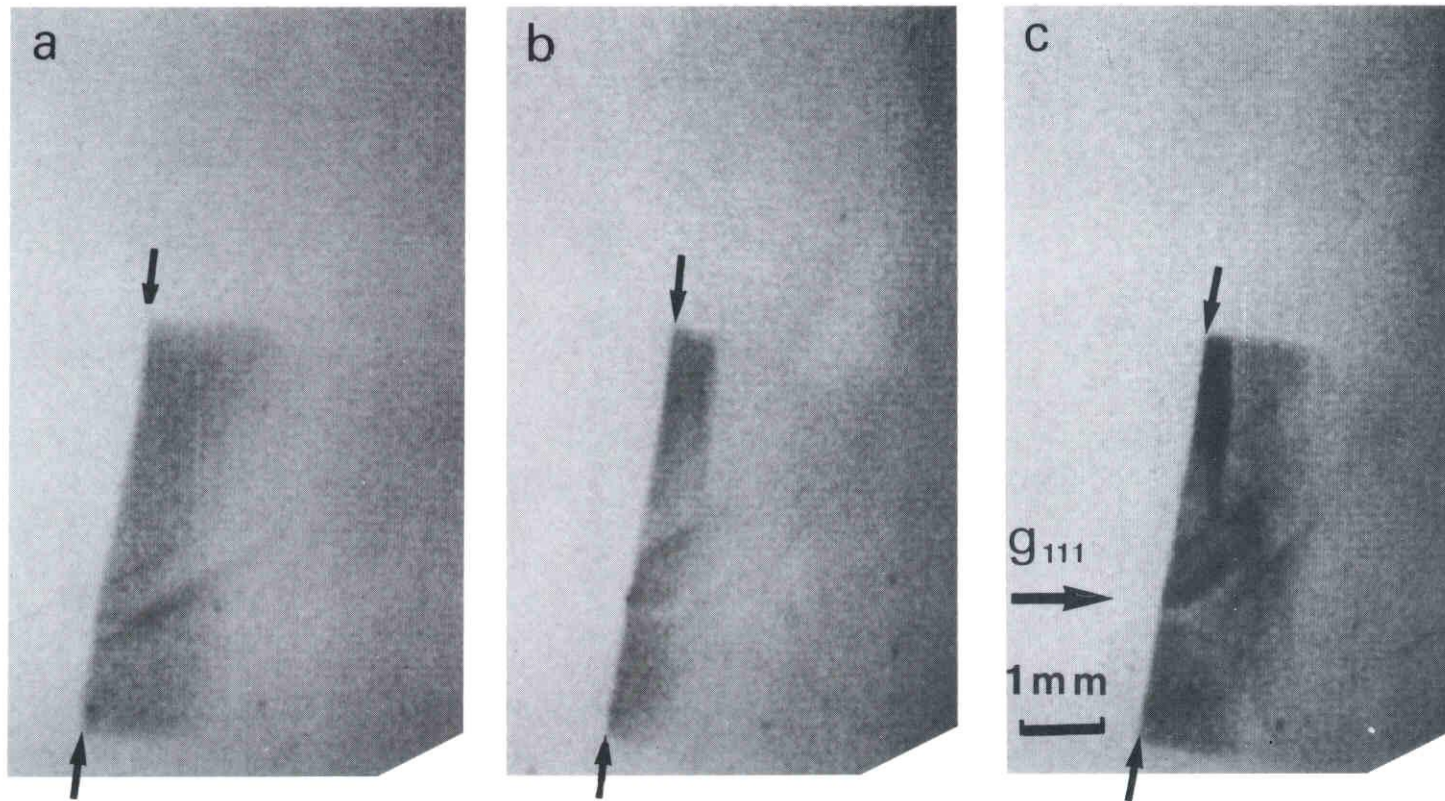
Figure 3.6   A series of X-ray topographs of aluminium (99.99%) during
horizontal melting along the direction normal to iso-thermal plane
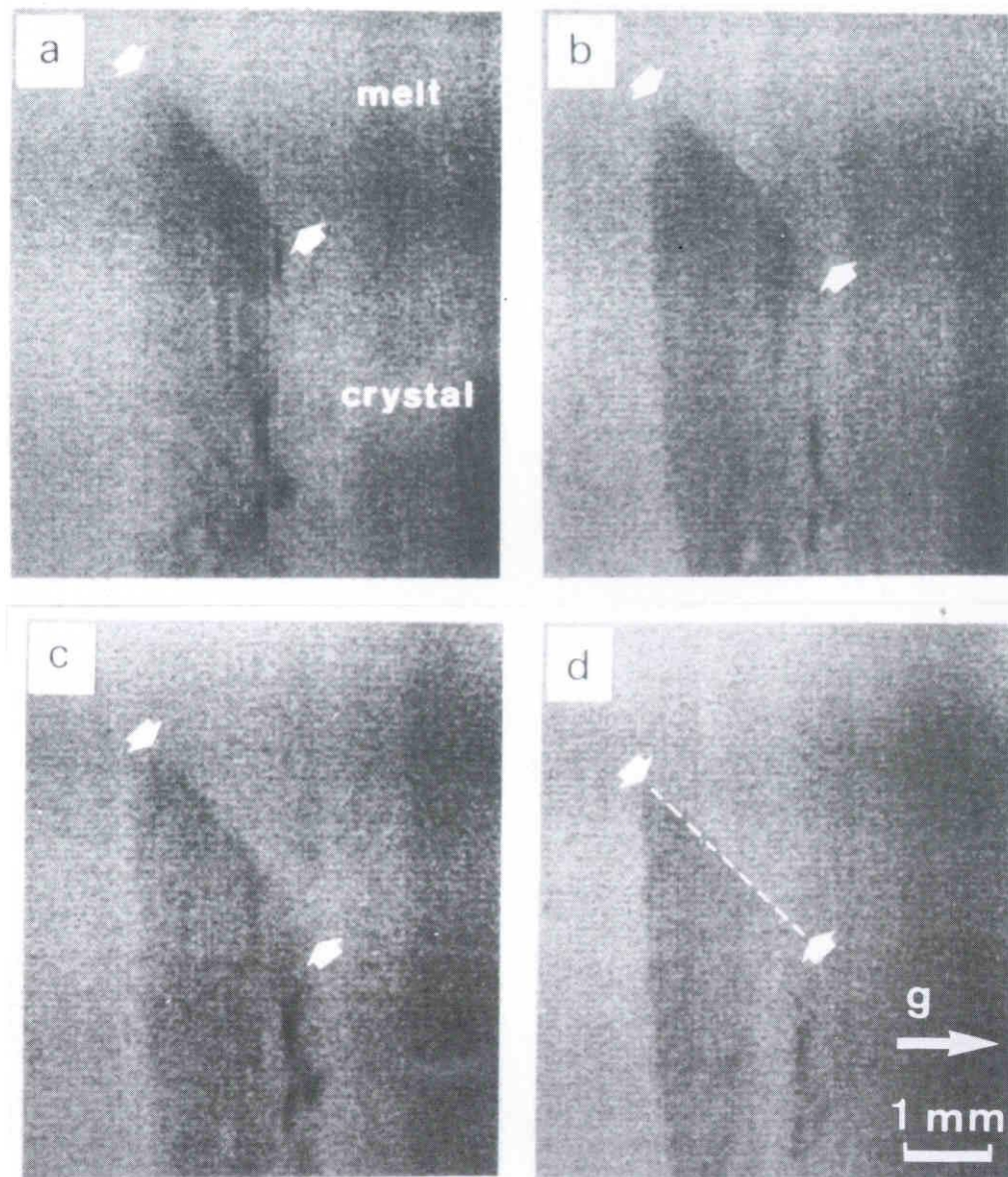(↑). Temperature gradient of the crystal was 1.0 K/mm.

Figure   3.7   A series   of   reflection topographs   of
        TV image during the melting process of gallium
        single crystal.   Temperature gradient of the
        crystal was about 0.4 K/mm.   The Solid-liquid
        interface is indicated by arrows and a broken
        line.

equilibrium state. The temperature gradient of the crystal was about 0.4 K/mm. The broad images observed on the right-hand side of the specimen were dislocations introduced during the preparation of the specimen. Neither an equal-thickness fringe nor any intensity enhancement was observed in the vicinity of the interface during the melting or in equillibrium state. These accord well with the results on aluminium.

3.3.2. Observations of Solid-Liquid Interface during Growth

Growth process of aluminium single crystals

Figure 3.8 is a series of topographs of the same crystal shown in Fig. 3.4 taken during the continued growth process by lowering the heater temperature. The mean growth rate was about 20 μm/s in Fig. 3.8 (a) to (c). The solid-liquid interface (indicated by bold arrows) is macroscopically flat and extends along the isotherms of the crystal. Contrast change, which was observed in Si [7], is not observed in the melt near the interface. The boundary between the seed crystal (unmolten part of the crystal) and the newly grown crystal is indicated by a broken line. A comparison between Fig. 3.4 and Fig. 3.8 shows that the perfection of the crystal just after the solidification in Fig. 3.8 is better than that in the unmolten region in Fig 3.4. Dislocation bundles, which were inherited from the seed (indicated by the arrow with dg.) intersect with the interface and disappeared out of the
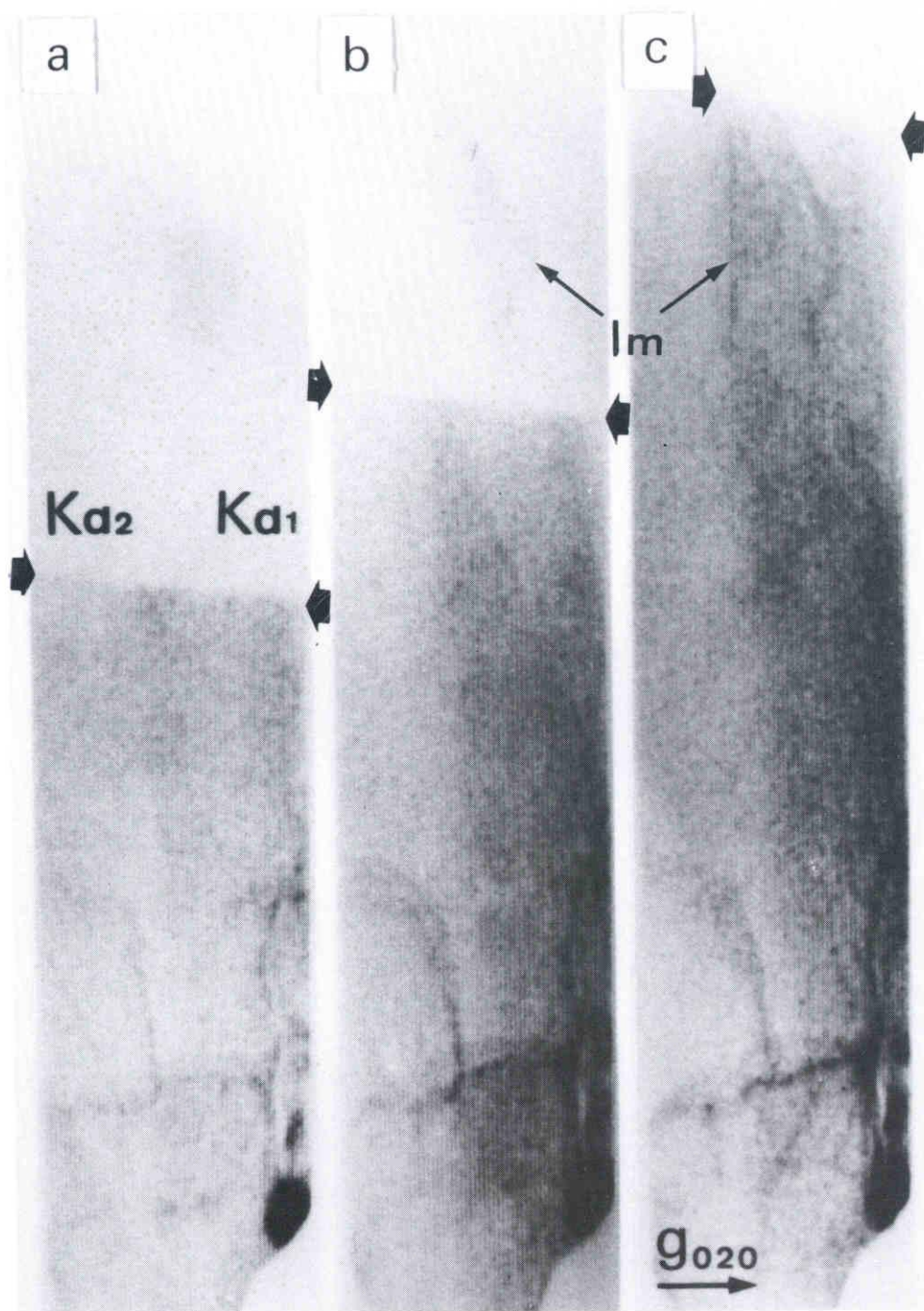
Figure 3.8   A series of X-ray topographys of aluminium during subsequent growth of the crystal shown in Fig. 3.4.   Mean growth rate was 20 um/s in (a) to (c).   Solid-liquid interface is indicated by bold arrows.   The arrows with Im indicate images of mica used for thermal shield.

crystal early in the growth.

Figure 3.9 shows the process of growth in the horizontal direction with a vertical iso-thermal plane, continued from the equilibrium state shown in Fig. 3.6 (c). The reflecting plane was nearly parallel to the solid-liquid interface. No contrast change along the interface was observed in this case, either. The broad images observed in the crystal are subgrain boundaries inherited from the unmolten part of the crystal. The growth rate was about 19 μm/s.

Figure 3.10 illustrates another series of transmission X-ray topographs during the growth process of another aluminium single crystal of 99.999 % in purity. The growth rate of Fig. 3.10 (a)-(c) was about 20 μm/s and that of Fig. 3.10 (d)-(f) was about 45 μm/s. It is obvious that the perfection is better for slowly grown crystal than for that rapidly grown.

The observation of other crystals during growth showed that when a crystal grows at a rate greater than a certain rate (about 30 μm/s in the present case) many dislocations are suddenly generated into the newly grown region of a crystal. No contrast change along the solid-liquid interface is observed in this high purity crystal, either.

Growth process of gallium single crystals

Many types of facet plane which were inclined to the iso-thermal plane in the liquid were observed during uni-directional solidification of gallium single crystals.

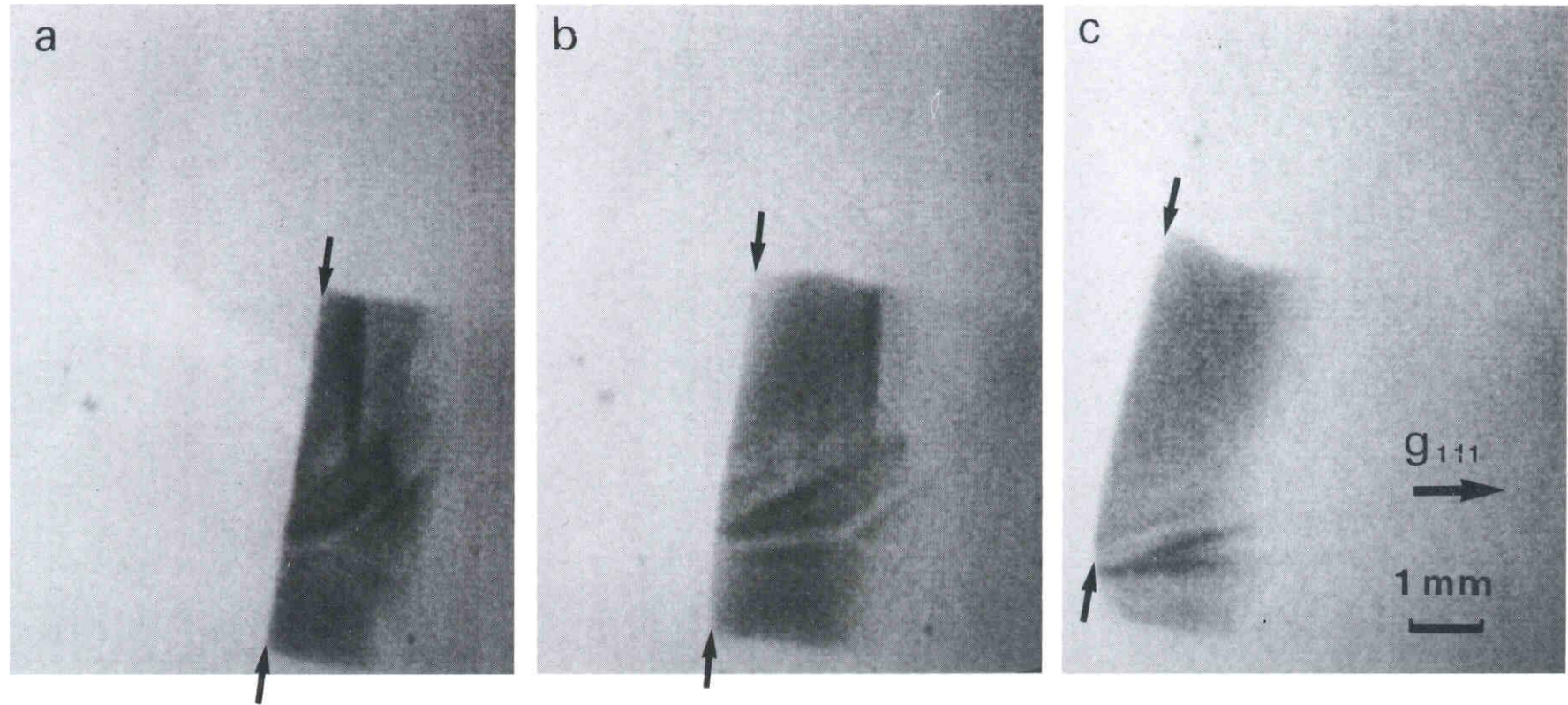A typical example of such faceted growth is shown in Figures

Figure 3.9 A series of X-ray topographs of aluminium obtained in the growth process subsequent to Fig.3.6. The growth rate was about 19 um/s.

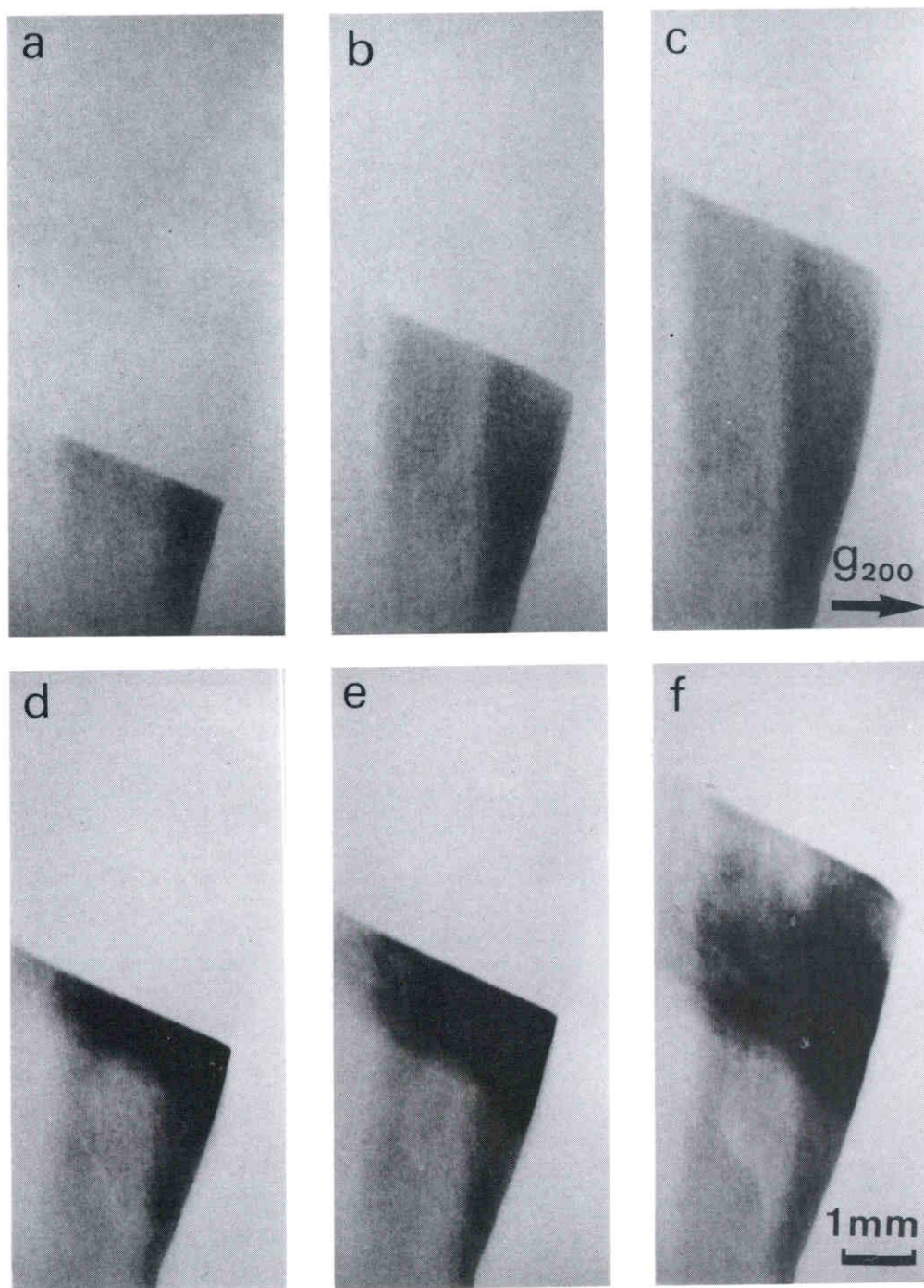Figure 3.10 A series of X-ray topographs of aluminium (99.999%) during growth process. The growth rate of (a) - (c) was about 20 μm/s and that of (d) - (f) was about 45 μm/s.

3.11 with TV image of the transmission topographs. In this case, two crystallographically equivalent (011) facets appeared and competed with each other. Each facet inclines to the iso-thermal plane to gain the required supercooling for faceted growth, and the nucleation for growth takes place at the corner of right- and left-sides for the (0$\bar{1}$1) and (011) facet respectvely. In Figure 3.11 (a), many black lines due to bundles of dislocations are visible and some of them are left behind the facet although two bundles of dislocations intersect with the right (0$\bar{1}$1) facets. By examining their image contrast with various reflections after growth, it is found that they have no common Burgers vector. But this facet does not shrink by the intersection of the dislocation bundles. Moreover, these bundles are also left behind and the newly grown region of the crystal seems to be dislocation-free, as seen in Fig. 3.11 (c) and (d). In this case, the dislocation bundles which intersected almost perpendicular with the interface did neither propagate into newly grown crystal nor influence the faceted growth.

In another case, dislocation bundles, which propagated into newly grown crystal and intersected with the interface, were observed, as shown in Figure 3.12. Fig. 3.12 is a series of TV images taken during the growth process by reflection topography. Fig. 3.12 (a) is the state of the seed crystal just before the growth starts. The macroscopic interface appears along the iso-thermal plane, and a broad black line which is the image due to a bundle of many dislocations is visible. As the crystal grew (cf. Fig. 3.12(b)), ($\bar{1}$10) and (010) facets appeared, and the dislocation bundle propagated into newly grown crystal. If nucleation occurred at the intersection of the bundle, ($\bar{1}$10)
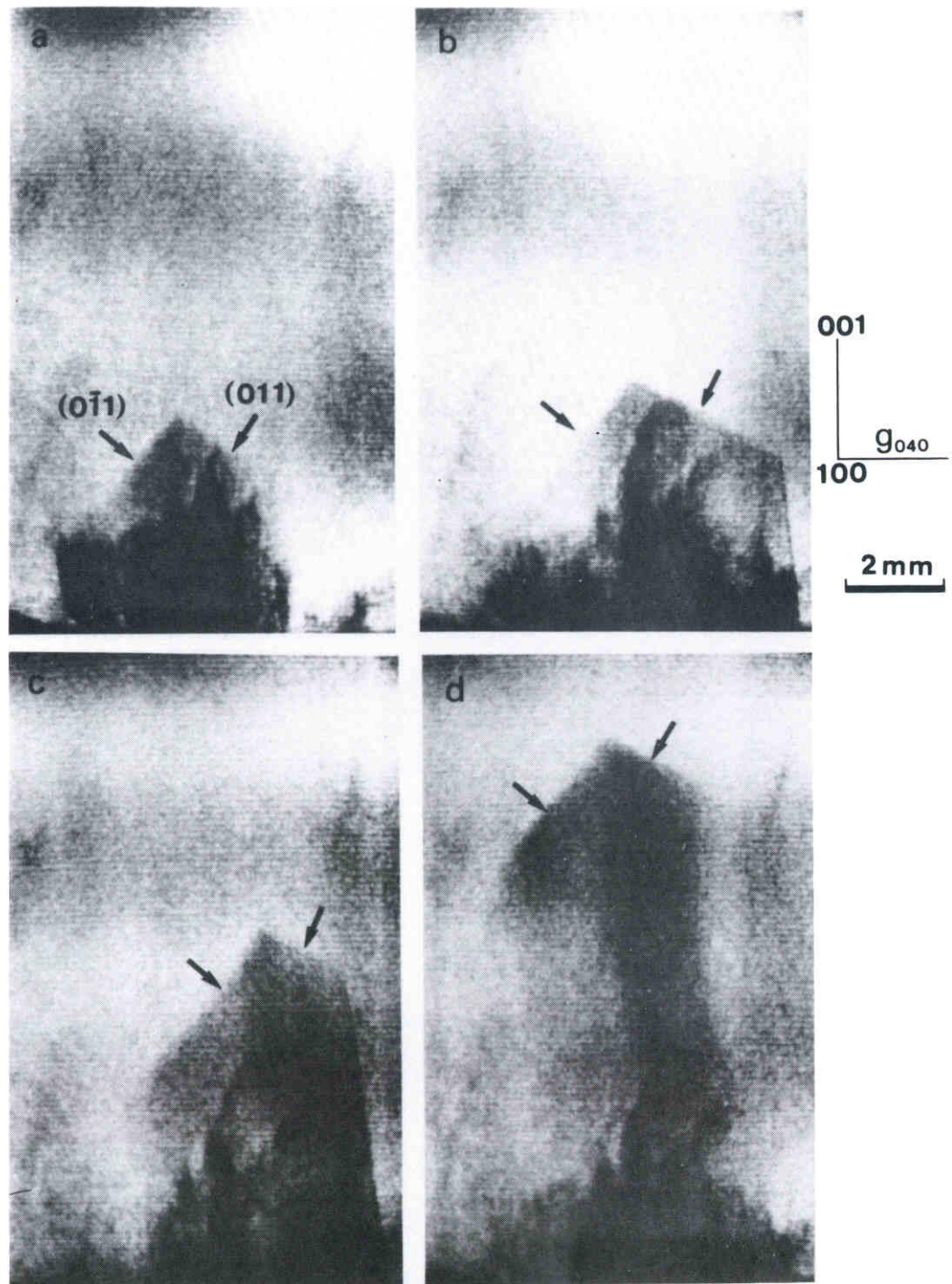
Figure   3.11   A series of X-ray topographs during   growth   of
gallium. These images are TV images with an interval of
about   100   s.   Faceted interface along (011) and   (011)
between   the melt and   crystal are indicated by   arrows.
The   growth rates normal to each facet are   as   follows:
(a)-(b)   0   um/s,   (b)-(c) 4 um/s,   (c)-(d) 17 um/s   for
(011) facet and (a)-(b) 5 um/s,   (b)-(c) and (c)-(d)   12
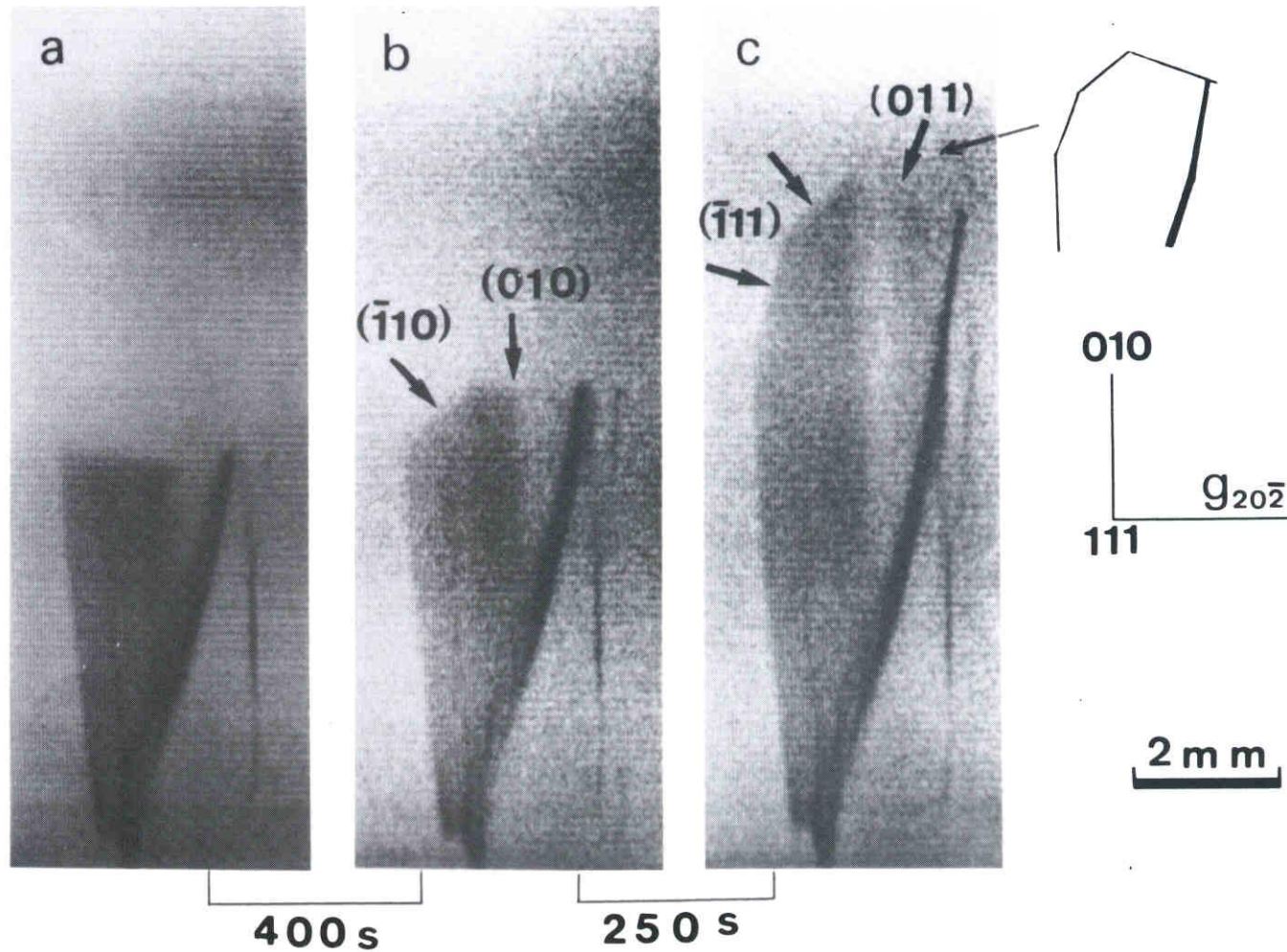um/s for (011) facet.

Figure 3.12 A series of reflection topographs of (a): equilibrium state and (b), (c): growth process. The intervals of each topograph are indicated under the topographs. ($\bar{1}$10) and (010) facets appear on (b) and ($\bar{1}$11), ($\bar{1}$10) and (011) facets on (c), and indicated by arrows. (d) is a schematic diagram of a faceted interface of (c).

facet, which is inclined to the iso-thermal plane, would not appear. Moreover, $(\bar{1}11)$ and (011) facets appeared in Fig. 3.12 (c) and the dislocation bundle propagated into newly grown crystal without affecting the faceted growth.

Similar behavior of dislocations was observed in the transmission topograph as shown in Figure 3.13. In Fig. 3.13 (a) which is the TV image of growth process, many dislocations intersect with $(\bar{1}01)$ and $(\bar{1}10)$ facets. In Fig. 3.13 (b), (011) facet appears and the dislocations propagate into newly grown crystal intersecting with the facets. The $(\bar{1}01)$facet seems to shrink by dislocation effect (cf. Fig. 3.13 (c)) but as seen in Fig. 3.13 (d), growth on the $(\bar{1}01)$ facet and $(0\bar{1}1)$ facet stops during the periods of the preferential growth on the $(\bar{1}10)$ facet, then the (101) facet seems to develop although many dislocations propagate into newly grown crystal, intersecting with the $(\bar{1}01)$ facet. The $(\bar{1}10)$ facet shrinks (cf Fig. 3.13 (d) and Fig. 3.13 (e)), and the $(0\bar{1}1)$ facet shrinks as the $(\bar{1}01)$ facet keeps stopping.

3.3.3. Growth Kinetics and Measurement of Growth Rate as a Function of Super-Cooling

The measurement of super-cooling using the crucible shown in Fig. 3.3 (a) was unsuccessful, because the supercooled layer in the melt is too narrow to be detected by means of thermocouples of 0.1 mm in diameter. Therefore, super-cooling of the melt was determined from cooling curves measured with the aid of the
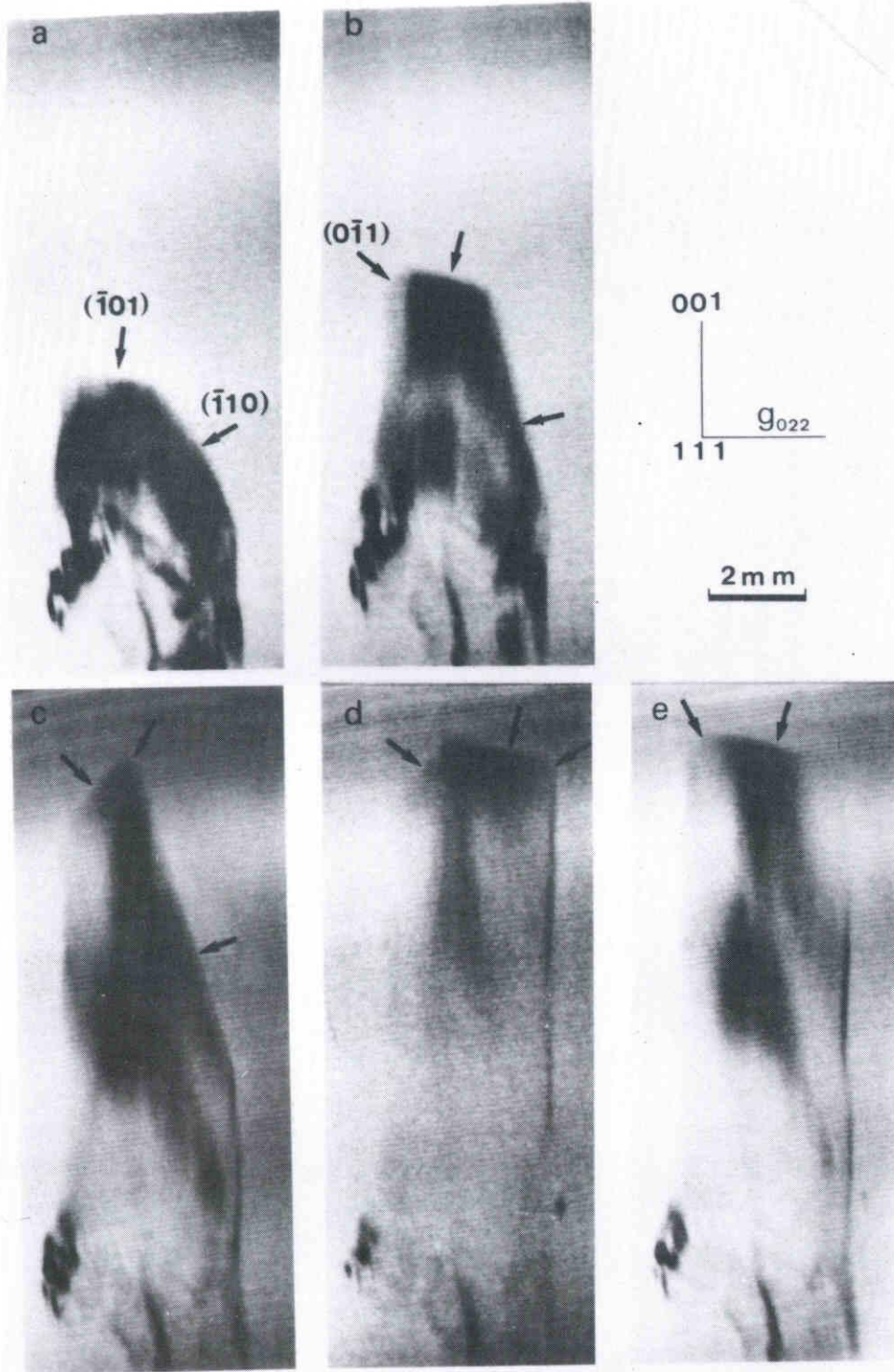
Figure 3.13 Transmission topographs during growth of gallium. (101), (110) and (011) facets appear and compete with each other. The growth rates normal to each facet are as follows: (a)-(b) 13 um/s, (b)-(c) 12 um/s and (d)-(e) 0 um/s for (101) facet, (b)-(c) 5 um/s, (c)-(d) 0 um/s, (d)-(e) 1 um/s for (011) facet, and (a)-(b) and (b)-(c) 2 um/s, (c)-(d) 3 um/s, (d)-(e) 0 um/s for (110) facet.

crucible shown in Fig. 3.3 (b).

Figure 3.14 shows typical heating and cooling curves measured during melting and growth processes of aluminium crystal under condition of high temperature gradient (10 K/mm). Each point on the curves indicated by arrows shows the temperature measured at the moment when the solid-liquid interface passed through the hot junctions of the thermocouple. Scales of time and temperature are indicated in the figure.

Figure 3.15 shows the relations between growth rate and super-cooling measured from the cooling curves during the growth in the [110] and [111] directions. It is obvious from the graph that growth in the [111] direction is more rapid than that in the [110] direction. Growth kinetics of aluminium in the [110] and [111] directions seem to be that of normal (or adhesive) growth. However, the growth kinetics obtained in this experiment may not be very accurate, because many dislocations were likely to be generated around the thermocouple in contact with the melt.

3.4. DISCUSSION

Melting process

In the X-ray topographs taken during the melting process of aluminium shown in Fig. 3.4 and Fig. 3.5, no intensity enhancement was observed in the vicinity of the interface. In the cases shown in Fig. 3.4 and Fig. 3.5, the reflecting planes used were nearly perpendicular to the solid-liquid interface. By taking into account the criterion that topographic images show no
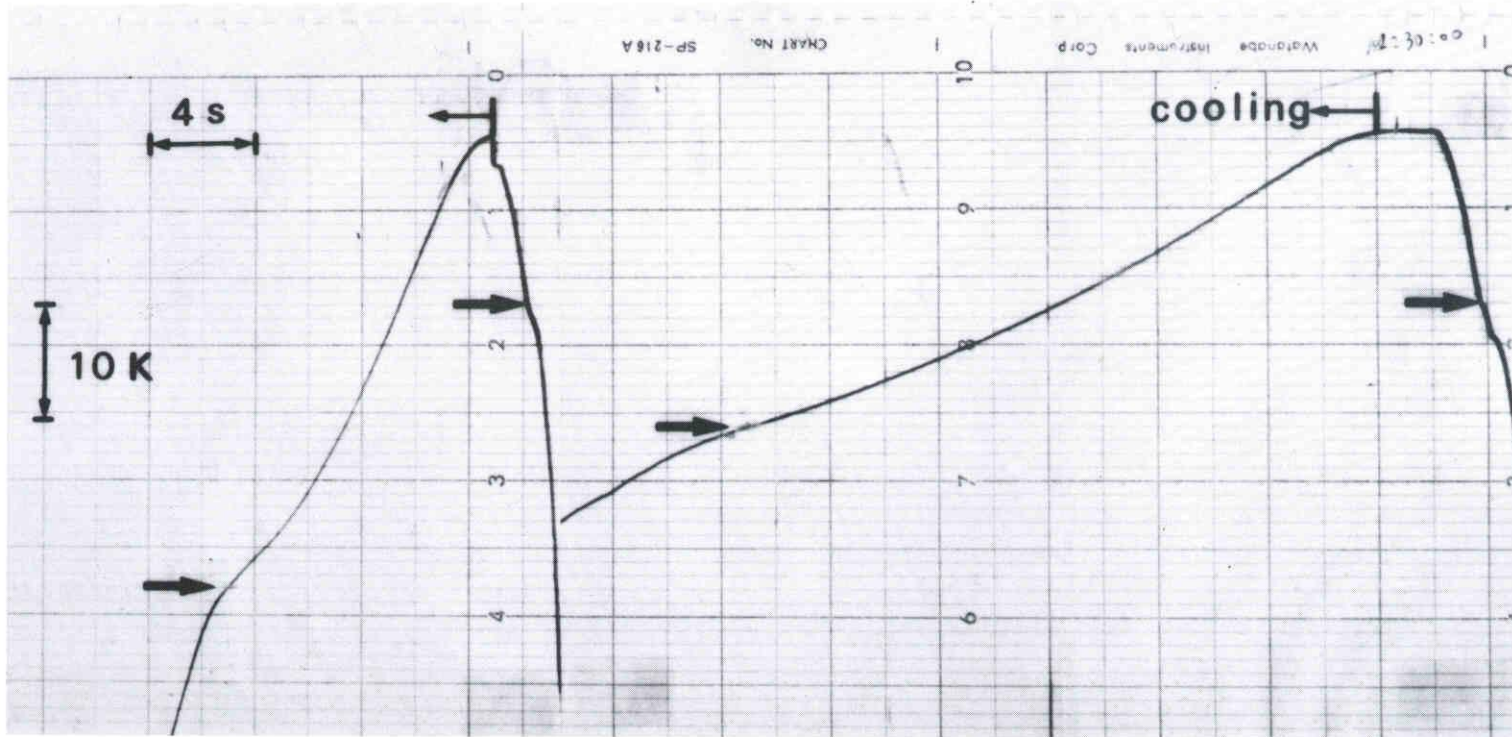
Figure   3.14 Typical heating   and   cooling curves using the   crucible
        shown   in   Fig.   3.3 (b) measured during melting   and   growth
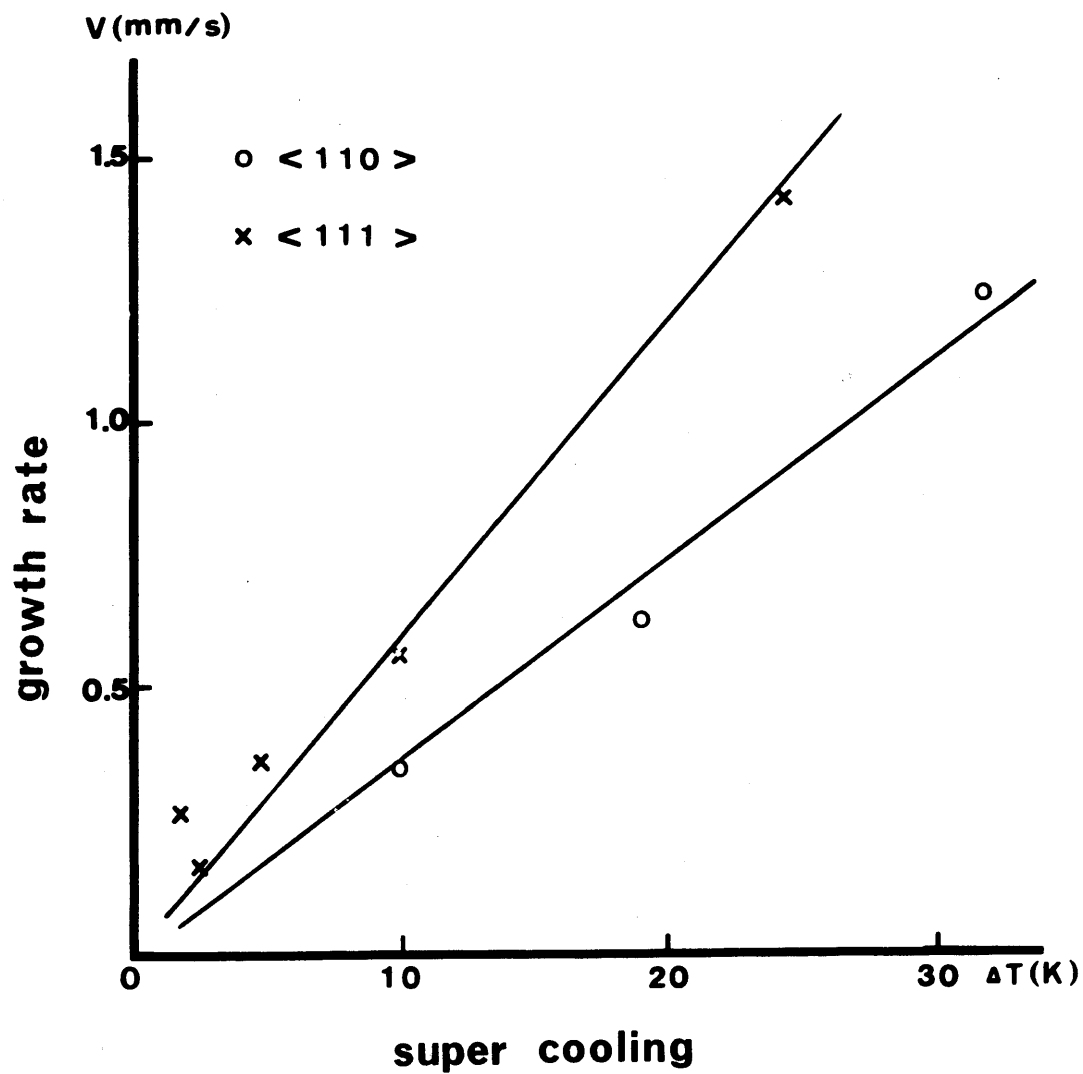   processes   of   aluminium.

Figure 3.15 Relations between growth rate and supercooling of aluminium single crystals obtained during the growth in the [110] and [111] directions.

contrast for the reflecting plane to which the displacement of atoms is parallel, there is a possibility that we cannot detect the distortion perpendicular to the interface in Fig. 3.4 and Fig. 3.5. However, in the observation of the melting process shown in Fig.3.6, the reflecting plane was nearly parallel to the solid-liquid interface, and no intensity enhancement was observed in the vicinity of the interface. Consequently, there is little lattice distortion in the aluminium crystal near the interface within the limit of resolution of the X-ray topographic imaging system, (in spite of existance of volume change between the liquid and the solid).

In the observations mentioned above, no equal-thickness fringe was observed near the solid-liquid interface. From this, it can be said that the crystal surface in contact with its melt was nearly planar, and that the temperature gradient in the crystal was almost completely uni-directional. Therefore, we can relate the morphological changes which should appear during growth directly to the mechanism of crystal growth.

The continuous observations mentioned above also showed that dislocations introduced during the temperature rise up to the melting point did not move until they came into contact with the interface. This observation conflicts with the results observed on Si [7] and Sn [8]. According to the observations during the growth process of aluminium, however, dislocation in the region of high perfection ought to be detected, within the resolution of the present imaging system used although it is not as good as that of the system used by Chikawa et al. and Nittono et al. (less than 10 μm). This can be explained by considering that the thermal stresses caused by temperature gradient in the crystal (1.0 K/mm

to 10 K/mm) heated by the present furnaces was too small to move dislocations.

The lattice distortion near the interface and the behavior of dislocations in gallium crystal were similar to that of aluminium. The volume change of gallium crystals at the melting point is negative, although that of aluminium crystals is positive. In spite of this, the results of observations on the lattice distortion and the behavior of dislocations during the melting process is almost the same for aluminium and gallium.

Microscopical structure of the solid-liquid interface of aluminium and gallium

From the observations of interfacial morphology during the growth process and dislocation effect on the growing interface, the structure of the solid-liquid interface on atomic scale is discussed here, and compared with the theoretical expectations.

K. A. Jackson [9] introduced the concept of roughness and classified the roughness of the interface of materials into two categories using the two-dimensional Ising model, that is, smooth interface and rough one.

D. E. Temkin [10] proposed the concept of diffuseness of the interface on the basis of a multilayer model which was an expansion of Jackson's two-level model.

J. W. Cahn [11] used a continuous model to describe the interface. According to his theory, the surface energy of an interface depends on the mean position of the interface with

respect to the atomic plane, and therefore, the surface energy should vary periodically as the interface moves.

The solid-liquid interface of aluminium during the growth was observed to lie always along the iso-thermal plane of the crystal throughout the observations shown in Fig. 3.8 to Fig. 3.10, and no facet appeared at the growing interface even in the case of growth under low temperature gradient (1.0 K/mm), shown in Fig. 3.9. Furthermore, the morphology of the interface never changed by the intersection of dislocations with the interface. From this, the solid-liquid interface of aluminium should be rough in terms of it can be concluded that Jackson's roughness (when α for Al is less than 2), or diffuse interface in terms of Temkin's diffseness.With respect to Cahn's theory, neither growth by the lateral mechanism nor that by transitional mechansim, which are predicted in his theory, has been observed within the range of temperature gradient and the supercooling realized in the present study.

In the case of gallium, (010),(110),(011) and (111) facets were observed at the solid-liquid interface during growth (Fig. 3.11 - Fig. 3.13). The structure of the solid-liquid interface on atomic scale, which is related to the faceted growth and which is expected from the Jackson's theory, ought to be the smooth interface and that from the Temkin's theory ought to be sharp or a diffuse one with steps.

These types interface are schematically illustrated in Figure 3.16.

If the observed surface structure of the (010), (110), (011),and (111) facets was the smooth interface expected from the Jackson's theory, these facets would advance and reduce in size by
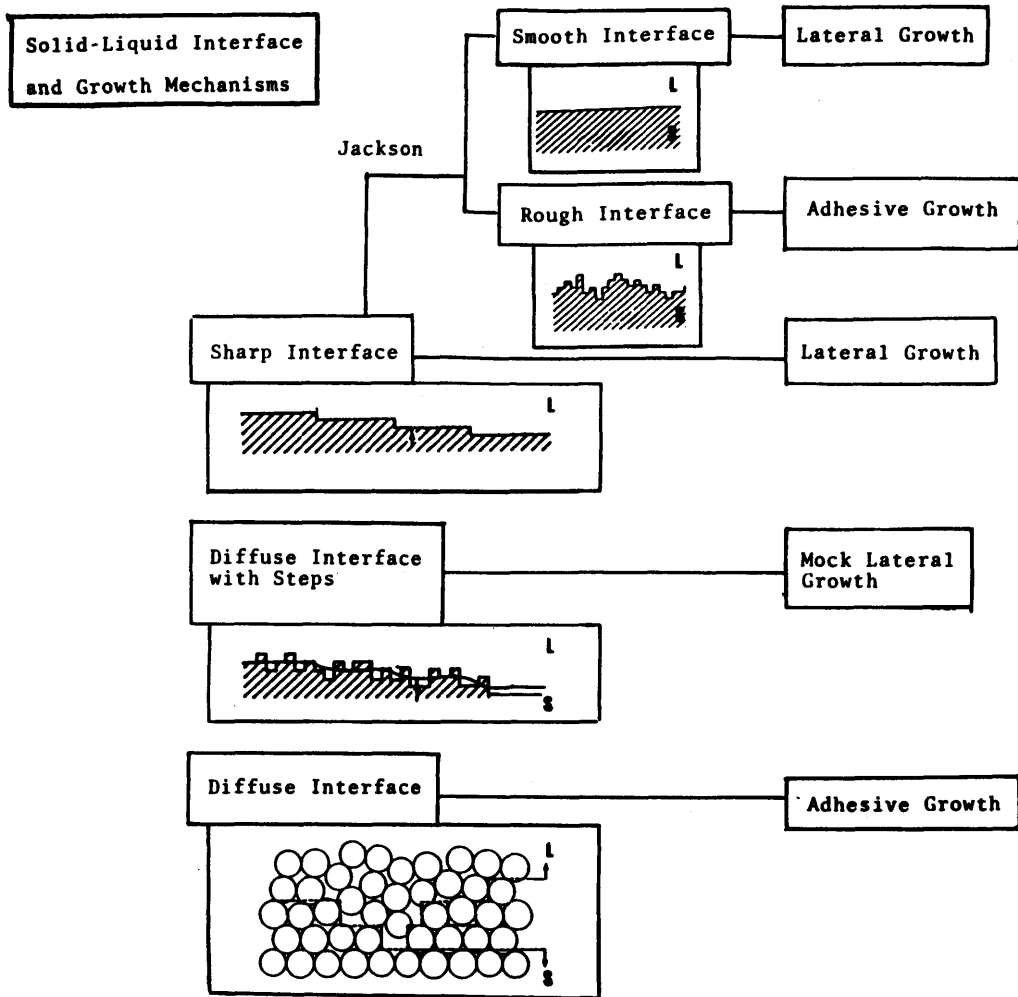
Figure 3.16 Schematic illustrations solid-liquid interface and growth mechanism.

the intersection of screw dislocations. However, The bundle of dislocations with different Burgers vectors did not affect the faceted growth as in the Fig. 3.13. Further were, many facets such as (110), (011),and (111) facets, which cannot be expected to appear from Jackson's theory because of the fact that the Jackson's parameter α of these facets is 1.12, have been observed (c.f. Fig.3.11 - Fig. 3.13).

One possible explanation of this discrepancy is a modification of Jackson's parameter α by considering the second nearest neighbor atoms, as follows: For gallium,

$$L/kT_m = 2.24 \quad \text{and} \quad v = 4$$

When the first nearest neighbor atoms are considered, $n_i = 2$ for (110) and (011) plane. However, the distance to the first nearest neighbor atoms and to the second nearest neighbor atoms in (110) plane is 4.45 and 4.52, respectively, and almost the same. If the first and the second nearest neighbor atoms are taken into consideration, (therefore, $n_i=4$), α is calculated as follows,

$$\alpha = (L/kT_m)(n_1/v) = 2.24$$

In this case,(110) surface should be smooth and (110) facet should appear. Thus,faceted growth observed on (110), (011), and (111) in Fig. 3.11 - Fig. 3.13 can be explained by the modification of Jackson's theory, although there may be another way of modification of Jackson's theory for example, by introducing structural difference between a crystal and its liquid [13].

With respect to Temkin's theory, sharp interface can be related to the faceted growth when the crystal surface in contact with its melt is smooth. Furthermore, the fact that the (011) facet observed in Figure 3.13 stopped advancing to gain the supercooling necessary for a further growth denies the

possibility of growth on the Temkin's diffuse interface with steps.

Therefore, Jackson's theory is, roughly speaking, valid for the faceted growth of gallium. However, in details, Jackson's theory is in conflict with the experimental result that dislocations observed in Fig.3.12 and Fig. 3.13 do not affect the faceted growth. Some modification of the theory should be necessary as mentioned above.

With respect to Cahn's theory, a major disadvantage is that there is no other way to determine the diffuseness of the interface than curve-fitting with the theory [1]. In the present study, the breaks from lateral growth kinetics to continuous growth kinetics which are expected according to his theory, have not been observed. Therefore, his theory can not be applied to the present findings.

Mechanisms of crystal growth from the melt of aluminium and gallium

From the result of observations of the solid-liquid interface during growth and the speculation about the microscopical structure of the solid-liquid interface mentioned above, the mechanism of crystal growth of aluminium from the melt is discussed here.

The solid-liquid interface of aluminium always appears along the iso-thermal plane of the crystal and advances normal to the iso-thermal plane in the system. Therefore, it can be said that the growth of aluminium crystals is isotropic. Consequently,

the growth mechanism of aluminium is considered to be continuous growth, or adhesive growth.

Also from the microscopical structure of the interface of aluminium presumed to be rough or diffuse, crystal growth of aluminium is considered to be continuous or adhesive growth.

Now let us infer the growth mechanism from the result of real time observation of faceted growth of gallium. According to the theories of Jackson [1] and Temkin [11]; macroscopical faceting of the interface is formed by growth rate anisotropy. In the temperature gradient realized in the present experiment, anisotropic growth implies that the growth is governed by a lateral growth mechanism.

In Figure 3.13 (b) to (d), ($\bar{1}$01) facet which is in the center of the solid-liquid interface repeats shrinking and spreading in turn as the crystal grows, This is illustrated schematically in Figure 3.17. In this case, preferential nucleation may occur at the center facet (($\bar{1}$01) facet) resulting in preferential growth of the center facet (Fig. 3.17 (a)). Consequently, the center facet appears to shrink, as is seen in Fig. 3.13 (c). As a result of preferential growth, this facet cannot gain the supercooling necessary for growth by the latent heat generated at this facet. Therefore, growth on this facet stops(see Fig. 3.13 (d)). During this process, growth on the (0$\bar{1}$1) and ($\bar{1}$10) facets which are located on the both sides of the crystal keeps stopping. This indicates that the rate of the lateral spread of nuclei is low ; it is almost same as the rate of nucleation.

On the contrary, if the nuclei spreads rapidly compared with the nucleation on facets as shown in Fig. 3.17 (b), the
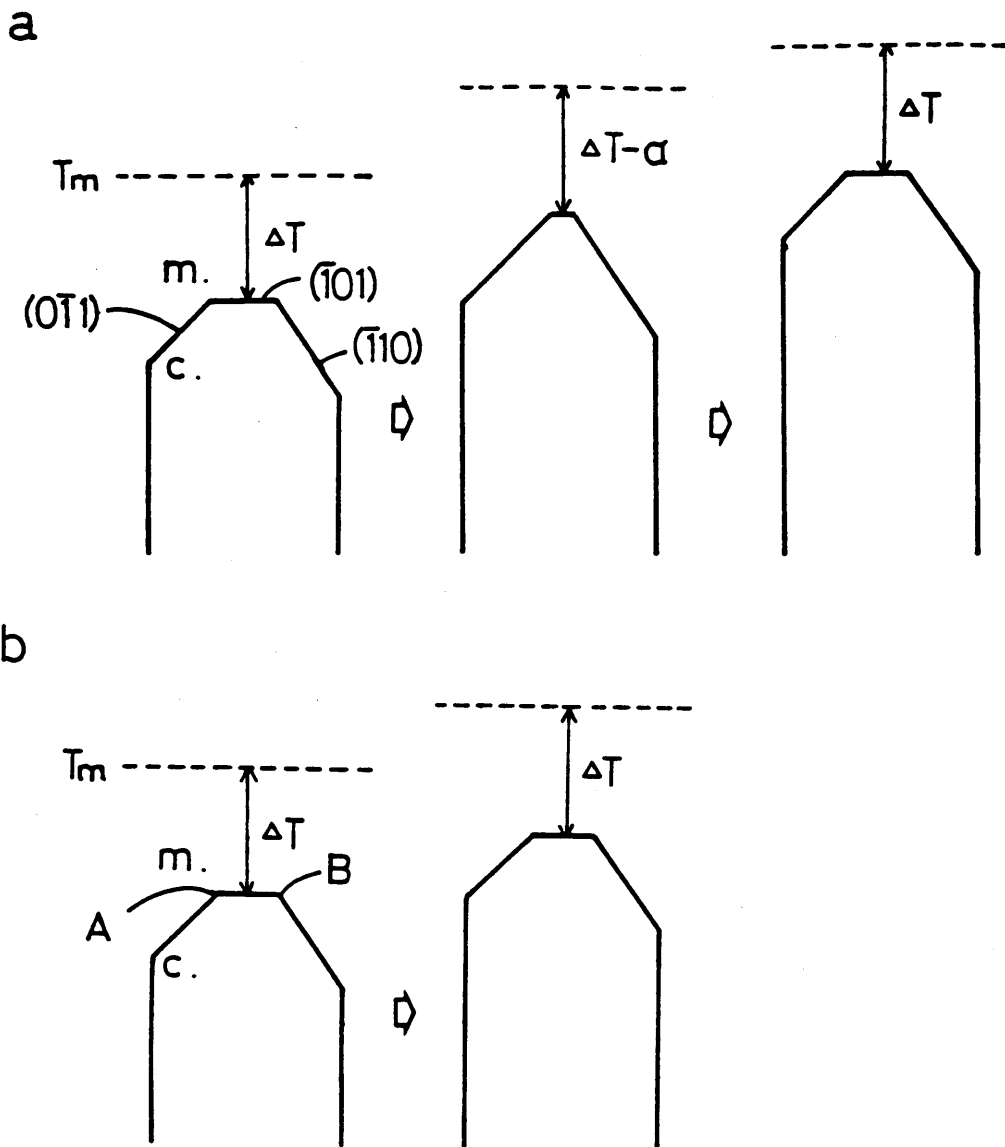
-75-

Figure 3.17   Schematic illustrations of faceted interface observed during growth of Fig. 3.13. (a) is for the case of growth on a singular interface with a low rate of nucleus spread and (b) for the case on a singular interface with rapid lateral spread. The dotted lines indicate the isothermal plane in the melt, T supercooling.

nuclei would spread from the edges of the center facet (A,B) to the side facets and growth would also occur at these facets almost at the same speed as the center facet.

From this, it is concluded that gallium crystals grow by lateral mechanism on smooth interface, and that the rate of lateral spread of nuclei is almost the same as the rate of two-dimensional nucleation on the surface. This conclusion is favorable to the Jackson's theory.

Kinetic experiment on the growth of aluminium

According to the theoretical predictions by Jackson and Temkin based on the lattice model of the melt [1],[10], growth rate anisotropy on the adhesive growth should not be observed in aluminium. Computer experiment on the kinetics of growth from the melt of f.c.c. metals [11] shows that growth on the rough interface should be isotropic. However, the difference of growth on (110) and (111) is observed in Fig 3.14. This growth rate anisotropy, which was not expected from the theories for the growth of aluminium from the melt indicates that the mechanism of growth from the melt can not always be predicted by these theories.

CHAPTER SUMMARY

Real time observations with X-ray topography have been made during the melting and growth processes of aluminium and gallium

single crystals. The microscopical structures of the solid-liquid interface and mechanisms of growth from the melt of aluminium and gallium are clarified as follows ;

(1) The solid-liquid interface of aluminium during growth is most probably rough.

(2) The growth mechanism of aluminium is continuous growth.

(3) The solid-liquid interface of gallium during growth is smooth and boundary layers of crystallites with the thickness of a few atomic distances exist in the crystal surface in contact with the melt.

(4) The growth mechanism of gallium is lateral growth and the rate of lateral spread of nuclei is almost the same as that of nucleation.

(5) These results are favourable to the Jackson's theory.

Real time X-ray topography also showed that dislocations which intersect with the interface did not affect either the interface morphologies or the growth of aluminium and gallium. Some facets which are not predicted from the Jackson's theory have been observed on gallium during the growth from the melt. The theories of interface morphology introduced by Jackson and Temkin are roughly valid for aluminium and gallium, but the morphology of solid-liquid interface of these crystals can not always be predicted from these theories.

Theories of crystal growth from the melt which were developed from that of crystal growth from vapor phase or solution, are roughly applicable to the growth of aluminium and gallium from the melt, but they can not predict all mechanisms of crystal

growth from the melt.

REFERENCES

(1)   K. A. Jackson: J. Cryst. Growth 1 (1967) 1

(2)   K. A. Jackson: "Liquid Metals and Solidification" (American Society for Metals, Cleveland, 1958) p.174

(3)   T. Abe : J. Cryst. Growth., 24/25 (1974) 463

(4)   J. Chikawa and F. Sato : "Defects and Radiation Effects in Semiconductors, 1980" edited by R. R. Hashiguti (The Institute of Physics, London, 1981) p.95

(5)   K. Kamada * Prog. Crystal Charact. 3 (1981) 309

(6)   B. Noest : Phil. Mag. 11 (1965) 183

(7)   J. Chikawa and F. Sato : "Defects and Radiation Effects in Semiconductors, 1980" ed. R. R. Hasiguti (The Institute of Phisics, London, 1981) p.95

(8)   O. Nittono, T. Ogawa, S.K. Gong and S. Nagakura : Jpn. J. Appl. Phys. 23 (1984) L581

(9)   K. A. Jackson : "Liquid Metals and Solidification" R. H. Doremus and D. Turnbull eds. (American Society for metals, Ohio, 1958) 170

(10)   D. E. Temkin : "Crystallization Process" (Consultant Bureau, New York, 1966) 15

(11)   J. W. Cahn : Acta. Met. 8 (1960) 554

(12)   G. M. Gilmer and K. A. Jackson : "1976 Crystal Growth and Materials" E. Kaldis and H. J. Scheel eds. (North-Holland,

Amsterdam, 1977) p.80

(13) T. Sawada : J. Cryst. Growth **60** (1982) 349

CHAPTER 4   ORIGIN OF DISLOCATIONS INTRODUCED DURING CRYSTAL GROWTH

4.1. INTRODUCTION

The growth of dislocation-free or low dislocation density single crystals has been of great interest because such crystals are necessary for basic research on crystal characteristics and because they are required for semiconductor technology. The preparation of dislocation-free crystals of silicon [1] and germanium [2] has played an essential role not only in physics but also in semiconductor technology.

In the crystal growth from the melt, the following three origins of dislocation generation can be considered.

(1) Propagation of dislocations into the growing crystal from the seed crystal.

(2) Generation of dislocations by segregation of solute atoms or impurities.

(3) Generation of dislocations by thermal stress, and/or mechanical interaction of crystal with the crucible walls in the case of growth in a crucible.

Besides these, the following two models of intrinsic dislocation generation have been proposed in connection with the formation mechanism of dislocation in the crystal growth from the melt.

(4) Inheritance of dislocations from the liquid state which can be modelled as a coagulation of a large number of dislocations [3]-

(9).

(5) Tranformation of vacancy clusters, which are formed by excess vacancy condensation, into dislocation loops [1]-[2].

According to vacancy condensation mechanism, it is assumed that the initial vacancy concentration is equal to the equiliblium value at the melting-point for melt-grown crystals. Any excess vacancies that arise through temperature decrease will condense in many cases, on the atomic planes to form vacancy clusters or discs. The formation of dislocation loops from these clusters of vacancies will occur as long as the excess free energy due to dislocation loops is less than that for the clusters.

On the other hand, dislocation models of the liquid state have been developed by Mizushima [3], Ookawa [4], Kuhlman-Wilsdorf et al [5],[6], Cotterill et al. [7] and Suzuki [8] and growth theories based on these models have been put forward [7]-[9]. In Ookawa's theory[9], for example, it was assumed that a free energy barrier between the liquid and the solid phase can be easily surmounted without the aid of thermal activation when a suppercooling exists. Although the dislocation density decreases in the solidification process, part of the dislocations in the liquid phase are inherited into the solid phase. The number of these inherited dislocations will decrease in a short time with the corresponding decrease of free energy in the solid phase. Ookawa calculated the time necessary for recovery (i.e., the reduction of dislocation density) and the change of dislocation density, and concluded that dislocations of the number about 10^3 cm/cm^3 inevitably remain in a bulk solid phase of ordinary-metals such as Al and Cu under usual experimental growth conditions.

The most suitable experimental method to investigate how dislocations are introduced in the growing crystal is in situ observations of dislocations near the solid-liquid interface during the growth process of a crystal and the cooling process after solidification. If dislocations are introduced by the vacancy condensation mechanism, no dislocations should be observed in the crystal near the solid-liquid interface, because some degree of undercooling is necessary to obtain the excess concentration of vacancies required to form vacancy discs or dislocation loops. On the other hand, if dislocations are inherited from the liquid phase into the crystal, many dislocations should be observed in the crystal that has just solidified near the solid-liquid interface.

4.2. EXPERIMENTAL PROCEDURES

The method of real time observations of the process of crystal growth by X-ray topography using a 90kW-class rotating anode X-ray generator [10],[11] has been described in detail previously (Chapter 2, 3).

Single crystals of aluminium (5N) were prepared by the strain-anneal method and single crystals of gallium (6N) with low dislocation density were grown by Bridgman method. These single crystals were cut into small pieces with a size of about 30 x 5 mm^2. The thickness of these specimens was 0.7 mm for the aluminium crystals and 0.1 mm for the gallium crystals.

By using a furnace set on a goniometer stage of a Lang camera

[12], the real time observations of the generation and propagation of dislocations have been made during the unidirectional solidification. The temperature gradient in the specimen was about 1.0 K/mm for aluminium near its melting point (933 K) and 0.4 K/mm for gallium.

Because of a comparatively low yield stress of metallic materials at elevated temperatures, dislocations in metal crystals are very sensitive to the thermal stresses and move very easily by a small fluctuations of temperature. Therefore, it is difficult to record the images of dislocations at high temperature on a nuclear research plate, since in the ordinary experimental condition the exposure time necessary to record dislocation images is about 100 s. For this reason, the X-ray topographic observations were made mainly using an X-ray sensing TV camera. Since the signal-to-noise ratio (S/N) of one frame image (30 frames/sec) was not high enough to observe individual dislocations in the aluminuim crystal, an averaging of 8 to 32 TV frames was made to improve the S/N ratio. Since the averaging of n TV frames improves the S/N ratio by a factor of $(2n-1)^{1/2}$ and since the exposure time of 0.27 to 1.1 s was needed for this superposition of 8 to 32 TV frames, it was necessary to grow the crystals at a slower speed. Therefore, the growth rate used in the present experiments was in the range of about 5 to 50 μm/s.

4.3.   EXPERIMENTAL RESULTS

4.3.1   Dislocation Behavior near the Solid-Liquid Interface of

Aluminium during Crystal Growth

Fig. 4.1 is a series of X-ray topographs taken during the growth process of aluminium. These images are enhanced by averaging 32 TV frames using the real time image processor. The growth rate was 9 μm/s and the temperature gradient in the crystal near the solid-liquid interface was 1 K/mm. A straight and oblique black line is an image due to sub-boundary, which was inherited from a seed crystal and propagated into newly grown crystal, intersecting with the interface. The lower part of the crystal appears black due to the existence of many dislocations generated in the course of temperature decrease after solidification. But in Fig. 4.1 (a), no dislocation is seen in a region near the interface, the width of which is about 1 mm. This region should be dislocation free, because many dislocations can be observed in other regions. This dislocation free region indicated by arrows followed the interface, as seen in Fig. 4.1 (b), keeping its width almost the same as that of Fig. 4.1 (a), and many dislocations were generated behind this region as the interface advanced. It is also seen in Fig. 4.1 (c), and the width of the dislocation-free region is almost the same as before.

To observe the configuration of dislocations in newly grown crystal region in more detail, topographic images were recorded on Ilford-L4 nuclear research plate.

Figure 4.2 (a) to (c) are TV images of X-ray topographs during the melting and growth processes and Fig. 4.2 (d) and (e) are magnified images of the area indicated in Fig. 4.2 (a) and (c), recorded on nuclear research plates just before melting and just after growth respectively. By comparing Fig. 4.2 (d) with
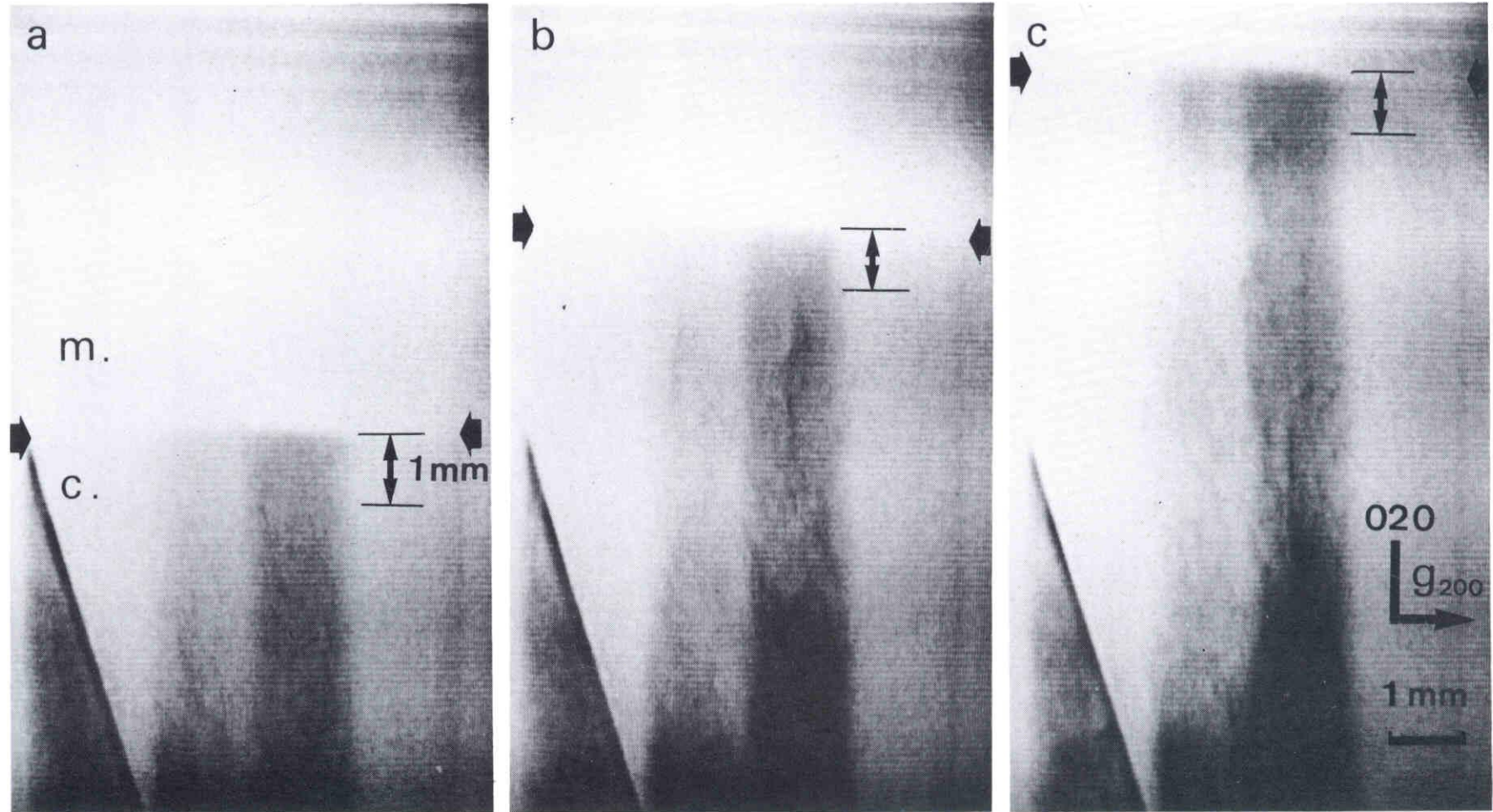
Figure 4.1 A series of X-ray topographs showing growth process of aluminium single crystal. Each topograph is a TV image which is an average of 32 TV frames by real time image processor.
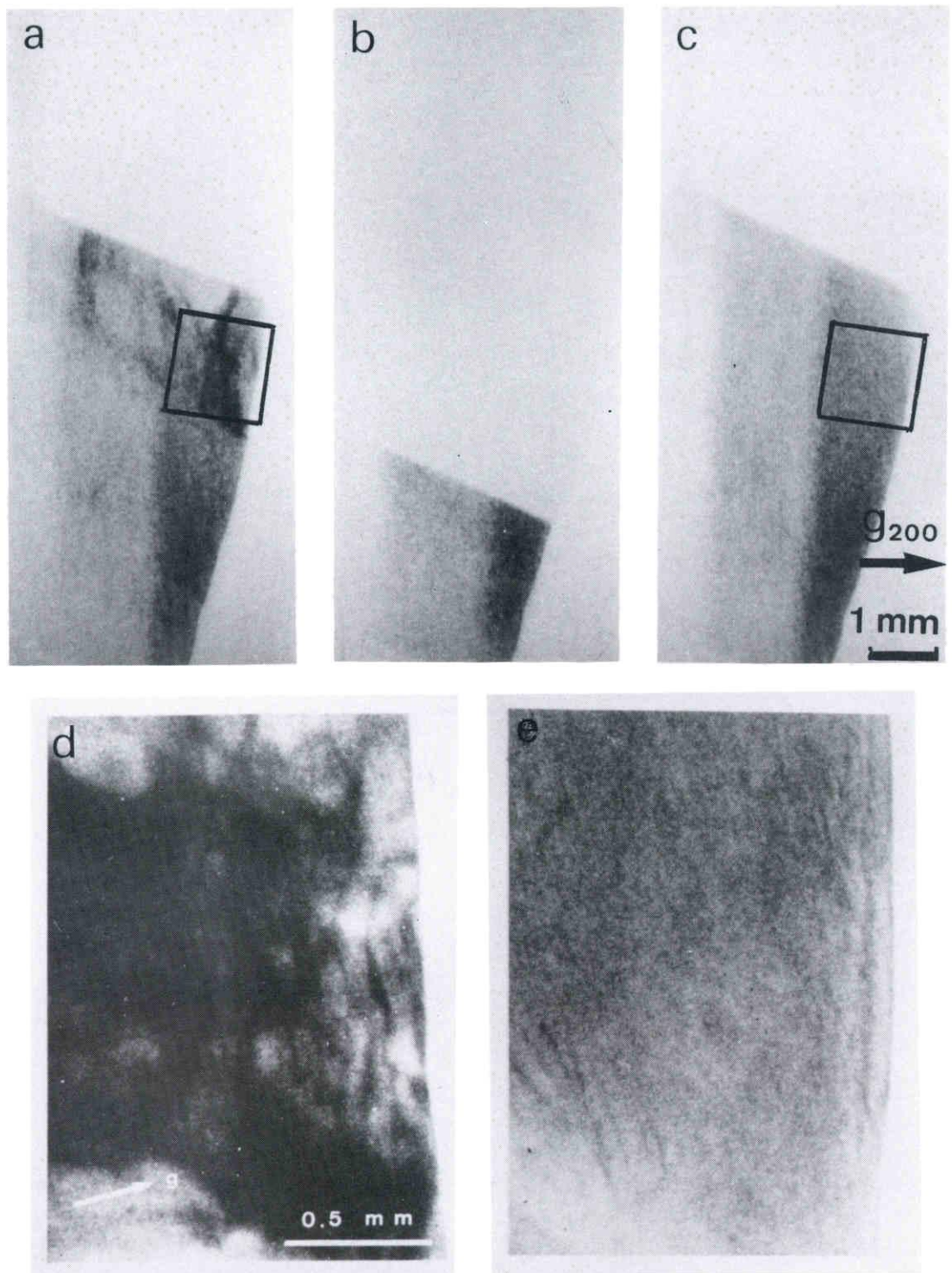
Figure 4.2 A series of X-ray topographs recorded on a video tape during melting (a), in equilibrium (b) and during growth (c). (d) and (e) are magnified images of the area indicated in (a) and (c), recorded on nuclear research plates just before melting and just after growth, respectively.

(e), we can conclude that newly grown crystal is highly perfect just after growth, except for the presence of invisible point defect. In Fig. 4.2 (c), some vague images are seen, which are dislocations introduced after growth by mechanical interaction with oxide film formed on the surface of the crystal. Therefore, it can be concluded that there is a region of high perfection (probably, dislocation-free) in the crystal behind the solid-liquid interface during growth.

To investigate the influence of the growth rate on the perfection of crystal, the growth rate was suddenly changed during the growth process. Figure 4.3 shows the process in which many dislocations were generated by change of growth rate. These images are produced by averaging 8 TV frames. Broad linear images are a bundle of many dislocations. Fig. 4.3 (a) is a topograph taken just before the change of growth rate. The previous growth rate was 20 μm/mm. After changing growth rate from 20 μm/mm to 42 μm/mm, many dislocations were generated from the dislocation bundle. The growth rate between Fig. 4.3 (b) and (d) was 42 μm/s. In Fig. 4.3 (b), however, generation of dislocations was not observed in the region far from the dislocation bundle at this moment, however, many dislocations were suddenly generated in the whole crystal which had been grown after the change of growth rate (Fig. 4.3 (c)). Subsequently, they increased in number in the region except for the region near the solid-liquid interface, as seen in Fig. 4.3 (d).

Thus, an increase in growth rate results in an increase in dislocation density, but this increase occurs in the crystal apart from the solid-liquid interface.
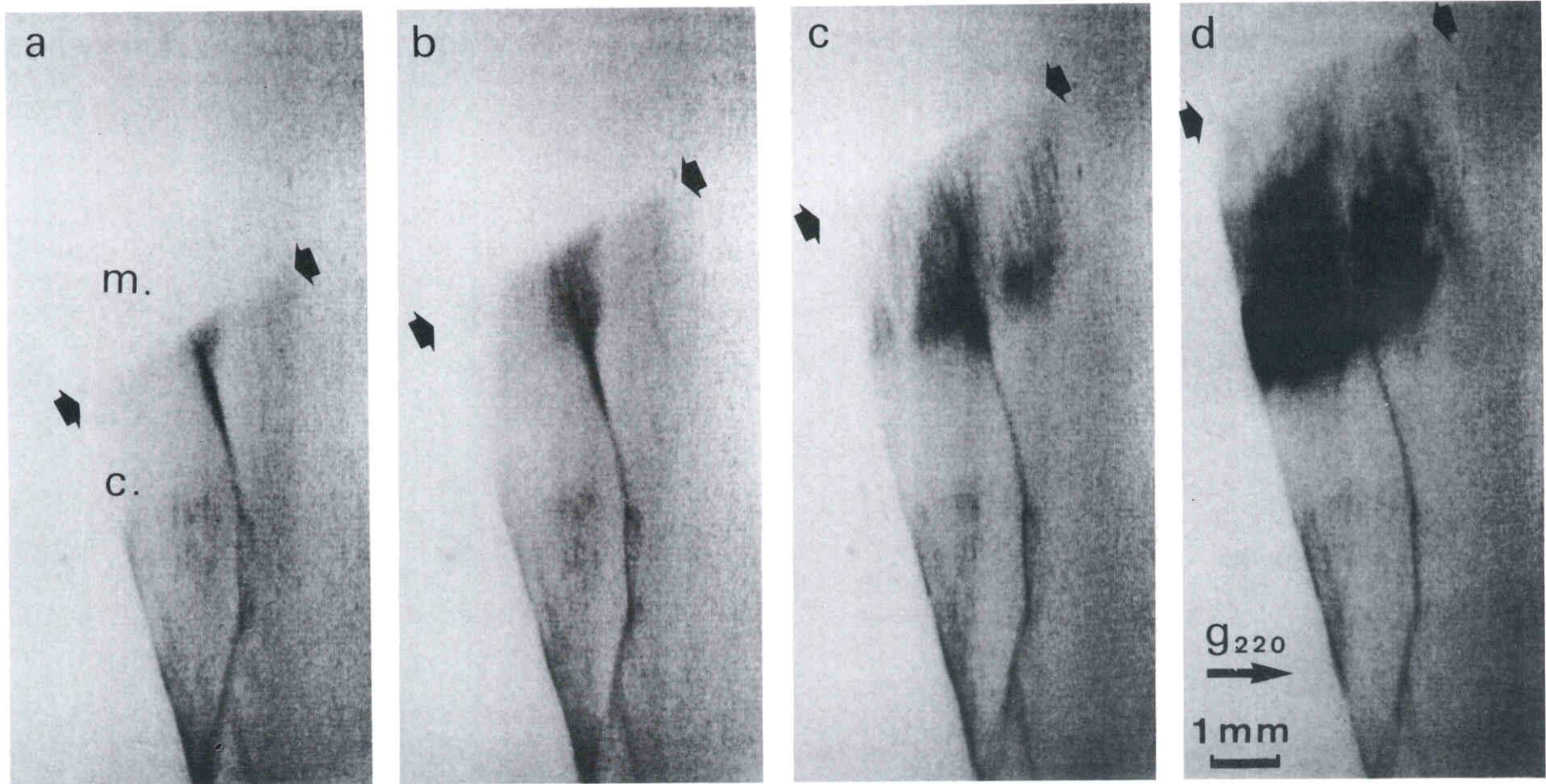
Figure 4.3 A series of X-ray topographs which was taken after the change of growth rate from 20μm/s to 42 μm/s. Many dislocations were suddenly generated after the change of the growth.

4.3.2 Dislocation Behavior in Aluminium during Cooling after Solidification

Figure. 4.4 shows the propagation of dislocation during cooling just after the solidification of Fig. 4.1. Each image is enhanced by the image processor. The temperature of the top of the crystal was 931 K and 928 K in Fig. 4.4 (a) and (b), respectively. The cooling rate was about 5 K/h. and the temperature gradient of the crystal was 1 K/mm. In this way, many dislocations were generated and propagated from the bottom (the region of lower temperature) to the top (the region of higher temperature) of the crystal by decreasing the temperature. At the same time, a part of these dislocations was concentrated to form a bundle of dislocations with the multiplication of them visible in Fig. 4.4 (b).

Fig. 4.5 is a series of topographs taken during successive cooling after Fig. 4.4. The temperature of the specimen was 924 K for Fig. 4.5 (a) and 920 K for Fig. 4.5 (b) and (c). The cooling rate between (a) and (b) was 12 K/h. and the time interval between (b) and (c) was 2 fours. With decreasing temperature, further multiplication of dislocation occurred as shown in Fig. 4.5 (a) and (b). But in contrast to this, subgrain boundaries were gradually formed by holding at a constant temperature and perfection of the inside of sub-boundaries was improved. From these observations, it may be concluded that the multiplication of dislocations arises from the decreasing of temperature and a change of configuration of dislocations to form dislocation bundles or subgrain boundaries is due to the effect of thermal annealing.
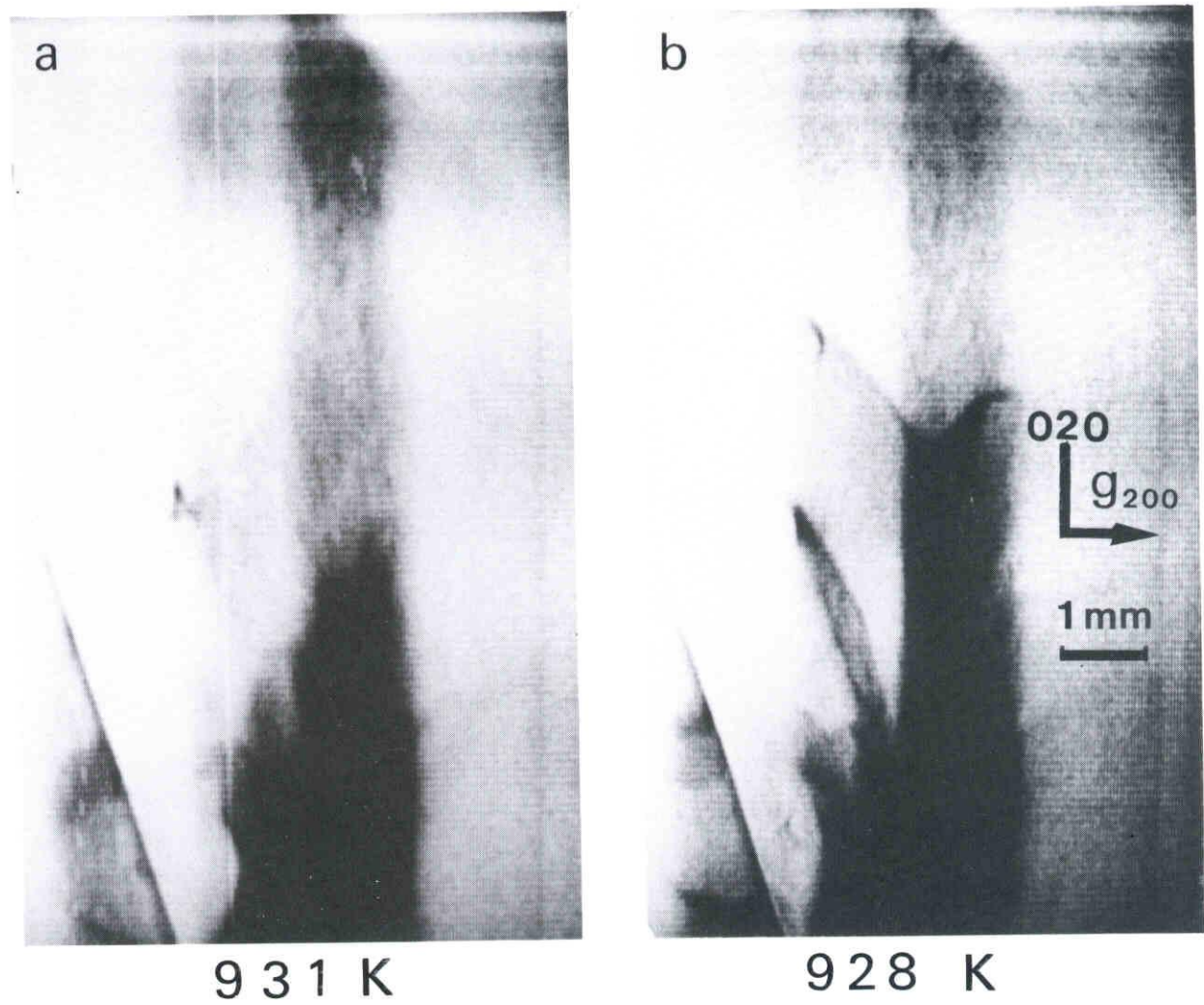
Figure 4.4   X-ray topographs of aluminium during cooling process.
Temperature of the top of the crystal was 931 K and 928 K in
(a) and (b), respectively. Cooling rate was about 5 K/h and
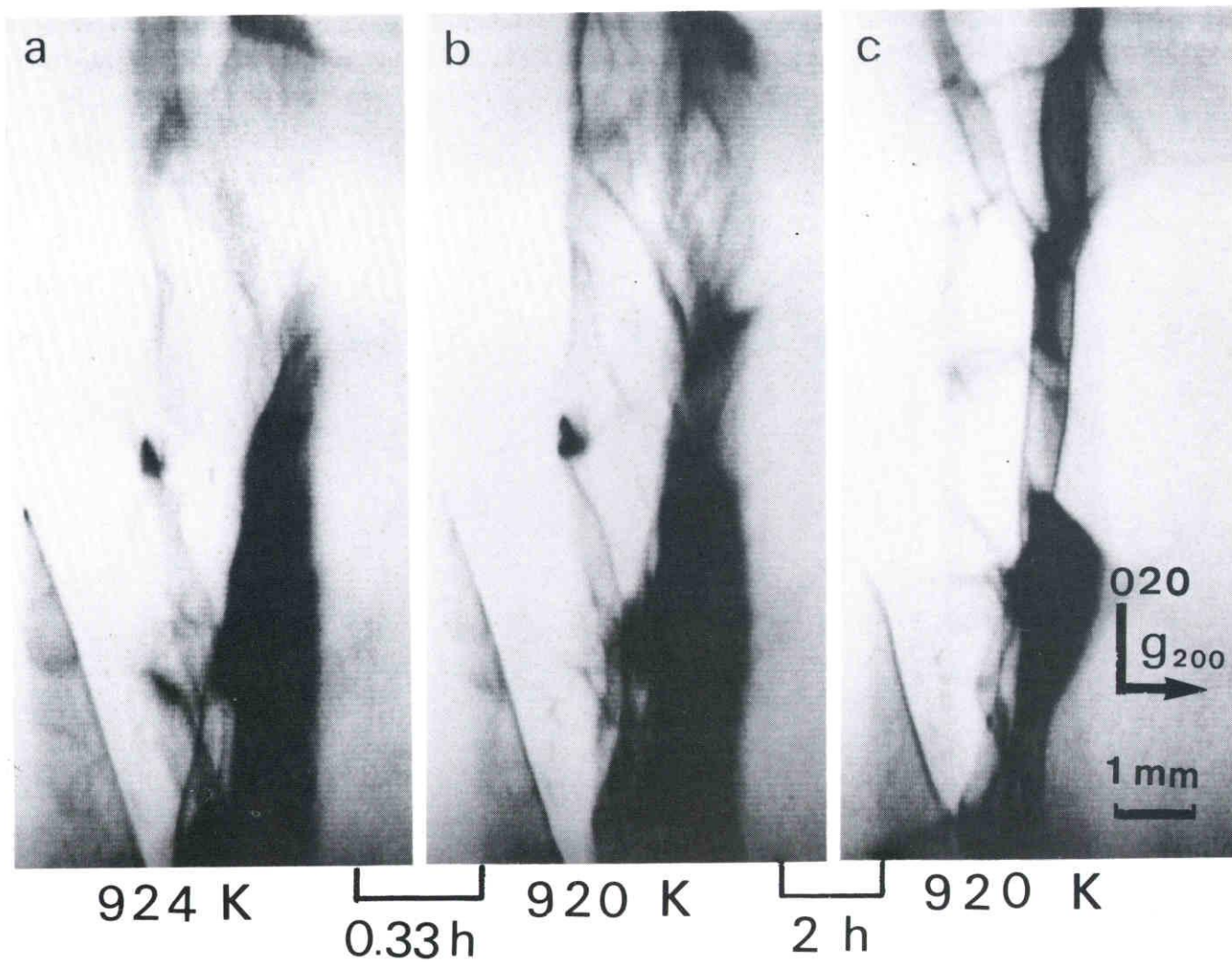temperature gradient of the crystal was 1 K/mm.

Figure 4.5   A series of X-ray topographys during sequential colling to Fig. 4.4.   Temperature of the crystal was 924 K for (a), 920 K for (b) and (c).   Cooling rate between (a) and (b) was 12 K/h and time interval between (b) and (c) was 12 K/h.

4.3.3 Dislocation Behavior near the Solid-Liquid Interface of Gallium during Crystal Growth

Figure. 4.6 is a series of topographs of TV images showing a growth process of gallium single crystal. Contrast of each image is enhanced and averaged by the image processor. Facets of (110) and (1$\bar{1}\bar{1}$) crystallographic planes were observed at the solid-liquid interface. The growth rate of each facet was about 3 µm/s. In this case, the seed crystal was highly perfect and no dislocations were observed to propagate from the seed crystal as shown in Fig. 4.6 (a). Further, generation of dislocations did not occur over the whole crystal during the following growth (Fig. 4.6 (b) and (c)).

In other observations shown in Fig. 3.11 to Fig. 3.13, no other dislocations besides for those propagating from the seed crystal have been observed generating in the crystal.

Consequently, dislocation-free single crystal of gallium can be grown under a proper growth condition.

4.4 DISCUSSION

In the observations of Fig. 4.1 to Fig. 4.5, no evidence of individual dislocations was obtained. Although, the low resolving power of the TV imaging system employed is not so good as that of nuclear research plate, in view of that a generation or multiplication of bundles of dislocation during growth and cooling processes could be observed successfully using a imagie processor,
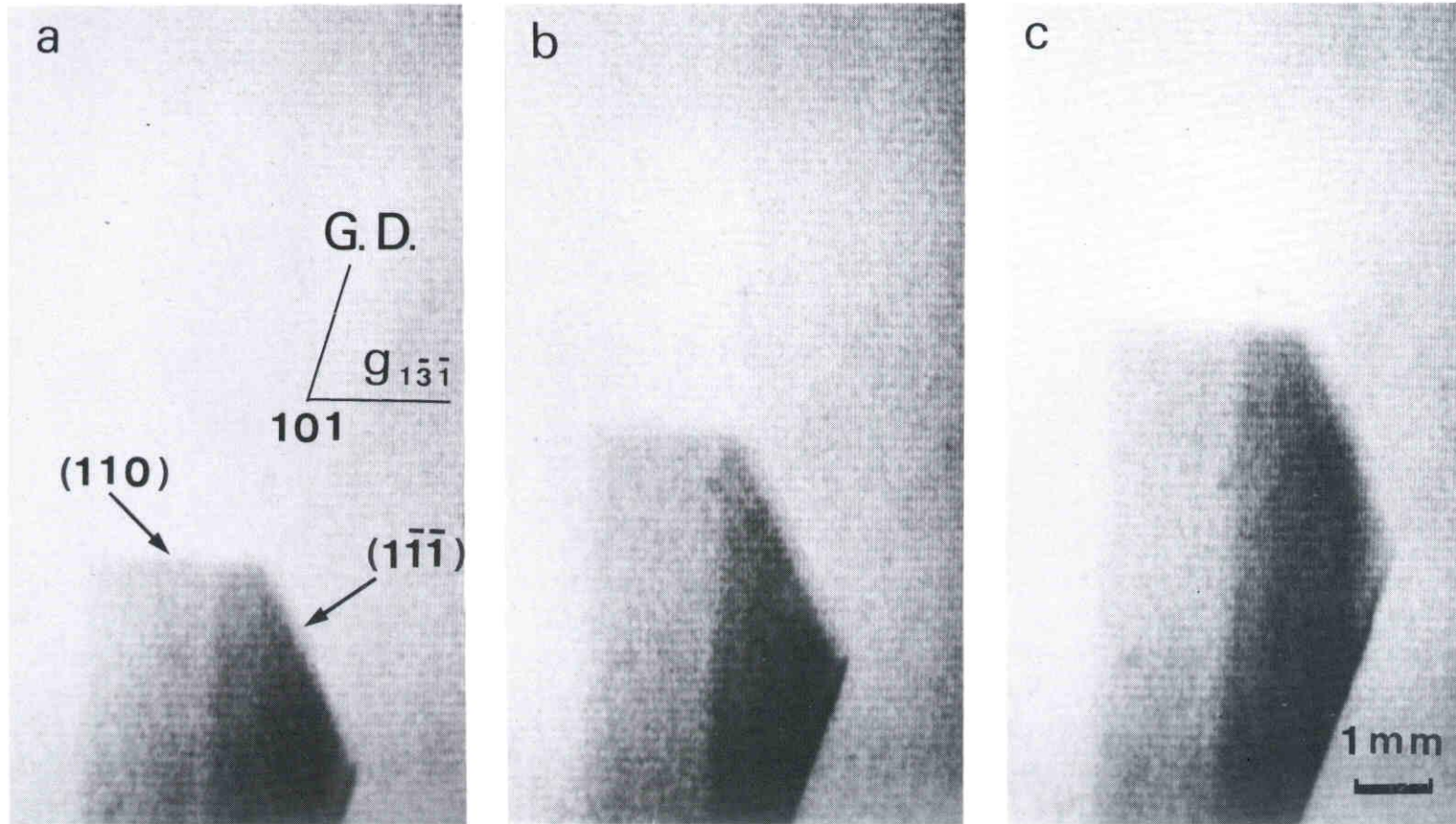
G.D.

$g_{1\bar{3}\bar{1}}$

101

(110)

(1$\bar{1}\bar{1}$)

1 mm

Figure 4.6   A series of X-ray topographs showing the growth process of a gallium single crystal.   Growth rate was about 3 um/s.   Facets of (110) and (111) at the solid-liquid interface are indicated by arrows.   These topographs are TV images recorded on a video tape.

it may be concluded that newly grown crystal of aluminium in adjacent to the advancing front at a slow rate (less than about 40 μm/s in the present study) are actually free from at least dislocation bundles and, most probably, isolated dislocations.

As is already mentioned in 4.1, possble origins of dislocations during growth and cooling of a metal crystal can be classified in two groups, i.e., the intrinsic ones and extrinsic ones. They may be summarized as follows.

Extrinsic origins:

(1) Propagation of pre-existing dislocations fron the seed.

(2) Generation of dislocations due to the segregation of solute atoms and/or impurities.

(3) Generation of dislocations due to a thermal stress.

Intrinsic origins:

(4) Inheritance of dislocations from the liquid state itself.

(5) Condensation of vacancies.

In the present observations described above, no evidence of the extrinsic origins of dislocations ((1)-(3)) were obtained. Thus, we can concentrate on the intrinsic origins ((4) and (5)), and these will be discussed in some detail in the following.

Dislocation inheritance from the liquid

Dislocations are considered as being inherited from the liquid, which is medelled as a coagulation of a large nember of dislocations.

The formation mechanism of dislocations based on the consideration of the liquid structure has been put forward by Ookawa[9]. In a practical time scale of growing and annealing of a crystal, dislocations of at leaset about 10^3 cm/cm^3 remain

inevitably in the crystal according to his calculation. However, this conflicts with the present result in which the crystal near the growing interface is dislocation-free, as was shown in Fig. 4.1.

Suzuki [8] proposed that under a small supercooling, phase separation with respect to the dislocation density must occur in the solid-liquid interface and the dislocation-free phase (solid phase) and that with numerous dislocations (liquid phase) can exist stably. The density of dislocation changes stepwise at the interface from zero to the density of the liquid. Therefore, the crystal always grows without dislocations. This prediction coincides with the observations of Fig. 4.1, i.e., that a dislocation free region exists near the interface. However, this theory of Suzuki also apparently contradicted with the fact that slight increase of growth rate causes the generation of dislocations in the crystal, which was observed in Fig. 4.4 and Fig. 3.10.

According to Kamada [13], the mechanism of dislocation generation can be explained by a dislocation model based on Cotterill's theory. Cotterill[7] believed that dislocations in the interface escape out of the region to the bulk melt and that at the same time the crystal grows without dislocations, and that these excess dislocations will annihilate each other to keep the thermal equilibrium concentration of the bulk melt. This mutual annihilation of dislocations will produce the latent heat of solidification. Based on these assumptions, Kamada evaluated the velocity with which a dislocation escapes out of the interface in to the bulk melt and concluded that this dislocation velocity theoretically arrived at agrees with the upper limit of the growth

rate needed for dislocation-free growth.

According to Kamada's hypothesis, therefore, if the growth rate of crystals exeeds the characteristic growth rate mentioned above, dislocations would be generated at the interface. This expectation is in conflict with the observation in Fig. 4.3 of there being an incubation period in the generation of dislocations during growth. This difficulty applies also for the expectation of Suzuki's theory.

Vacancy condensation

The other model is based on collapsing of vacancy discs which are formed by condensation of excess vacancies. If dislocations are introdeced by the vacancy condensation mechanism, no dislocations should be observed in the crystal adjacent to the solid-liquid interface, because some degree of undercooling is necessary to obtain the excess concentration of vacancies required to form vacency or dislocation loops. However, there have been criticisms against this type of theories.

For instance, Shoeck and Tillar [1] assumed that any excess concentration of vacancies arises solely from a temperature change and that initial vacancy concentration is the equilibrium value at the melting point. However, this equilibrium concentration of vacancy cannot explain the observed density of the vacancy discs or dislocation loops. The argument which had been made against the vacancy condensation mechanism is that high supersaturation of vacancies is needed to form vacancy discs or dislocation loops which can be obtained at quite low temperatures [12],[13].

Bolling and Fainstein [2] tried to modify the theory of vacancy condensation mechanism from the assumption of the trapping of vacancies. They assumed a diffuse interface following Temkin

[14] and suggested that vacancies contained in the liquid would be trapped at the solid-liquid interface advancing into the crystal and concluded that defects due to excess vacancies could be formed at high temperature. This theory can explain the observations shown in Fig. 4.1 to Fig. 4.3 that an increase in the growth rate results in an increase in the dislocation density, because an increase in the growth rate will result in an increase in the number of those vacancies that are trapped by the interface.

Therefore it can be concluded that present observations support the vacancy condensation mechanism of Bolling and Fainstein [2], although actual number of excess vacancies trapped at the advancing interface may be greater than estimated by them, because many dislocation are generated during growth as shown in Fig. 4.3.

This vacancy trapping may occur in order to compensate for the difference of the density of the liquid and that of the solid, in other words, the structural difference of the liquid and the solid. In an ordinary metal such as aluminium, the density of the liquid is less than that of the solid. In other words, the liquid of such metals may contain numerous vacancies. Therefore, it may be presumed that numerous vacancies are trapped at the crystal surface in contact with its melt. Consequently, dislocations are likely to be generated during growth by vacancy condensation mechanism.

On the contrary, in materials such as silicon and gallium, in which the density of the liquid is greater than that of the solid, the number of vacancies trapped at the solid-liquid interface may be less than that in an ordinary metal. Therefore, crystals with high perfection may be obtainable in these

materials. However, this presumption must be confirmed from observations on other materials, such as bismuth and antimony.

To grow crystals with high perfection, this presumption on the origin of dislocations necessitates certain growing conditions such as that crystals should be thin and the temperature gradient should be small.

Growth theories based on the dislocation models of liquid [1],[2], seem to have some shortcomings at the present time.

4.5.   CHAPTER SUMMARY

In the observation of dislocation configuration during growth process, a region without dislocation was observed near the solid-liquid interface in aluminium single crystal. In the case of rapid growth faster than 40 μm/s in the present experiment, numerous dislocations were generated in the crystal after the passage of the interface.

In the growth of gallium single crystal from a highly perfect seed, dislocations were not generated over the whole crystal under the condition given in the present experiment.

From these observations, the most probable origin of dislocations associated with the growth is considered to be vacancy condensation.

From this result, unit process of crystal growth from the melt may be supposed to be "atom by atom" process or a process similar to it.

Growth theories which are based on the dislocation models of

the liquid state seem to be unsuitable at the present time.

REFERENCES

(1)　G. Shoeck and W. A. Tiller : Phil. Mag. **5** (1960) 43

(2)　G. F. Bolling and D. Fainstein : Phil. Mag. **25** (1972) 45

(3)　S. Mizushima : J. Phys. Soc. Japan **12** (1960) 70

(4)　A. Ookawa : J. Phys. Soc. Japan **12** (1960) 2191

(5)　D. Kuhlmann-Wilsdorf : Phys. Rev. **10A** (1965) 1599

(6)　I. A. Kotze and D. Kuhlmann-Wilsdorf : Phil. Mag. **23** (1971) 1133

(7)　R. M. Cotterill, E. J. Jensen, W. Damgaard Kristensen and R. Paetsch : J. de Physique **36** (1975) C2-35

(8)　H. Suzuki : Bull. Japan Institute of Metals, **13** (1974) 733

(9)　A. Ookawa : "Crystal Growth" (Shokabo, Tokyo, 1977) in Japanese

(10)　T. Kobayashi and T. Imura : Jpn. J. Appl.Phys., **23** (1984) 1632

(11)　T. Kobayashi, Y. Nishikawa and T. Imura : Jpn. J. Appl. Phys., **25** (1986) 345

(12)　K. A. Jackson : Phil. Mag. **7** (1962) 1117

(13)　K. Kamada : Prog. Crystal Growth Charact. **3** (1981) 309

(14)　D. E. Temkin : "Crystallization Process" (Consultant Bureau, New York, 1966) p.15

CHAPTER 5   DENDRITIC GROWTH OF Al-Mg ALLOY SINGLE CRYSTALS

5.1 INTRODUCTION

Most of ingots and castings have a dendrite structure and the fineness of dendrites affects the homogeneity of the mechanical properties of the materials. Therefore, numerous investigations have been made both experimentally and theoretically on the mechanism of the dendrite growth and on the factors which affect the fineness of dendrite structure.

For example, experimental investigations have been made on the transition layer between the dendrite arms [1], [2], the preferred orientation of dendrite arms [1], [3]-[5], the relationship between supercooling of the melt and growth rate [1], [6], the tip radius of the dendrite arm [7], [8], dendrite arm spacing [9]-[13], interface morphology [14], [15], etc. In addition, there have been many theoretical studies on the dendrite growth, such as the theory of isothermal dendritic growth [16], [17], the theoretical analysis of the primary arm spacing [18], the theoretical analysis on solute redistribution in dendritic solidification [19], etc. However, most of the experimental studies of dendrite growth which have been made so far are of the type "ex post facto" to the actual process of solidification. In particular, in metals and alloys which are not transparent to visual light, sequential growth of dendrite arms and microstructual change of morphology of dendrite arms during cooling after solidification could not be clarified.

This is the reason why complete clarification of dendrite

growth mechanism has not yet been obtained. Therefore, direct and real time observation has been highly desired to improve this situation.

There have been several reports on real time observations of the solidification process of alloys by optical-[20] and electron microscopy [21], [22]. However, optical microscopy is not powerful enough to observe microstructures of growing interface of alloys which are not transparent to visual light. Electron microscopy is not suitable for the observation of dendrite growth, in particular, for the determination of the spacing of dendrite arms because of the extreme thinness of the specimen used.

Taking the precedings into account, the attempt to use real time X-ray topography, which has already brought us valuable information on the growth mechanism of pure metals [23], has been made to study dendrite growth of alloys. By taking full advantage of real time X-ray topography, observations have been made in the present experiments on the following subjects :

(1) Sequential growth and morphology of the dendrite arms during solidifications as a function of growth rate.

(2) Morphological changes of dendrite arms as a function of Mg content.

(3) Morphological changes and solute redistribution during cooling and isothermal annealing after solidification.

(4) Observation of the melting process of previously grown dendrite.

In the observation of dendritic solidification process by real time X-ray topography, care must be taken in avoiding the

influence of size and free surfaces of the specimen used on the morphology of growth front. Therefore. specimen materials with a small μ. where μ is the linear absorption coefficient for Ag $K_{\alpha 1}$ radiation. and with a relatively low melting point are recommended.

5.2   EXPERIMENTAL PROCEDURES

The present observations have been made with aluminium alloys containing 0.5. 2.0, 4.0 and 7.0 at%Mg. The phase diagram of Al-Mg system is illustrated in Figure 5.1.

Because the strucure of only one grain can be imaged at the same time by the Lang method. Al-Mg single crystals of the compositions mentioned above were prepared by strain-anneal method at first. Hot rolled sheets of 2 mm thick for each composition were cold-rolled to produce sheets of a size about 200 x 20 x 1 mm^3. These sheets were chemically polished and pre-annealed at 800 - 870 K for 1.5 hours. Strains varying 1 to 5 % were introduced to these sheets by tension followed by annealing just under the melting temperature for 7 hours. Grains with a surface area of larger than 70 mm^2 were used as specimens for the observation. The crystallographic orientaions of the surfaces of the specimen thus prepared and the relationship between strain and grain size in the strain anneal method are shown in Figure 5.2. These single crystals were spark cut into smaller specimens of about 20 x 4 mm^2, and chemically polished in the solution of 3 parts HNO_3. 19 parts $HClO_4$ and 190 parts CH_3COOH (by volume). The specimens thus obtained had a length of about 20 mm. a width of
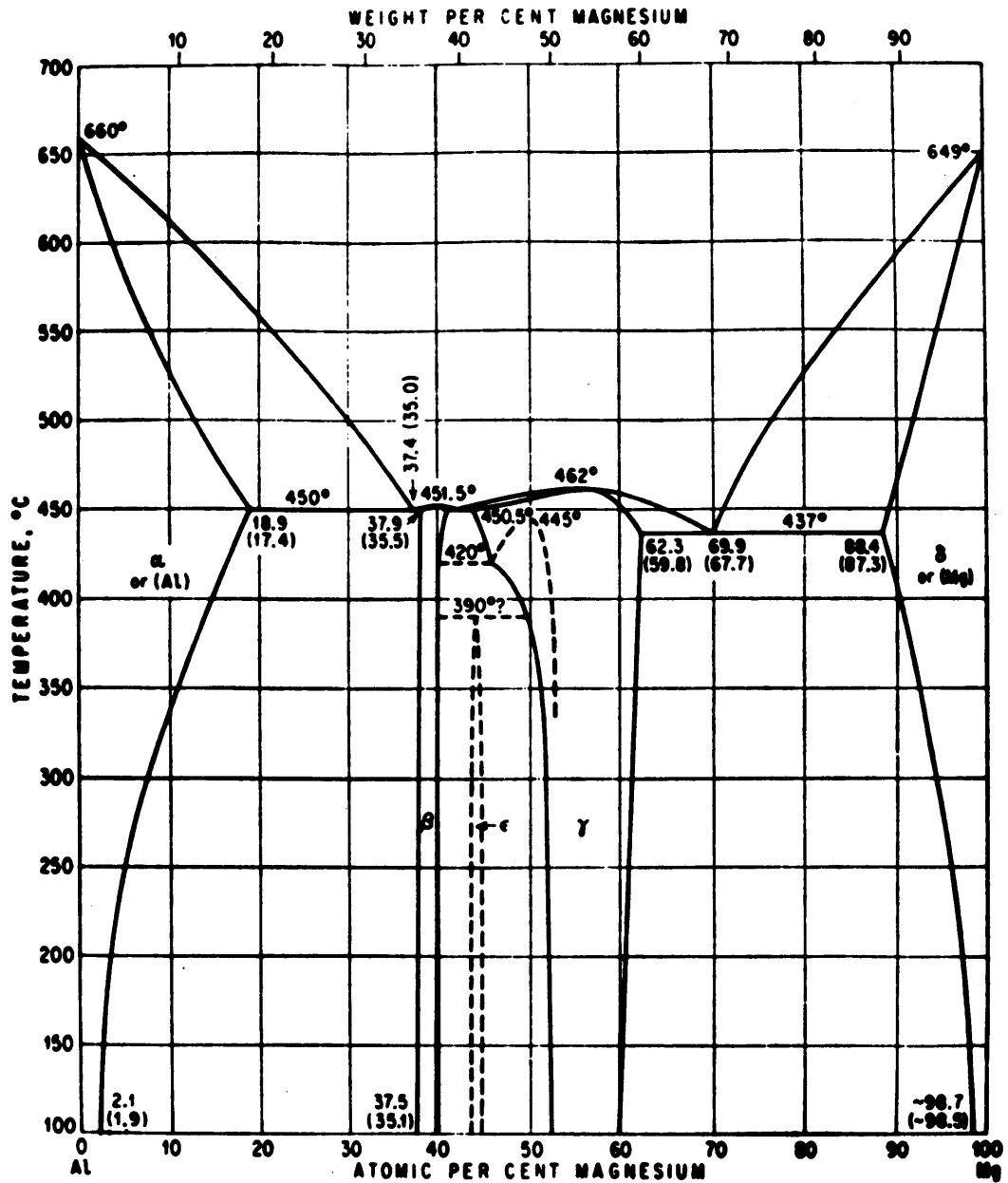
Figure 5.1 Phase diagram of Al-Mg binary system. Specimens used in the present study contain 0.5, 2.0 and 4.0 at % Mg.

about 4 mm and a thickness of 0.8 mm.

With the aid of the furnace[24] shown in Fig. 5.2, unidirectional melting and solidification processes were observed by real time X-ray topography. The topographic images were also recorded on Ilford-L4 nuclear research plates, if necessary, to observe at a higher resolution.

5.3   EXPERIMENTAL RESULT

5.3.1   Interfacial Morphologies as a Function of Growth Rate

Figure 5.3 shows topographs of dendrite morphologies in the solid-liquid interface in Al-4.0 at%Mg alloy recorded on nuclear research plates. In Fig. 5.3 (a), the growth rate of primary- or tertiary arms in the region indicated by A and B with arrows were 53 μm/s and 130 μm/s, respectively. In the present study, growth rate means that of primary arms, unless otherwise indicated. Higher-order (secondary, tertiary, and so forth) arms indicated by the arrows with the respective number can be seen in this figure. Here, "tertiary arms" means the arms which grow from secondary arms and "quaternary arms" means the arms which grow from so-called "tertiary arms", and so forth, in this paper. In Fig. 5.3, secondary arms and quaternary arms grew in the same <001> direction and their growth stopped before they impinged on each other. The secondary arm spacing of dendrites grown at a low growth rate (region A) is larger than that of more rapidly grown dendrite (region B). This agrees with the result of conventional
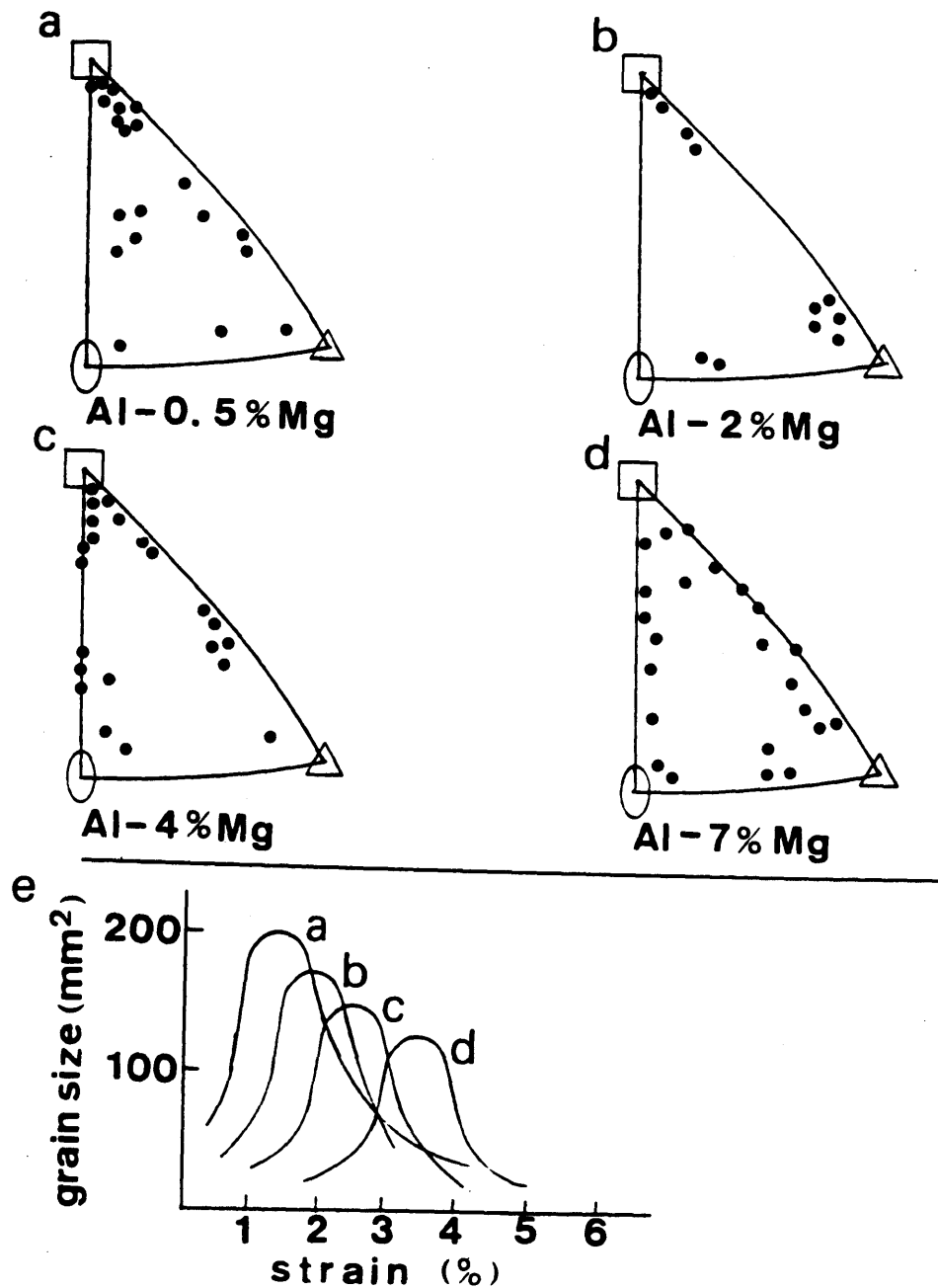
Figure 5.2 Stereo graphic projection of surface directions of recrystallized grains obtained by strain anneal method for Al-Mg alloy of various Mg content (a) (d) and (e) shows relationships between strain and grain size of the alloys illustrated.
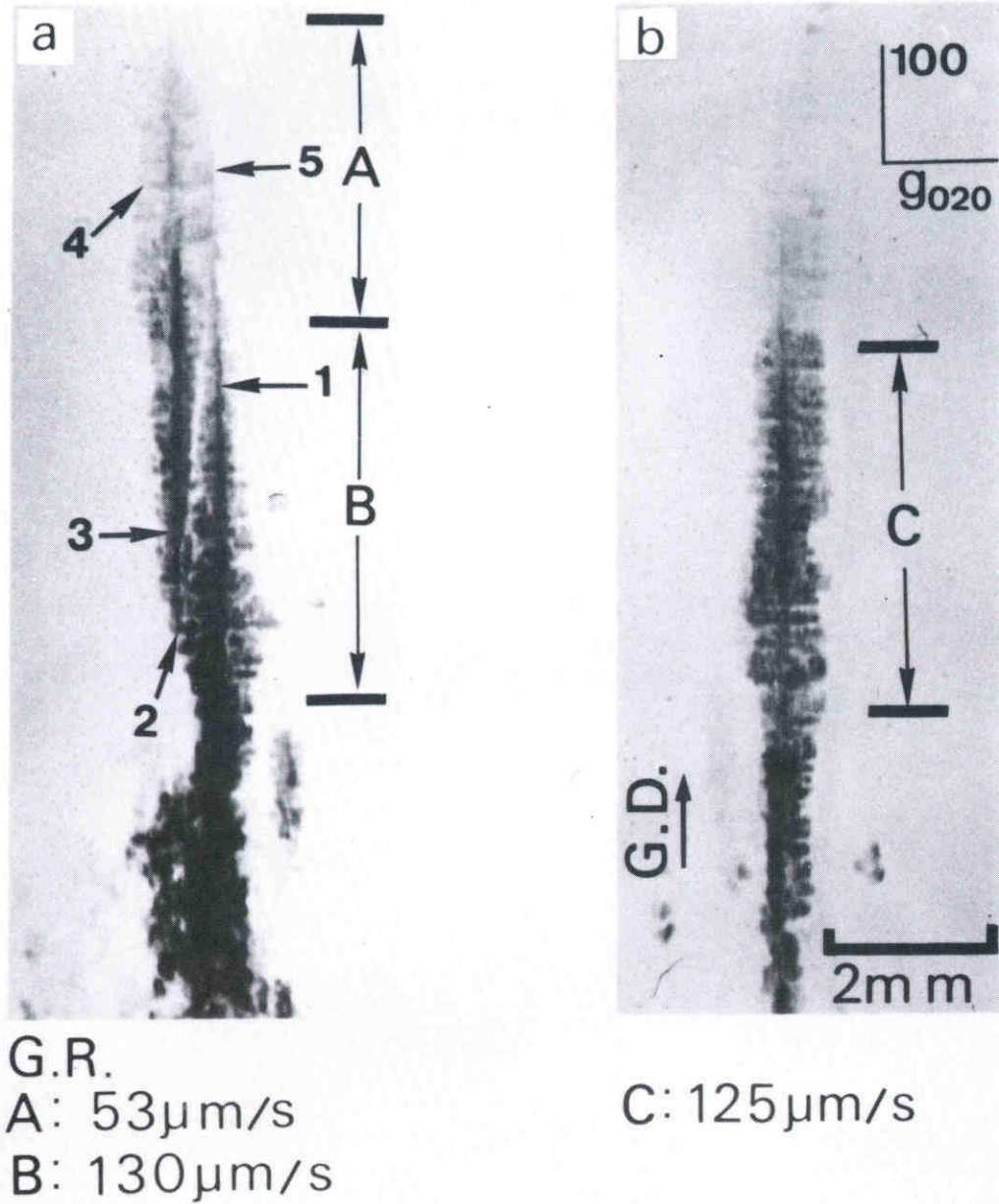
Figure 5.3 X-ray topographs recorded on nuclear research plates showing morphological change of dendrite arms of Al-4.0 at % Mg alloys as a function of growth rate. Growth rate of primary and tertiary arms was (a) 53 μm/s and 130 μm/s in the region indicated by A and B with the arrows, and (b) 125 μm/s, respectively. The growth direction was [100] and reflection vector, g, was [020].

"ex post facto" experiments made on bulk crystals. Therefore, it may be said that growth conditions in the present study are similar to those of bulk crystals. The morphologies of secondary or quaternary arms varied with the change of growth rate. In the larger growth rate region (B), primary and secondary arms have made a right angle with each other. On the other hand, they crossed at an acute angle in the region grown slowly (A). In contrast to this, when the crystal was grown at a constant rate, primary and secondary arms crossed at a constant angle throughout the crystal.

Figure 5.4 is a series of TV images recorded on a video tape during the solidification with gradual increase in growth rate. Time intervals between each topograph and growth rate for each are indicated below each figure. As shown in Fig. 5.4 (a) and (c), secondary arms, which are developed near the tips of primary arms, are observed to make an acute angle to the primary arms. The angle between these secondary arms and the primary arm approached a right angle with the advancement of the tip of the primary arm (Fig. 5.4 (d) and (e)). On the contrary, if the growth rate became faster (Fig. 5.4 (f)), the secondary arms extended at an angle neary equal to a right angle near the growth front.

5.3.2 Morphological Change as a Function of Mg Content

Figure 5.5 to Figure 5.7 show morphological changes with the change of growth rate and Mg content. Each image was recorded intermittently on nuclear reseach plate with an exposure of 60 seconds during which dendrite growth was disrupted. In the present
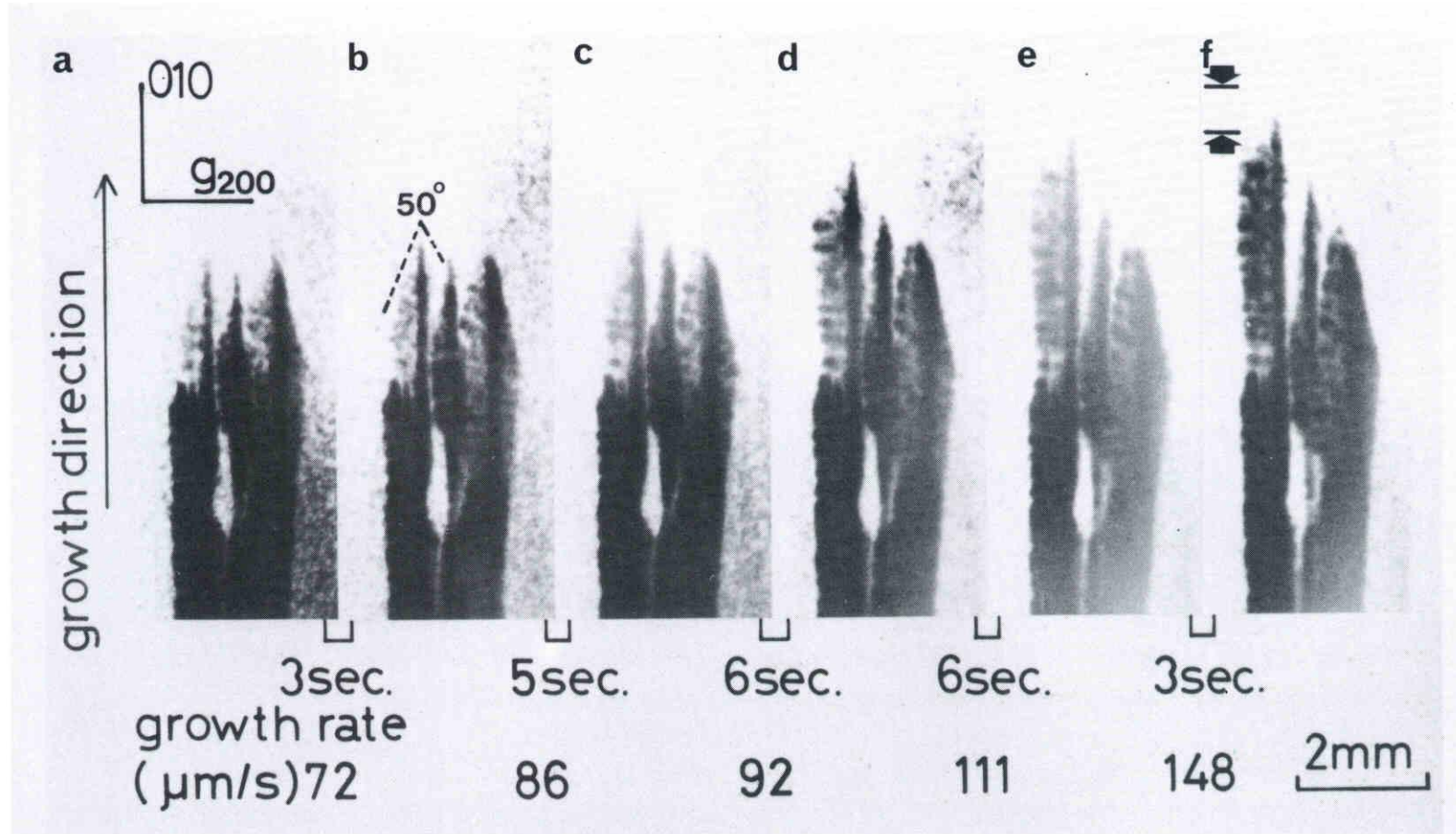
Figure 5.4   A series of X-ray topographs of Al-4%Mg in changing the growth rate continuously.

study, the angle between the primary and secondary arms was measured on the topographs. In an Al-4.0 at%Mg alloy, the angle between primary and secondary arms varied from 72 degree to 90 degree with increasing growth rate from 12 μm/s to 150 μm/s (Fig. 5.5). The same tendency was observed in an Al-2.0 at%Mg alloy (Fig. 5.6) and in an Al-0.5 at%Mg alloy (fig. 5.7). Furthermore, at the same growth rate of 150 μm/s, the angle between the primary and secondary arms was different, i.e., 90 degree in an Al-4.0 at%Mg alloy and 69 degree in Al-0.5 at%Mg alloy, respectively.

Interrelations among the angle between primary and secondary arms, growth rate and Mg content are indicated in Figure 5.8. The observation could not be made on growth rate faster than 150 μm/s because it was very difficult to interrupt the growth immediately. However, it may be predicted, for example, in an Al-0.5 at%Mg alloy that secondary arms would make a right angle to the primary arms at a growth rate exeeding 200 - 300 μm/s.

5.3.3   Dendrite Morhpologies Solidified in other Crystallographic
         Orientations in Comparison with <100> direction

Figure 5.9 shows dendrite morphology at the solidi-liquid interface of Al-4.0 at%Mg crystal solidified in <110> direction. These images were obtained with the same crystal and recorded on nuclear research plates during 60 second interruptions in the case of growth rate of 90 μm/s. Fig. 5.9 (b) is an image recorded by rotating the crystal 0.05 degree around the vertical axis relative to the angle of Fig. 5.9 (a).

In <110> direction grown crystals, the dendrite assembly

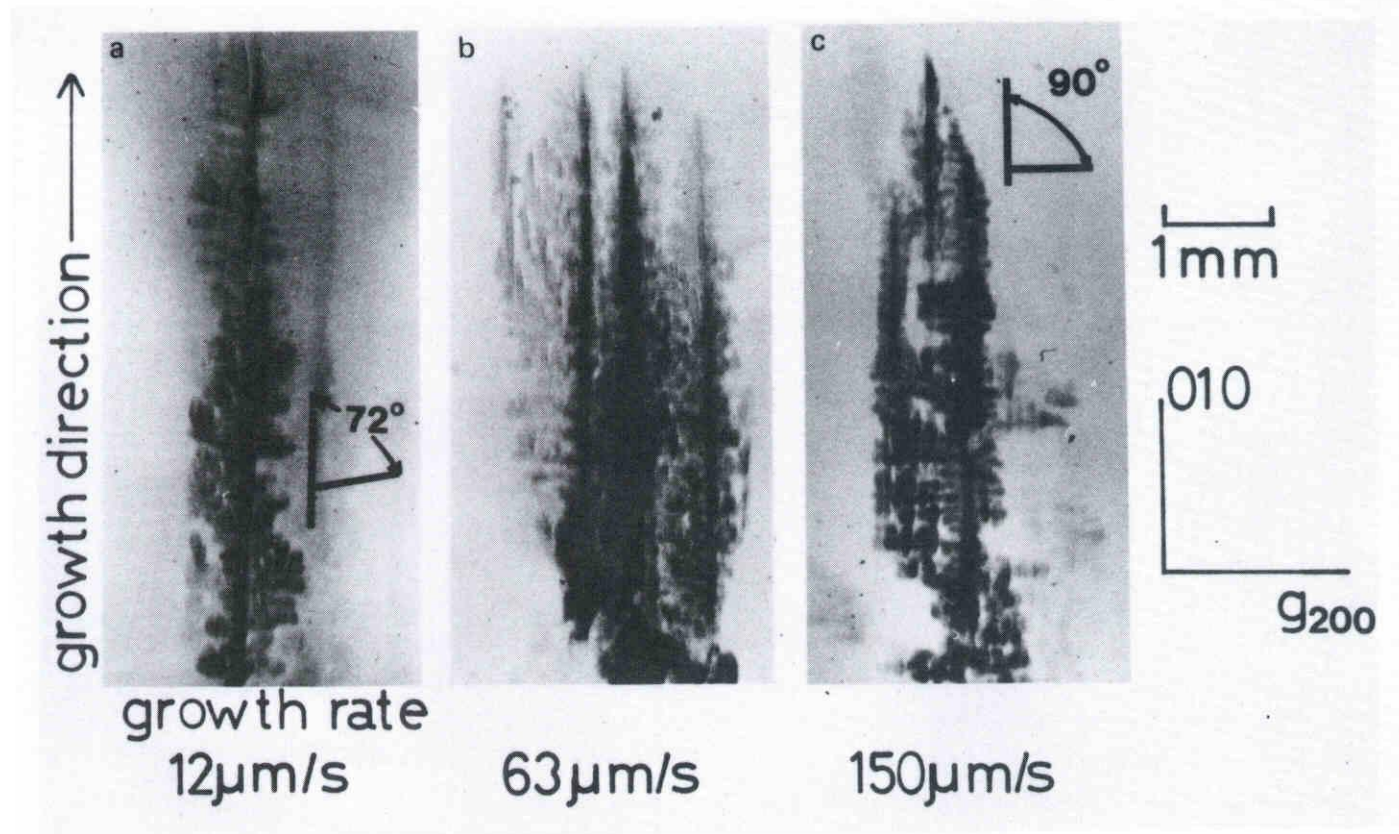Figure 5.5 X-ray topographs illustrating morphological change of dendrites of Al-4%Mg in chaging growth ratefrom 12 - 150 μm/s.
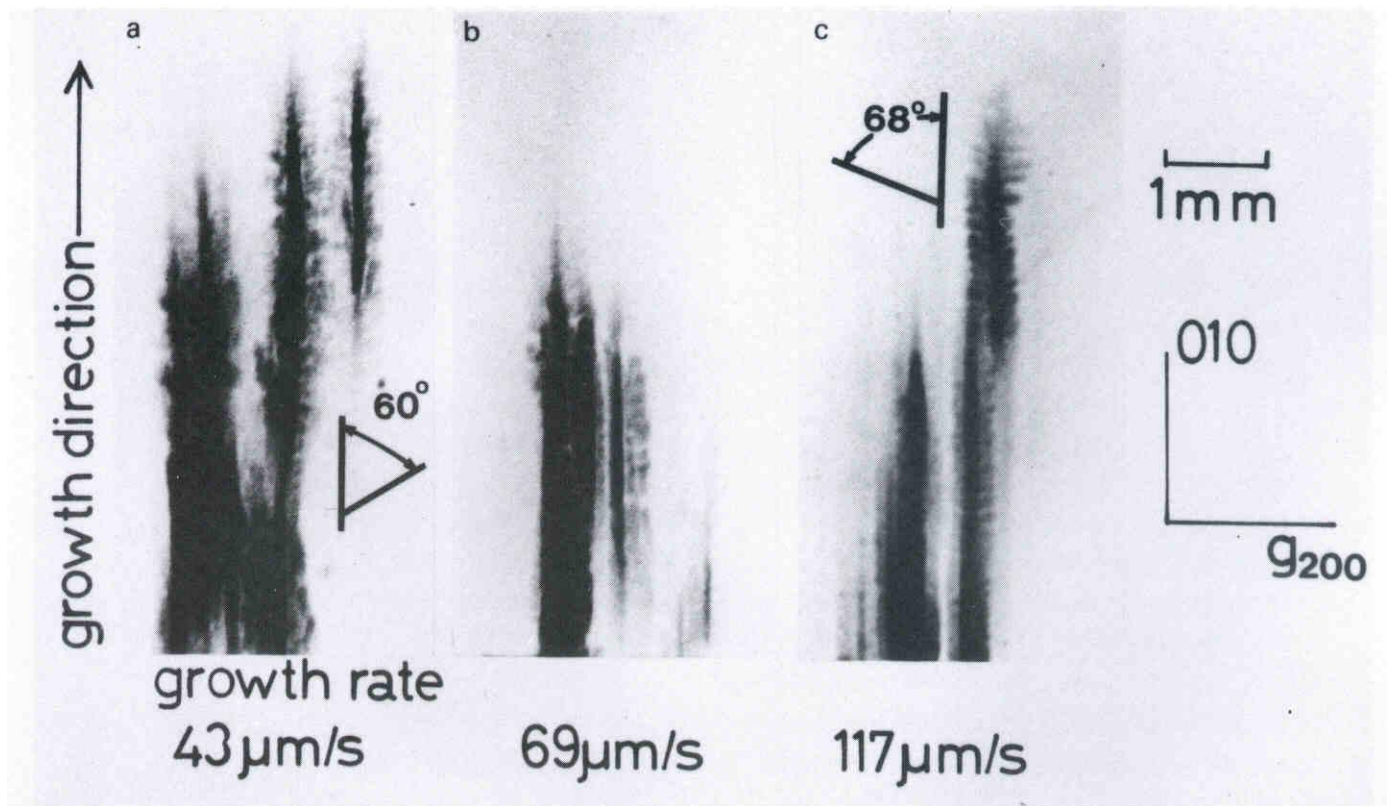
Figure   5.6   X-ray   topographs   illustraing   morphological   change   of
dendrites of Al-2%Mg in chaging growth rates from 43 - 117 μm/s.
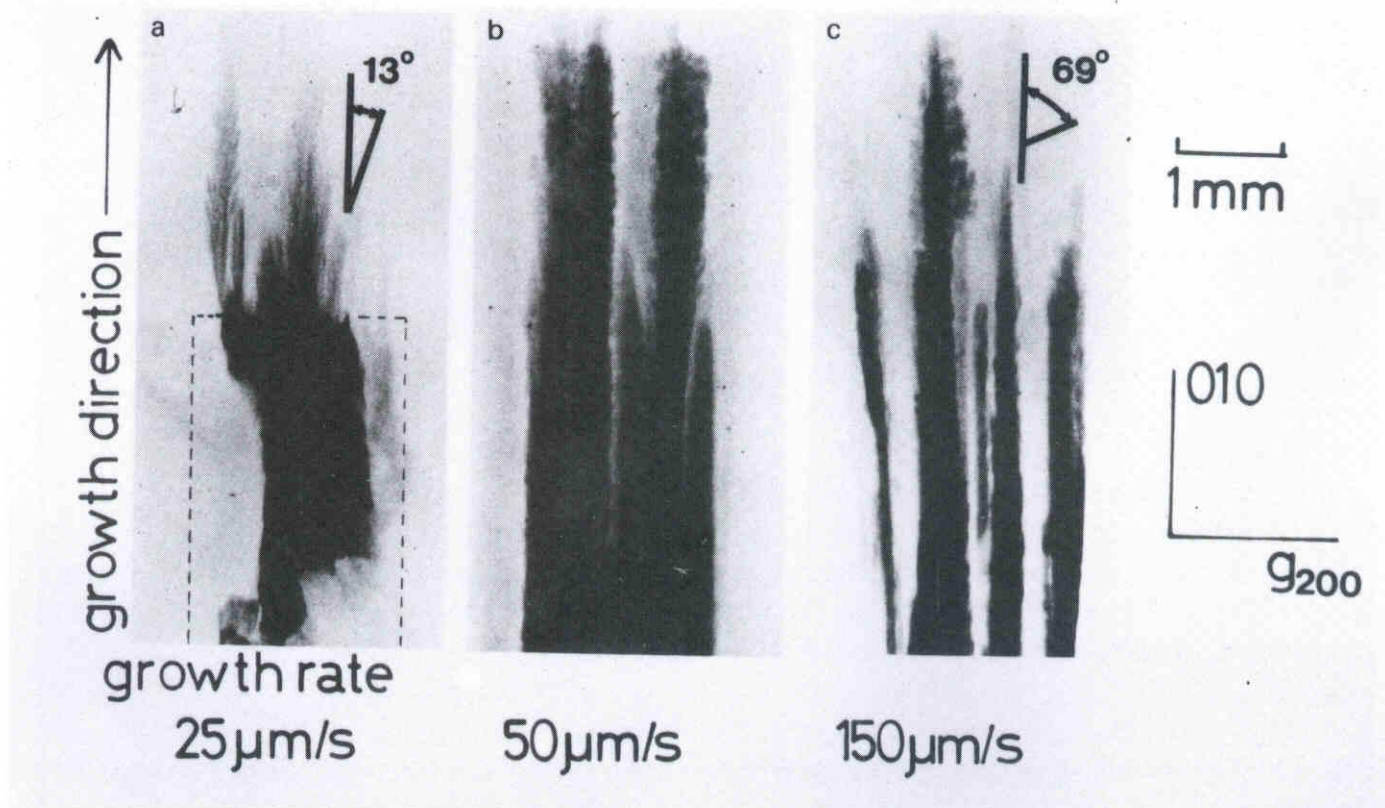
Figure 5.7 X-ray topographs illustrating morphological change of dendrites of Al-0.5%Mg in chaging growth rates from 25 - 150 μm/s.
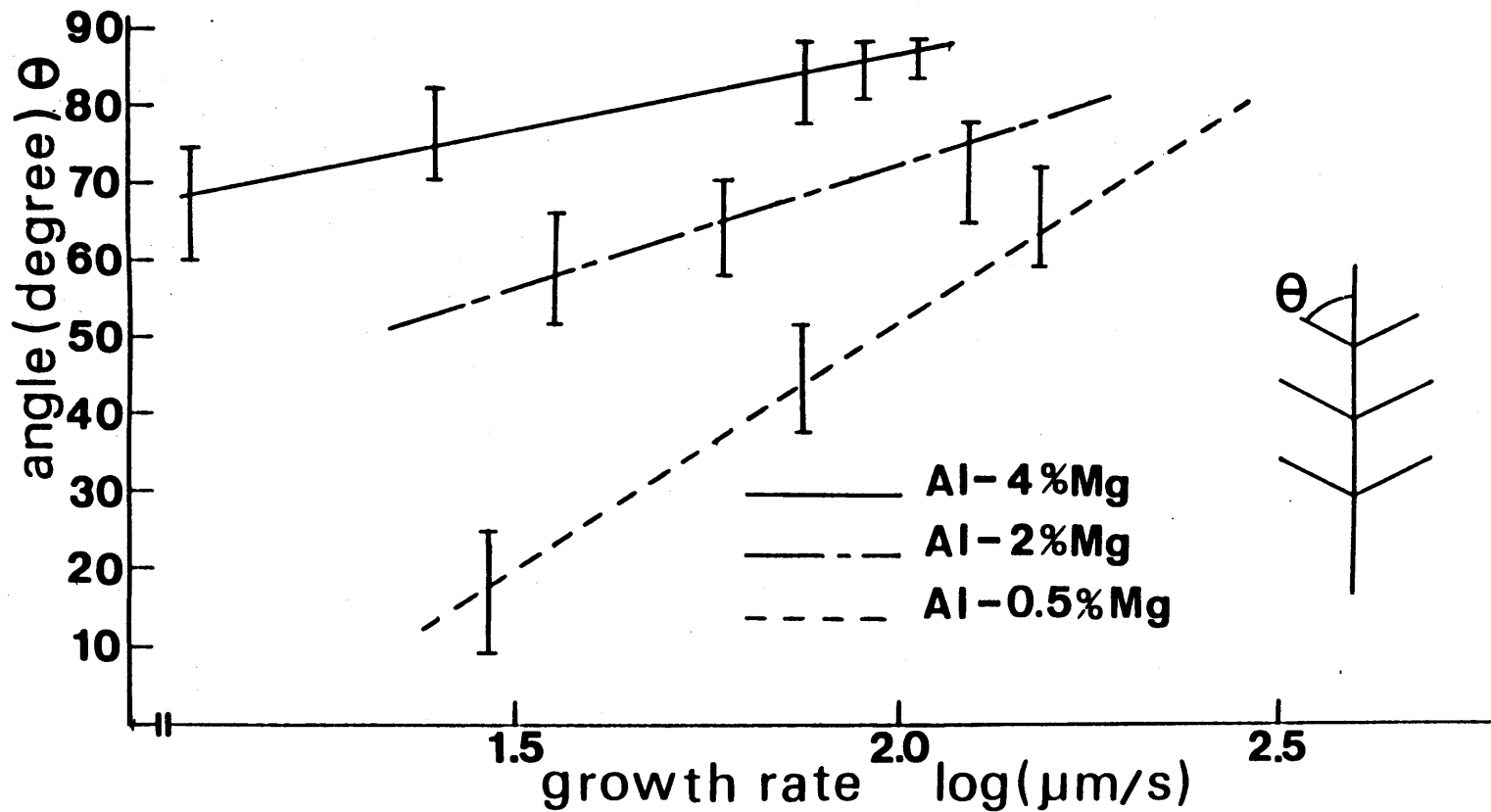
Figure 5.8   Effect of the growth rateand Mg content upon θ.   θ ;   the

angle between primary arms and secondary arms of Al-Mg. The

temperature gradient : 1 K/mm.

showed a "V" type structure[25]. These dendrite arms grew toward two equivalent <100> directions making an angle of 45 degree to the growth direction. No primary arm along <110> was observed and some arms along <100> acted as primary axis.

Figure 5.10 is a series of TV images observed during the solidification process of the same crystal shown in Fig. 5.9. From these topographs, the solidification process in <110> direction can be summarized as follows: i) Two dendrite arms are generated at the same origin and extend in two equivalent <100> directions. ii) These two primary arms grow preferentially and are accompanied by upward growth of secondary arms (Fig. 5.10 (b)). iii) Secondary arms grow upward at a slow speed making right angles with the primary arms. iv) Preferential growth of one of these secondary arms occurs. v) The secondary arm acts like the primary arm and this process of i) to iv) is repeated. The process mentioned above is illustrated schematically in Fig. 5.9.

Dendrite morphology near the solid-liquid interface during solidification in <111> direction is shown in Figure 5.11. These images are recorded on nuclear research plates with a short interruption of growth. In this case, three primary arms should grow in three equivalent <100> directions making an angle of 54.7 degree to the growth direction. However, only one of these arms was observed to grow preferentially owing to the deviation of growth direction from the intended growth direction.

Figure 5.12 shows dendrite morphology of Al-0.5 at%Mg crystal during growth in <130> direction. In the growth rate of 40 μm/s and 10 μm/s, well-defined primary arms were observed to grow in <100> direction.
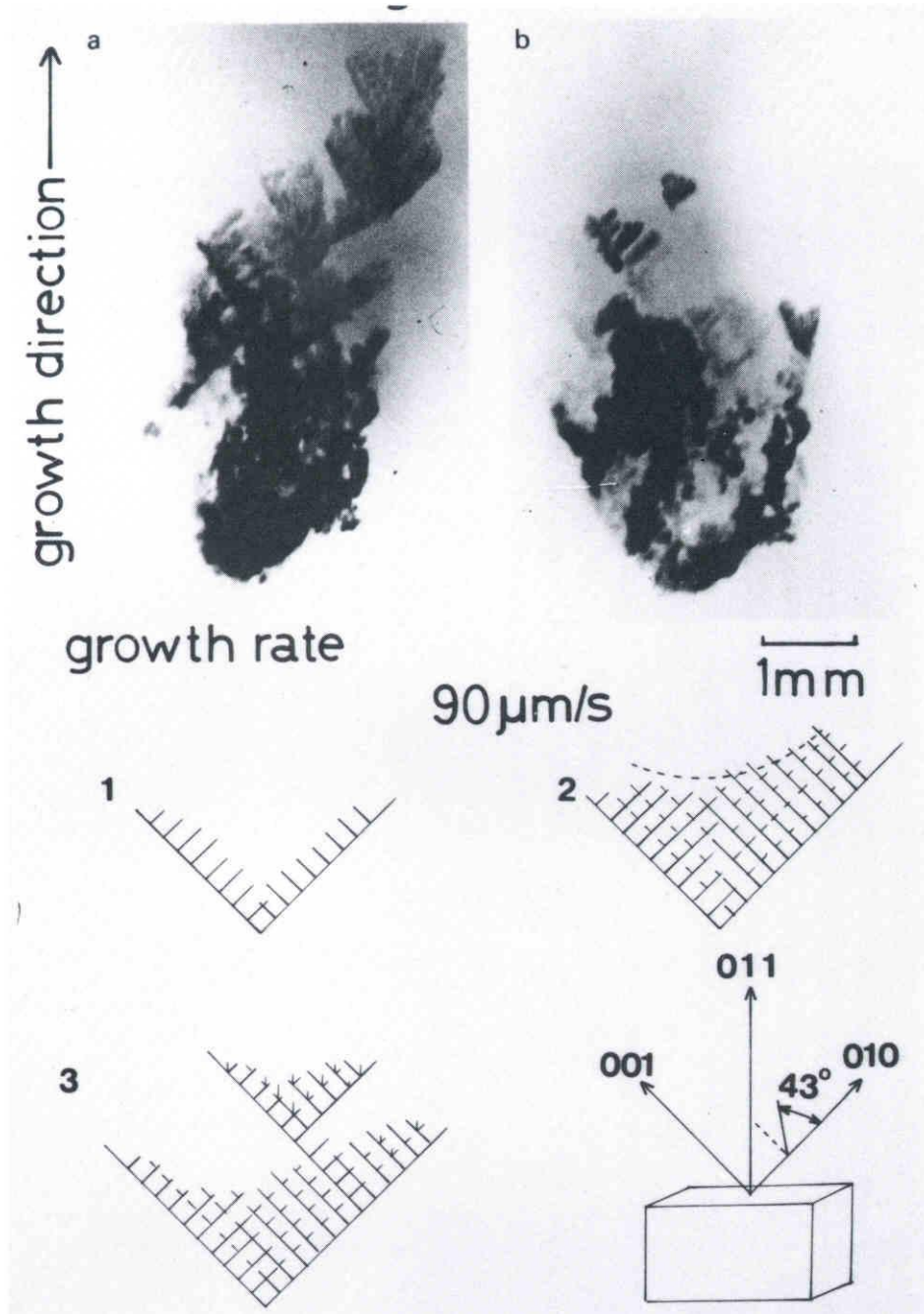
Figure 5.9 Illustration of the change of dendrite morphology of an Al-4.0 at % Mg recorded on nuclear research plates immediately after the growth while the crystal was kept at a fixed temperature during the growth in <110> direction at a rate of 90 um/s. The image (b) is an image recorded by turning the crystal 0.05 degrees around the vertical axis relative to the position of (a). (020) reflection was used.
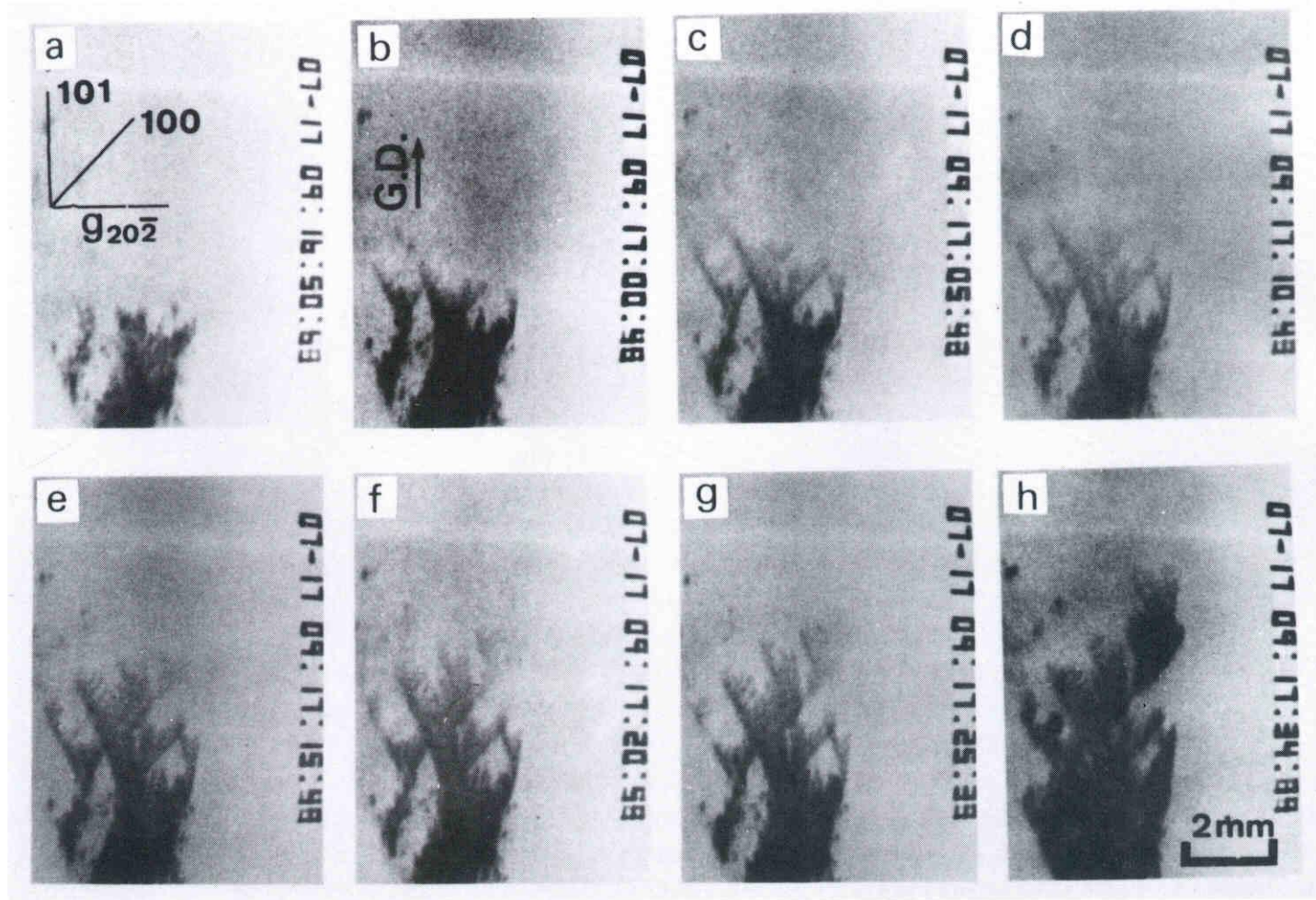
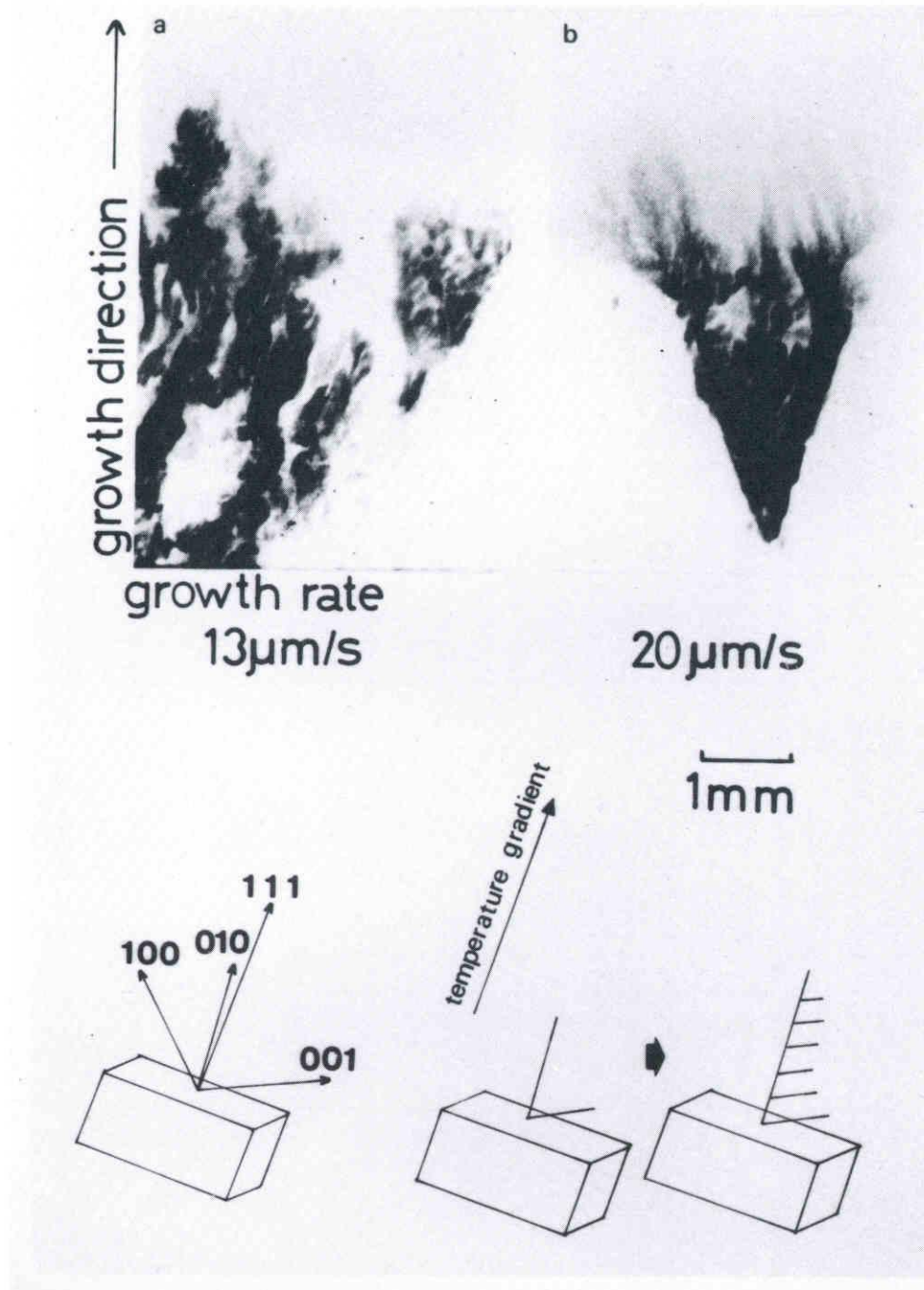Figure 5.10 A series of X-ray topographs of Al-4%Mg during the growing processes.

Figure 5.11 Dendrite morphology of an Al-4.0 at % Mg during ⟨111⟩ growth. The growth rate was (a) ; 13 μm/s and (b) ; 20 μm/s. These images are recorded on nuclear research plates with a short interruption of growth. (002) reflection was used.
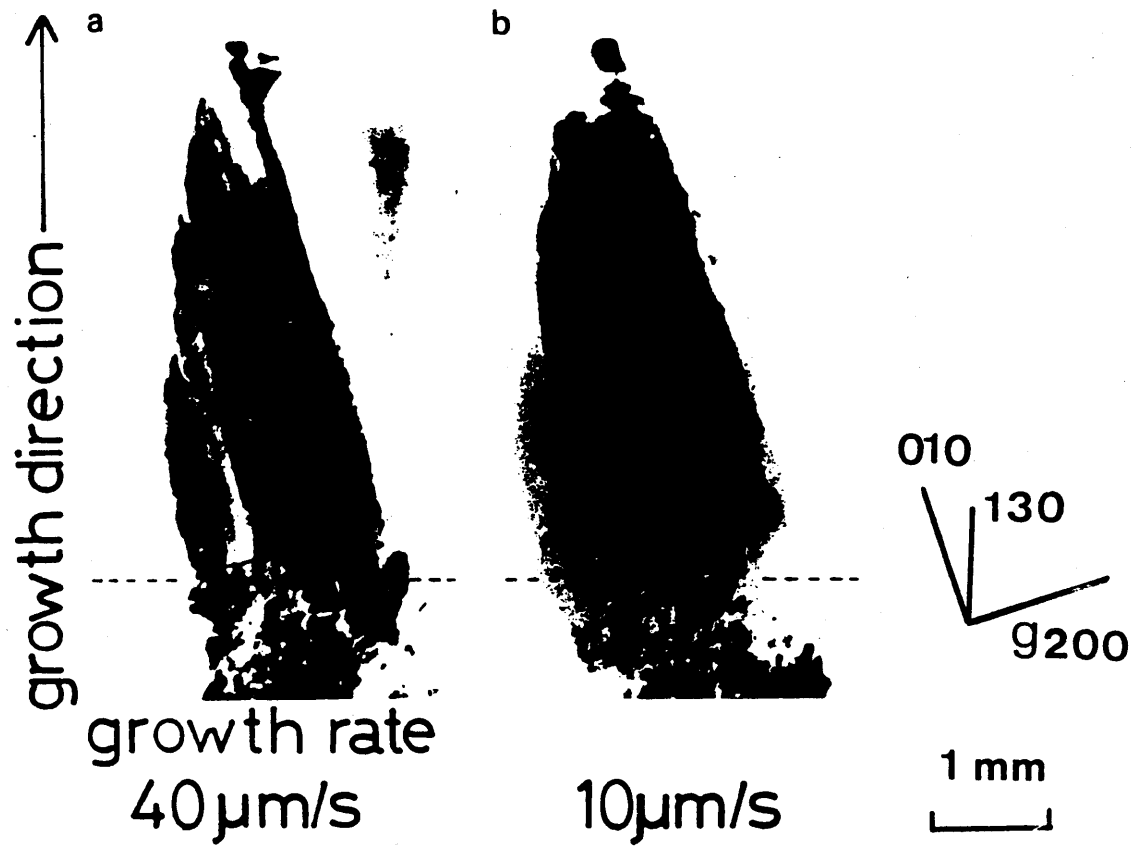
Figure 5.12 Dendrite morphology of an Al-0.5 at % Mg during <130> growth. The growth rate was (a) ; 40 μm/s and (b) ; 10 μm/s. These images are recorded on nuclear research plates with a short interruption of growth. (200) reflection was used.

5.3.4 Morphological Changes during Cooling and Isothermal Annealing after Solidification

Morphological changes of dendrites during cooling and also isothermal annealing were observed by X-ray topography. Topographs shown here were recorded on nuclear research plates except for Figure 5.14.

Figure 5.13 shows a change of dendrite structure of Al-4.0 at%Mg crystal during the cooling process after solidification. In Fig. 5.13 (a), it was observed that primary, secondary, and tertiary arms crossed each other at right angles. After gradual cooling to a temperature 10 K lower than the melting temperature, little change in dendrite morphology was observed. However, dendrite morphology had gradually changed with the decrease in temperature. These morphological changes observed here were mainly due to the change in lattice constant accompanied by the variation of the temperature. In this case of cooling at a relatively small rate, dendrite morphology did not change greatly.

Figure 5.14 shows the morphological change during a more rapid cooling process. Fig. 5.14 (a) to (d) are images of growth process and Fig. 5.14 (e) to (h) are that of subsequent cooling. These images are TV images and the cooling rate in Fig. 5.14 (a) to (h) was about 1 K/s. In Fig. 5.14 (c), the distortion of dendrite arm occurred at the location indicated by arrow, and then further distortions were observed at other locations (Fig. 5.14 (d) to (f)). In Fig. 5.14 (g) and (h), rapid change of dendrite morphology occurred over the whole crystal. The distortion of dendrite arms observed in Fig. 5.14 (a) to (f) is considered to be due to shrinkage at the crystal surface. This
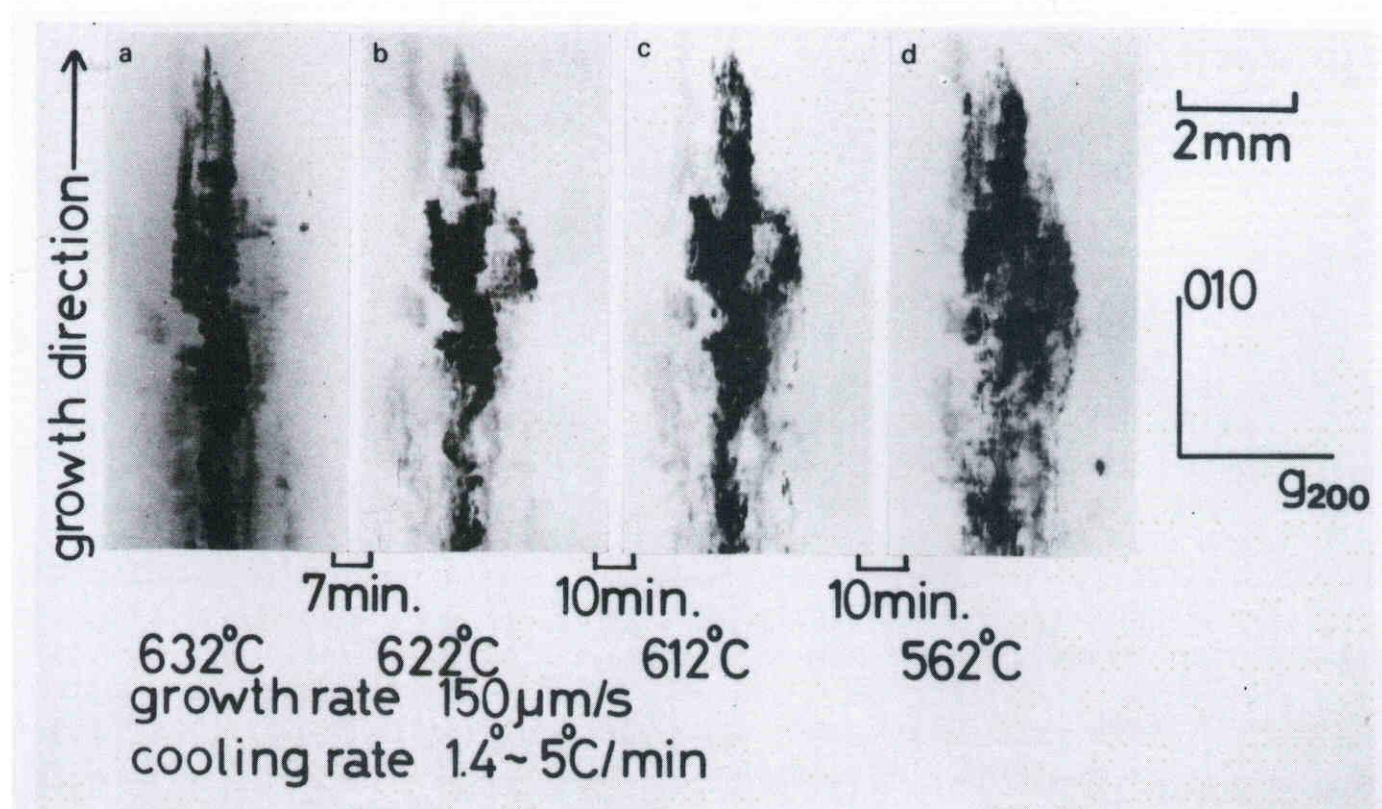
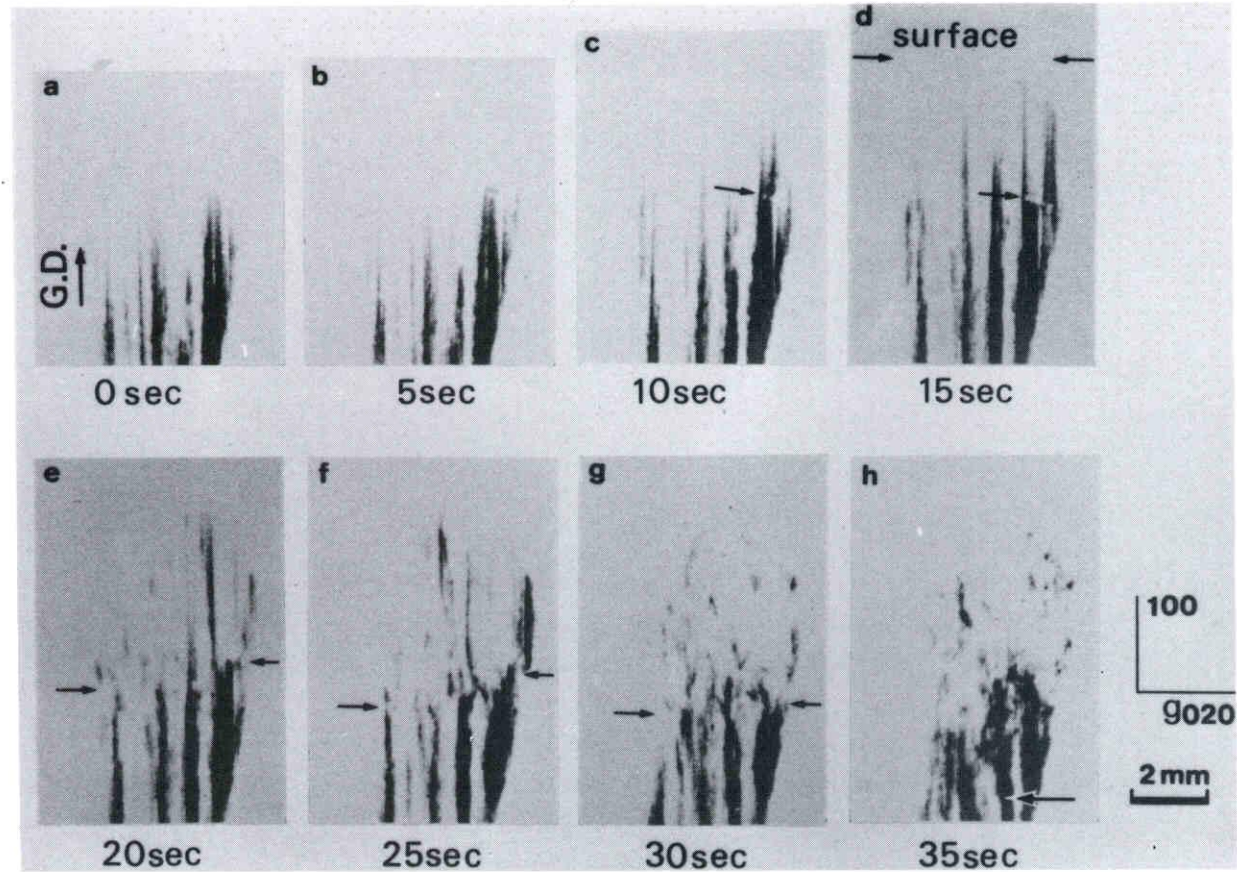Figure 5.13 A series of X-ray topographs of Al-4%Mg during the cooling process.

Figure 5.14 Morphological change of dendrite arms of Al-4.0 at %
Mg during growth ((a)-(d)) and following cooling ((e)-(h)).
Cooling rate was about 1 K/s and the time interval between
each successive topograph was 5 s.

lattice distortion of each dendrite arms is estimated to be about ± 0.3 degree from another observation. The rapid change of the morphology shown in Fig. 5.14 (g) and (h) may occur due to the stress which resulted from segregation of Mg atoms.

Figure 5.15 is a series of X-ray topographs taken during isothermal annealing near the melting temperature. Fig. 5.15 (a) is an image taken just after the growth of dendrite arms. After keeping the temperature constant for 3 minutes, morphological change was observed in Fig. 5.15 (b). Primary arms seemed to become thick by absorbing molten metal and/or secondary arms. However, little change in dendrite morphology was observed between the crystal annealed for 3 minutes and that annealed for 18 minutes at 657 K (Fig. 5.15 (c)).

Morphological change of dendrite arms were also examined during isothermal annealing at a temperature of 100 K below the melting temperature, as shown in Figure 5.16. In this case, little change of dendrite morphology was observed during the isothermal annealing.

Consequently, we conclude that morphological change of dendrite arms during isothermal annealing occurs near the melting temperature in the first few minutes.

5.3.5   Observation of Melting Process

Figure 5.17 illustrates TV images of a melting process after solidification shown in Figure 5.18 of Al-4.0 at%Mg crystal. In this figure, melting proceeds from high-order arms to low-order
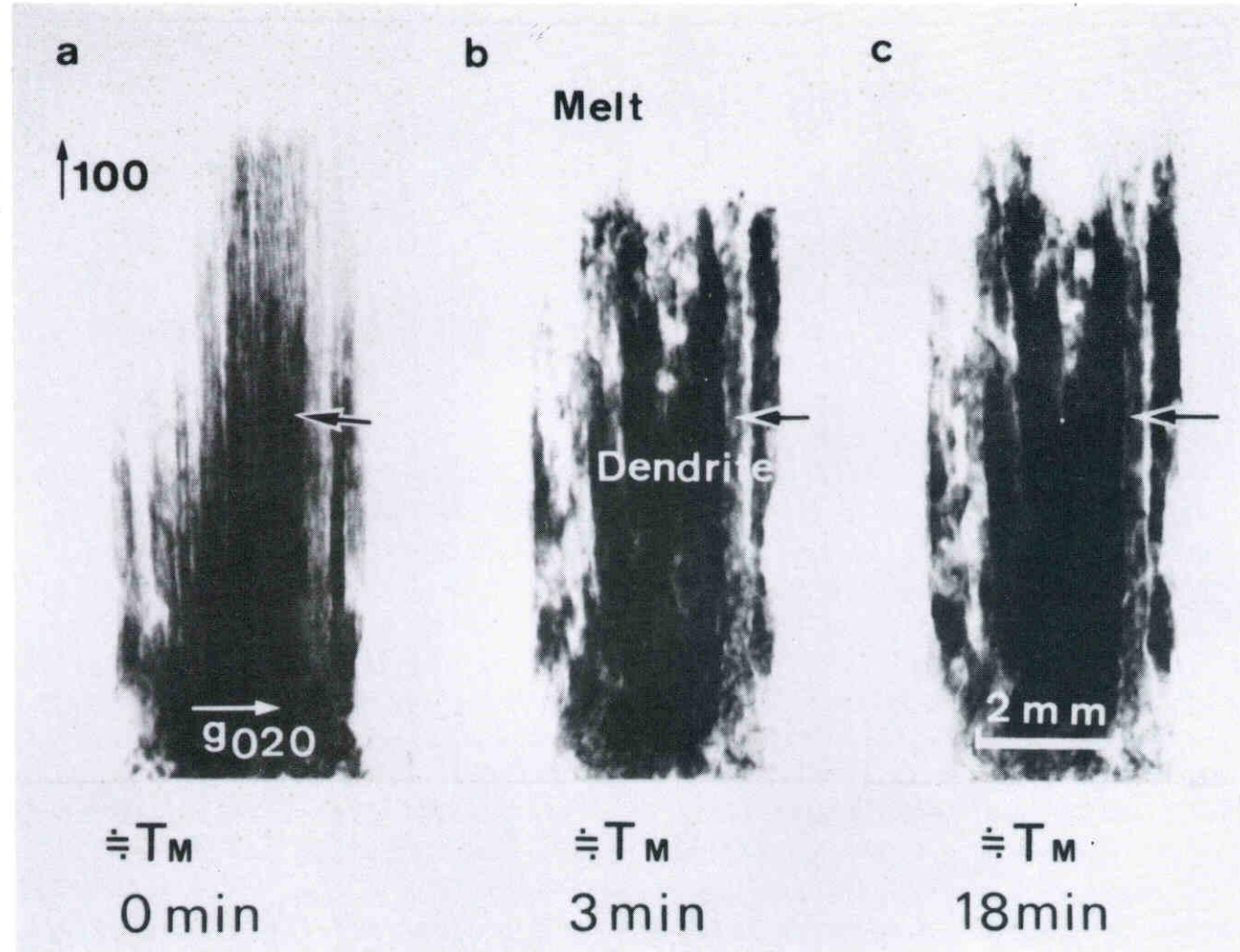
Figure 5.15 Morphological change of dendrite arms of Al-4.0 at % Mg during isothermal annealing near the melting point after solidification. (a) is an image of as grown crystal just after growth, and (b) and (c) are those of the crystal being kept for 3 and 18 minutes, respectively. Each images was recorded on nuclear research plate.
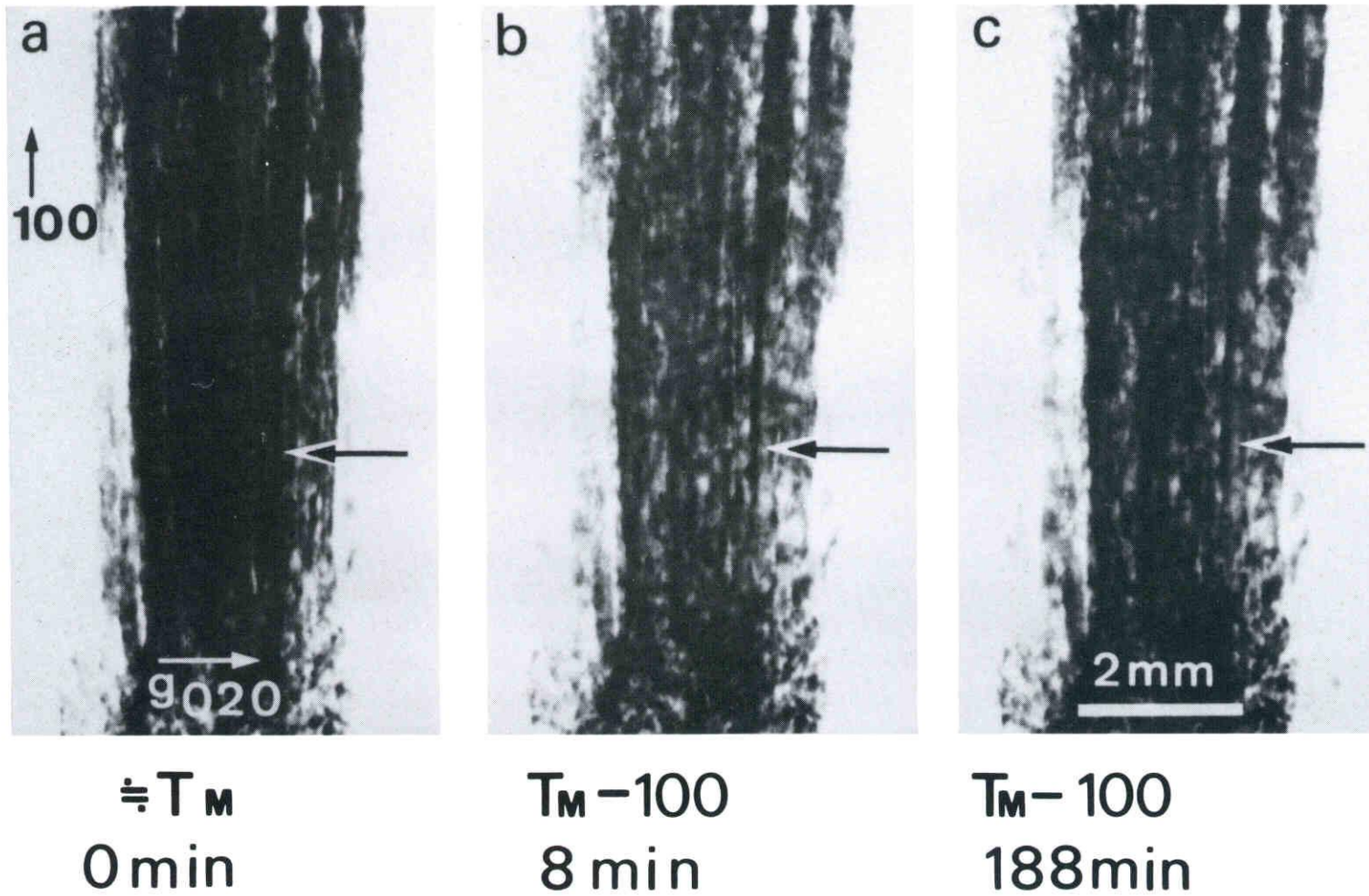
Figure 5.16 X-ray topographs of Al-0.5%Mg showing the morphological changes of dendrite by isothermal annealing at T_m-100 C.

arms. However, macroscopical melting occurred from upper dendrite arms (located at the part with high temperature) to lower arms (located at the part with low temperature). From these results, it can be said that solidification and melting process are not exactly reversed.

Figure 5.19 shows the melting process of an Al-4.0 at%Mg crystal grown in <100> direction. Melting occurred first in high-order arms (secondary or tertiary arms) located near the tip of primary arms (Fig. 5.19 (a),(b)) and melting propagated downward in the high-order arms with increase in tmeperature (Fig. 5.19 (c) to (f)). However, in contrast to the melting process of Fig. 5.17, melting of the primary arms occurred after almost all high-order arms have melted (Fig. 5.19 (g) to (j)).

The above results indicated that there is a difference in concentration profiles of Mg between the crystal grown in <100> direction and that grown in other direction. The observational result that the solidification and melting processes are not exactly reversed can be explained by considering a partial redistribution of solute atoms after solidification.

5.4 DISCUSSION

Morphological changes of dendrite arms as a function of growth rate and concentration of Mg content

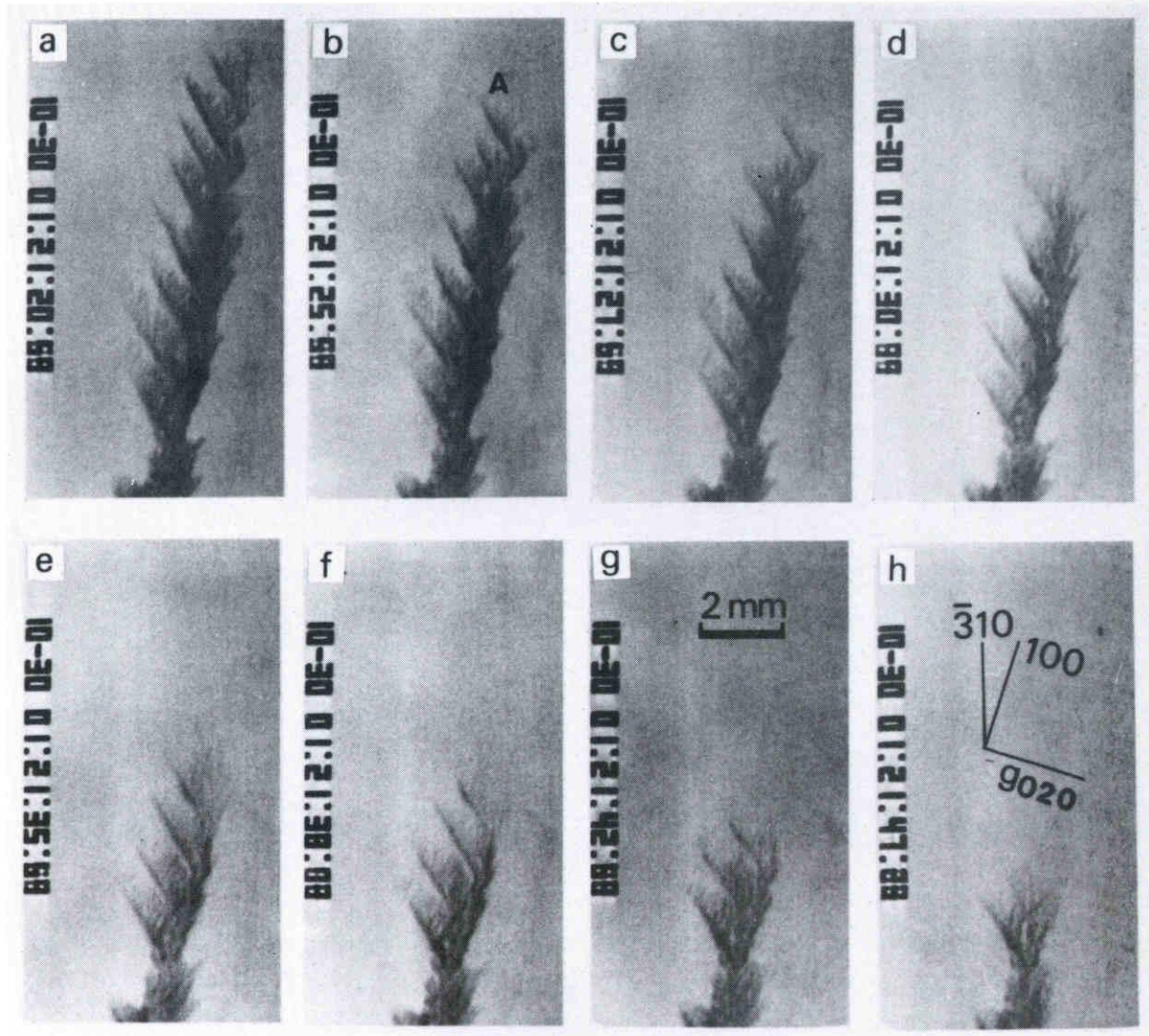The present real time X-ray topographic observations shown

Figure   5.17   A series of X-ray topographs of   Al-4%Mg
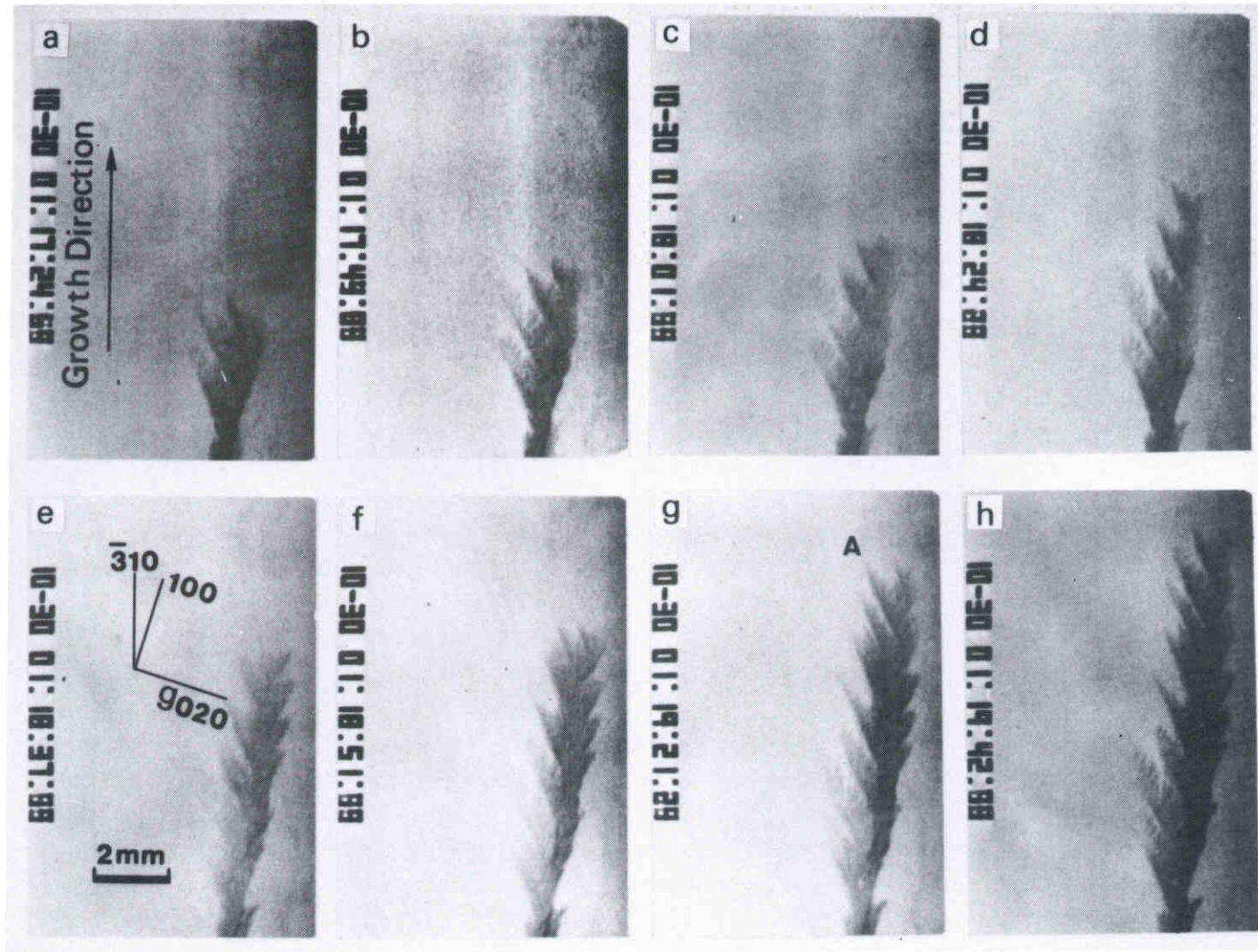during the melting process.

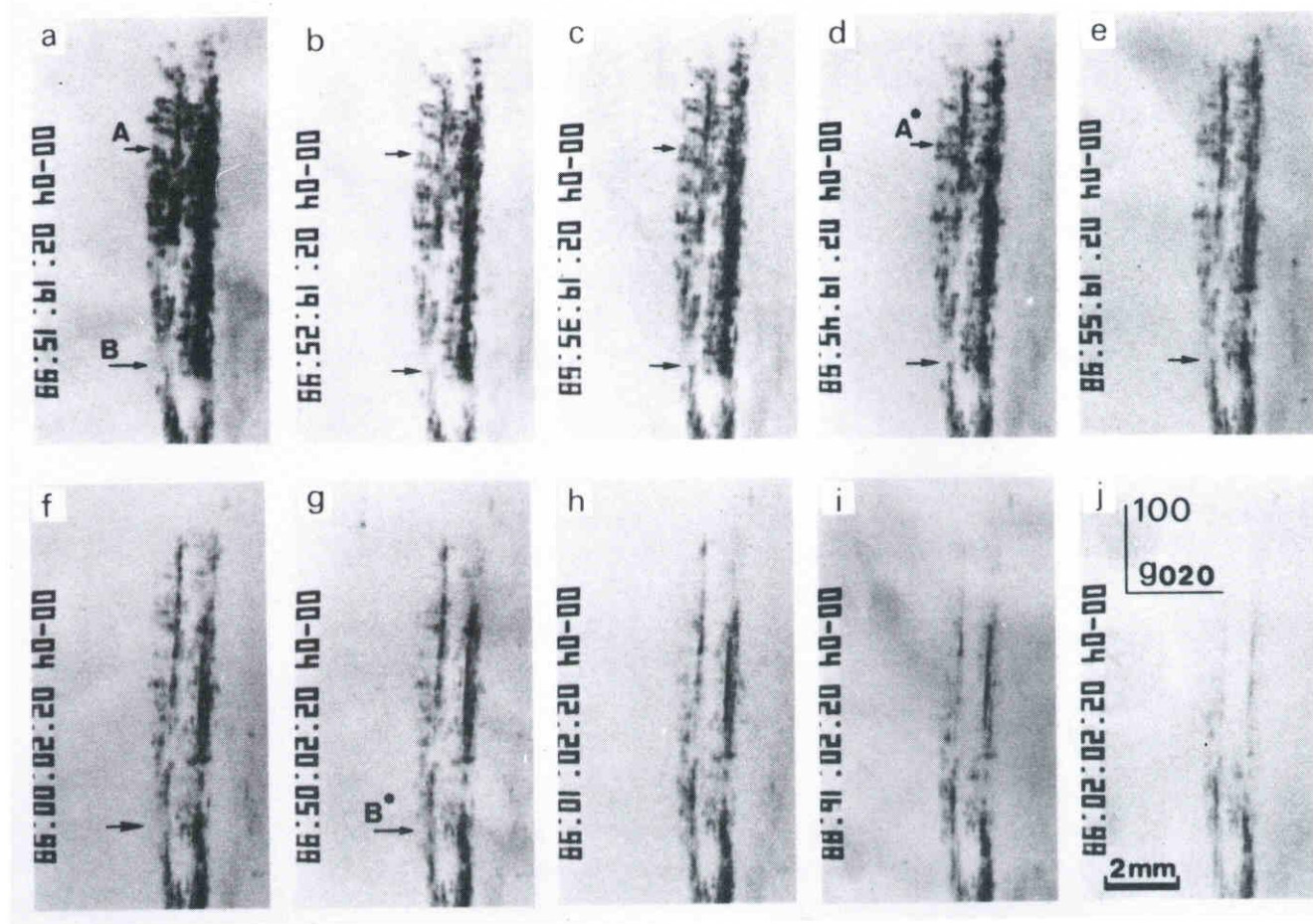Figure 5.18 A series of X-ray topographs of Al-4%Mg during the growing processes.

Figure 5.19 A series of X-ray topographs of Al-4%Mg during the melting process.

that, the angle between primary and secondary arms is found to be dependent on the growth rate and initial Mg concentration, and not necessarily to be a right angle (Fig. 5.3 and Fig 5.5 to Fig 5.7).

Parameters which are related to growth rate of secondary arms and concentration of alloying element in dendrite arms are considered by conventional "ex post facto" studies to be as follows:

(1) Tip radius of primary arms

The tip radius decreases with increase of the growth rate[26], namely, the tip radius at a low growth rate (Fig. 5.5(a), for example) is larger than that at a high growth rate (Fig. 5.5(c)). Secondary arms generate and extend so as to minimize the surface energy, i.e., they make a right angle to the surface of primary arms. Therefore, if the secondary arms generate at the tip of the primary arms, it is possible for the primary and the secondary arms to make an acute angle at a low growth rate. However, it has been pointed out [27] that the distance between the tip of the primary arm and the location at which secondary arms generate increases with the increase of the tip radius. Consequently, this tip radius may be independent of the angle between primary- and secondary arms.

(2) Temperature gradient in the system

The temperature gradient used in these observations is about 1.0 K/mm,which is quite small compared with that used in the conventional studies.

In the case of dendrite growth under a small temperature gradient, a relatively extensive region may be under cooled in the melt near the solid-liquid interface. If secondary arms generate to make an acute angle with primary arms for some reason, they can

grow in the direction which makes an acute angle with the primary arm because of the exsistence of an undercooled region. When the temperature gradient is large near the tip of primary arms, these secondary arms could not extend upward because of the increasing temperature along this direction.

Consequently, the temperature gradient near the tip of primary arms is responsible for the observed morphology of secondary arms.

(3) Concentration of Mg atoms in the dendrite arms

In the case of rapid growth, the concentration of Mg in the liquid near the solid-liquid interface became high because of the Mg content which had been exhausted from dendrite arms, and could not diffuse sufficiently into the liquid due to lack of time interval necessary for a complete diffusion. On the contrary, in the growth at a small rate, the concentration of Mg in the growing dendrite arms approaches the equilibrium concentration. From the observational result shown in Fig. 5.8, the angle between primary and secondary arms approaches the right angle with the increase of the macroscopical growth rate. Therefore, it can be supposed that the angle between primary and secondary arms changes with the concentration of Mg in the growing dendrite arms. This speculation is compatible with the experimental result that the angle is proportional to the initial concentration of Mg in the bulk crystal.

Consequently, the generation of secondary arms which make an acute angle with primary arms relates to the concentration of Mg in the growing dendrite arms.

Morphological change during cooling and isothermal annealing

after solidification

Rapid change of dendrite morphology was observed during growth and successive cooling at a rate of 1 K/s (Fig. 5.10). At first, lattice distortion of dendrite arms takes place during cooling, which may be due to stress generated by shrinkage of crystal. The subsequent change of dendrite morphology which occurs over the whole crystal may be caused by the internal stress originated from segregation of Mg atoms (Fig. 5.9). Therefore, morphology observed examined metallographically after the solidification may differ from that during or just after the solidification.

As can be seen in Fig. 5.11, the morphological change of dendrite arms also occurred during a few minutes after isothermal annealing near the melting temperature. In this case, primary arms seemed to thicken by absorption of secondary arms. This change of dendrite morphology was observed only near the melting temperature in the time interval of present observation. This morphological change may be caused by diffusion into the solid.

In this way, morphological changes of dendrite arms can be observed by real time observations using X-ray topography during cooling just after solidification with the temperature being kept near the melting temperature. This is one of the reasons why real time observations using X-ray topography are necessary to the study of dendritic growth.

Morphologies of dendrite in different crystallographic orientation

In the observations of Fig. 5.9 to Fig. 5.13, dendrite arms grow preferentially in $\langle 100 \rangle$ direction, and dendrite morphology depends on macroscopical growth direction. These findings on the morphology can be explained on the basis of the interrelation between preferential growth direction of $\langle 100 \rangle$ and macroscopical growth direction.

In the case of growth in $\langle 110 \rangle$ direction, two equivalent $\langle 100 \rangle$ directions make an angle 45 degrees to the macroscopical growth direction of $\langle 110 \rangle$ (Fig. 5.20). Therefore, there should be the arms preferentially grown in two equivalent $\langle 100 \rangle$ directions but no distinguished primary arms (Fig. 5.10, 5.20).

If a crystal grows macroscopically in $\langle 111 \rangle$ direction, three equivalent $\langle 100 \rangle$ directions make an angle 54.7 degree to the growth direction. In this case, three arms should preferentially grow in $\langle 100 \rangle$ directions. However, this ideal growth should be sensitive to the condition existing in the growing system. If one of these equivalent $\langle 100 \rangle$ directions approaches the macroscopical growth direction, preferential growth of dendrite arms should occur (Fig. 5.12).

In the case of growth in $\langle 130 \rangle$ direction shown in Fig. 5.12, primary arms were observed to grow along one $\langle 100 \rangle$ direction preferentially because there is only one $\langle 100 \rangle$ direction close to the macroscopical growth direction.

Consequently, it may be concluded that preferential growth directions of dendrite arms are unaffected by overall macroscopical growth direction.
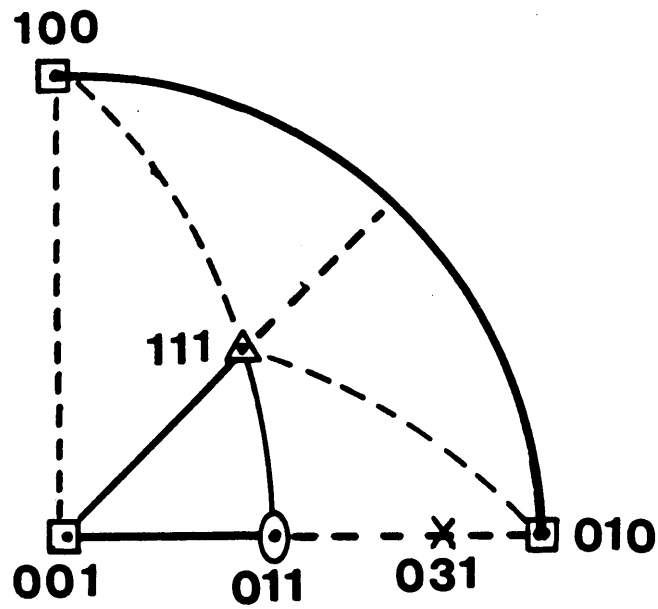

Concentration profiles of Mg

Figure 5.20   Relation between preferen-
tial direction of dendrite arms
{100} and macroscopical growth
direction.

From the observations of the melting process, concentration profiles of Mg at different parts of the dendrite arms have been estimated. According to the phase diagram of Al-Mg system, a part with a low melting temperature has a high concentration of Mg in the present range of concentration.

In <100> direction growth, the melting occurred at first in the high-order dendrite arms. After most of these arms had been melted, primary arms began to melt from tip to lower part. Therefore, it may be presumed that there is considerable difference in the concentration of Mg content between primary arms and other high-order arms.

The concentration profiles of Mg in columnar dendrite are estimated from these observations and illustrated schematically in Figure 5.21. Also, it may be pointed out that experimental results of concentration profiles obtained at room temperature with "ex post facto" method differ from the profiles of just after the solidification.

5.5   CHAPTER SUMMARY

Morphologies of dendrite arms during melting and solidification processes have been observed by real time X-ray topography. Important information, which can not be obtained from the conventional experiment with the static method, has been obtained as follows.

In the observations of dendrite morphologies with variation of growth rate and concentration of Mg, generation and growth of
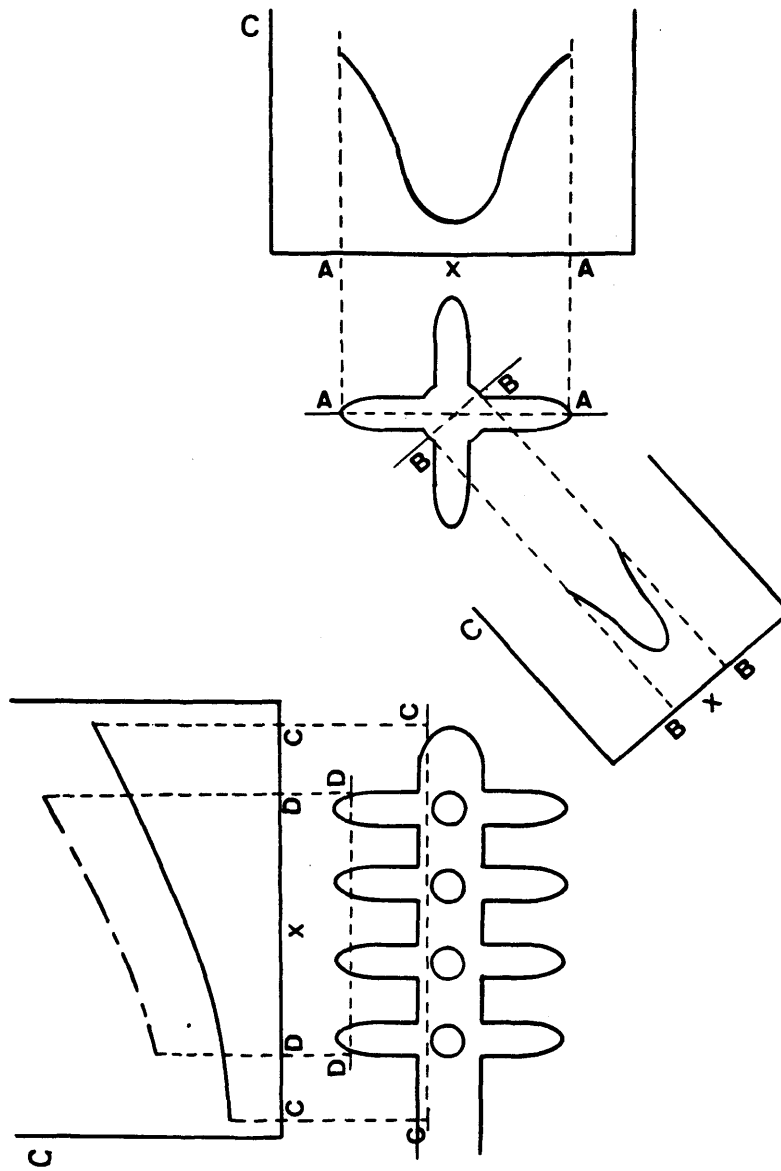
Figure 5.21 Schematic illustration of the concentration profiles of Mg in columnar dendrite.

secondary arms which make an acute angle with primary arms have been observed. The generation of these secondary arms is considered to be related to the growth rate and the concentration of Mg content in the growing dendrite arms. The temperature gradient in the liquid near the solid-liquid interface may be responsible for the growth of these secondary arms.

In the observations of morphological changes of dendrite arms have been observed during cooling and isothermal annealing. Morphology of dendrite arms changes just after the solidification during slow rate cooling such as 1 K/s. At first, lattice distortion of dendrite arms takes place followed by morphological change of dendrite arms over the whole crystal. These morphological changes may be caused by stress due to shrinkage of crystal or segregation of Mg atoms. During cooling at a speed less than 8×10^{-2} K/s, changes of dendrite morphology have rarely been observed.

Morphological change of dendrite arms has been also observed during isothermal annealing near the melting temperature. This change is caused by diffusion in solid.

In the observations of dendrite morphology with variation of crystallographic growth direction, dendrite arms alway grow in <100> directions at a proper growth rate. It is concluded that growth directions of dendrite arms are independent of macroscopical growth direction.

From the observations of melting process, concentration profiles of Mg in dendrite arms have been estimated and provided such information that there is considerable difference in the concentration of Mg between primary arms and other high-order arms.

REFERENCES

(1)   F. Weinberg and B. Chalmers : Can. J. Phys. **30** (1952) 488

(2)   F. Weinberg and B. Chalmers : Can. J. Phys. **29** (1951) 382

(3)   J. W. Cahn : Acta Met. **8** (1960) 554

(4)   G. Harvay and J. W. Cahn : Acta Met. **9** (1961) 695

(5)   G. A. Chadwick : Acta Met. **10** (1962) 1

(6)   R. Rosenberg and W. C. Winegard : Acta Met. **2** (1954) 342

(7)   G. Horvay and J. W. Cahn : Acta Met. **9** (1961) 695

(8)   G. F. Bolling and J. W. Cahn : J. Appl. Phys. **32** (1961) 2587

(9)   P. E. Brown and M. Adams, Jr. : Trans. Am. Founddrymen's Soc. **69** (1961) 879

(10)   H. D. Brody and M. C. Flemings : Trans. Met. Soc. AIME **236** (1966) 615

(11)   D. E. Temkin : Soviet Phys. Doklad. : **5** (1960) 609

(12)   W. Kurz and D. J. Fisher : Acta Met. **29** (1981) 11

(13)   D. G. McArtney, J. D. Hunt : Acta Met. **29** (1981) 1851

(14)   C. M. Claren, J. D. Verhoseven and R. Trivedi : Metallur. Trans. **11A** (1980) 1853

(15)   T. Okamoto and K. Kishitake : J. Cryst. Growth **29** (1975) 133

(16)   S. N. Tewari and A. M. Srioammurthy : Metallur. Trancs. **12A** (1981) 137

(17)   K. P. Toung and D. H. Kirkwood : Metallur. Trance **6a** (1975) 197

(18)   W. Morris, W. A. Tiller, J. W. Rutter and W. C. Winegard : Trans. ASM **47** (1954) 463

(19)   E. L. Holmes, J. W. Rutter and W. C. Winegard : Can. J. Phys. **35** (1957) 1223

(20)   H. E. Cline : Trans AIME **239** (1967) 1489

(21) C. Lemaignan, D. Camel and J. Pelisier : J. Cryst. Growth 52 (1981) 67

(22) R. Hamar and C. Lemaignan : J. Cryst. Growth 53 (1981) 586

(23) T. Kobayashi, Y. Nishikawa and T. Imura : Jpn. J. Appl. Phys. to be published

(24) T. Kobayashi and T. Imura : Jpn. J. Appl. Phys. 23 (1984) L632

(25) A. Watanabe, A. Sudo, U. Honma and S. Oya : Aluminium : 58 (1982) 346

(26) W. Kurz and D. J. Fisher : Acta Met., 29 (1981) 11

(27) K. E. Glicksman and P. W. Voorhees : Metallur. Trans. 15A (1984) 995

CHAPTER 6   SUMMARY AND CONCLUSIONS

Full understanding of the structure of crystal surface in contact with the melt is indispensable for elucidation of the mechanism of crystal growth from the melt. However, the structure of the solid-liquid interface of the metal crystals has not yet been elucidated satisfactorily by experiments.

Nevertheless, the structure of the solid-liquid interface has been investigated theoretically, and some models of it have been proposed (Chapter 1).

One of the effective experimental methods for investigating the growth mechanism is direct and real-time observation of the morphology of solid-liquid interface during growth and the effect of lattice defects on it.

The structure of the solid-liquid interface on atomic scale can be inferred from the observation of its effect on the morphology. Furthermore, the mechanism of crystal growth from the melt can be inferred by comparing the observed morphology of the solid-liquid interface with that theoretically predicted.

Real time X-ray topography is a most effective method for observing the morphology of solid-liquid interface during growth, particularly for metallic crystals which are opaque to visual light, because it enables us to observe directly the growth process of of a bulky metal crystal and, the introduction and role of lattice lattice defects, in particular, dislocations in the growing crystal.

For the purpose of the observation of melting and growth

processes of metallic single crystals with relatively high melting temperature continuously, a Lang type topography camera with a high temperature furnace for uni-directional solidification was constructed on a large goniometer of an ultra-high intensity X-ray generator (90 kW class) and a TV-VTR imaging system has been developed (Chapter 2).

With the aid of these facilities, real time observations of melting and growth processes of aluminium and gallium single crystals and growth of Al-Mg alloys have been made by X-ray topography.

In the first place, microscopical structure of the solid-liquid interface and the mechanism of growth from the melt of aluminium and gallium single crystals are clarified (Chapter 3).

In the case of aluminium, whose Jackson's parameter α is about 1.3, it is found under the temperature gradient of 1 - 10 K/mm and growth rate of 12 - 1400 μm/s that :

(1) The solid-liquid interface during growth is rough or smooth, depending on growth rate and growth direction.

(2) The growth is by the continuous growth.

(3) When a crystal grows at a rate greater than a certain value (about 30 μm/s in the present experiments) or when the growth rate is changed to exceed such value, many dislocations are suddenly generated into the newly grown region of the aluminium crystal.

In the case of gallium, whose α parameter ranges 1.12 - 2.24 depending on the growth direction, it is found under the temperature gradient of 0.4 K/mm that :

(1) The solid-liquid interface is smooth for (010), (100) , (110)

and (111) and a thin layer of crystallites with thickness of a few atomic distances exists in front of the crystal surface which contacts the melt.

(2)   The growth is by the lateral growth, and the rate of lateral spread of nuclei is almost the same as that of nucleation.

(3)   Some habit planes which can not be predicted from the Jackson's theories were observed such as (110) and (111) . So that,this theory . has to be modified althoug th theory seems to be of general validity.

One of the modification proposed is to take into account of the second nearest neighbour atoms in calculating α parameter.

As regards the origin of dislocation, there have been two models associated with the mechanism of crystal growth from the melt ; one is a model based on transformation of vacancy clusters and another is based on the dislocation model of the liquid state itself. To investgate the origin and role of dislocations, configurations of dislocations in the metallic crystal near the interface during growth was observed with real time X-ray topography (Capter 4).

In the case of aluminium, a dislocation free region was observed in adjacent to the advancing front. It was also observed that many dislocations were generated behind this dislocation-free region when the cooling speed was low.

In the growth of gallium single crystal from a highly perfect seed, dislocations were not generated over the whole growing crystals. From these observations, the origin of dislocations associated with the aforementioned growth mechanism is vacancy condensation. Accordingly, the aforementioned growth theories

based on the dislocation models of the liquid are considered to be invalid.

Real time X-ray topography, which had brought us valuable information on growth mechanisms of pure metals, was applied to the study of dendrite growth of Al-Mg binary alloys (Chap.5).

In the observations of dendrite morphologies as a function of growth rate and concentration of Mg, generation and growth of higher order arms, in particular, secondary arms, were observed. The generation of these secondary arms and others is considered to be related to concentration of Mg in the growing dendrite arms. Temperature gradient in the liquid near the interface seems to be responsible for the macroscopic growth directions of these secondary arms.

Morphological as well as microstructural changes of dendrite arms were observed during coolimg and isothermal annealing after solidification. Morphology of dendrite arms changes just after the solidification during cooling. At first, lattice distortion of dendrite arms takes place and morphological change as well as microstructural of dendrite arms followed over the whole crystal. These changes are likely caused by the stress due to shrinkage of crystal surface or segregation of Mg atoms.

Morphological and microstructural change of dendrite arms has also been observed during isothermal annealing near the melting temperature. This change is attributable to the solute redistribution caused by diffusion in solid.

In the observations of dendrite morphology with the variation of macroscopical growth direction, primary dendrite arms always grow in <100> direction at the growth rate examined in the present

experiments (10 μm/s - 90 μm/s). It is concluded that growth direction of dendrite arms is independent of macroscopical growth direction (i.e. the direction of temperature gradient).

From the observations of the melting process, concentration profiles of Mg in dendrite arms were estimated. It can be concluded that there is considerable difference in the concentration of Mg between primary arms and other high-order arms.

ACKNOWLEDGEMENT

LIST OF PUBLICATIONS

(1) "In Situ Heating Device for Real Time X-Ray Topography on Crystal Growth from the Melt" : T. Kobayashi and T. Imura, Jpn. J. Appl. Phys., 23 (1984) L.632

(2) " X線トポグラフィーによる 金属の融解, 凝固過程の動的観察 "
小林 達正 , 井村 徹, 坂 公恭 , 日本金属学会会報, 第23巻 (1984) P.952

(3) "Real-Time X-Ray Topographic Observation of Crystal Growth of Gallium from Melt" : T. Kobayashi, Y. Nishikawa and T. Imura, Jpn. J. Appl. Phys., 25 (1986) 345

(4) "Study of the Formation Mechanism of Dislocations during the Growth Process of Aluminium and Gallium Single Crystals from the Melt by Real Time X-Ray Topography" : T. Kobayashi, Y. Nishikawa and T. Imura, J. Cryst. Growth, 84 (1987) 489

(5) "Observational Study on Dendrite Growth of Al-Mg Single Crystals by Real Time X-Ray Topography" : T. Kobayashi, N. Kawabe and T. Imura, Jpn. J. Appl. Phys., 26 (1987) 1823